NASA CONTRACTOR REPORT

STUDY OF ACTIVE VIBRATION ISOLATION SYSTEMS FOR SEVERE GROUND TRANSPORTATION ENVIRONMENTS

by Peter C. Calcaterra, Richard D. Cavanaugh, and Dale W. Schubert

Prepared by
BARRY WRIGHT CORPORATION
Watertown, Mass.
for Langley Research Center

NATIONAL AERONAUTICS AND SPACE ADMINISTRATION • WASHINGTON, D. C. • NOVEMBER 1969

STUDY OF ACTIVE VIBRATION ISOLATION SYSTEMS FOR SEVERE GROUND TRANSPORTATION ENVIRONMENTS

By Peter C. Calcaterra, Richard D. Cavanaugh, and Dale W. Schubert

Prepared under Contract No. NAS 1-8611 by
BARRY WRIGHT CORPORATION
Watertown, Mass.

for Langley Research Center

NATIONAL AERONAUTICS AND SPACE ADMINISTRATION

For sale by the Clearinghouse for Federal Scientific and Technical Information
Springfield, Virginia 22151 – Price $3.00

STUDY OF ACTIVE VIBRATION ISOLATION SYSTEMS FOR SEVERE GROUND TRANSPORTATION ENVIRONMENTS

by Peter C. Calcaterra, Richard D. Cavanaugh
and Dale W. Schubert

ABSTRACT

An investigation is conducted to evaluate the application of active mechanisms for the protection of equipment and/or personnel from the severe dynamic inputs characteristic of ground transportation vehicles. For the purposes of the study, dynamic loads and isolation system performance are defined in terms of the maximum expected vertical excitations associated with the suspension system of high speed ground transportation vehicles, and conservative levels of allowable passenger acceleration. Selected configurations employ available hardware, and consist of a static load support fluidic spring in parallel with a 0.2 Hz resonant frequency electrohydraulic isolator, which: a) provides the desired degree of isolation from both discrete frequency and broad-band vibration excitations; and b) limits the payload deflections to within ± 6 inches under conditions of combined vibratory and transient dynamic loads. Rigid and flexible payloads of 1,000, 3,000 and 10,000 pounds per isolator are considered. The response of the selected isolation systems is presented in terms of absolute and relative transmissibility; payload acceleration; and relative displacement between the payload and the source of excitation for the vibratory, transient, and combined excitations. In all cases the effect of increasing the payload weight by twenty percent is shown. The results indicate that the selected active isolation systems are capable of protecting a range of payloads from severe vibratory and transient dynamic loads. System stability, estimates of flow and power requirements, system weight, reliability, and failsafe criteria considerations are shown. Recommendations are made regarding extension of the techniques to provide isolation in the combined vertical and lateral directions.

CONTENTS

STUDY OF ACTIVE VIBRATION ISOLATION SYSTEMS FOR SEVERE GROUND TRANSPORTATION ENVIRONMENTS

by Peter C. Calcaterra, Richard D. Cavanaugh and Dale W. Schubert

Barry Controls, Division of Barry Wright Corporation
Watertown, Massachusetts

SUMMARY

In order to select parameters for the investigation, the environment of a high-speed ground transportation vehicle is chosen as representative of severe dynamic inputs. Based on assumptions made regarding the type and level of the expected excitations, discrete and broad-band vibratory inputs and a step force at the payload are selected. The level of desired isolation is that associated with human comfort. A range of payload weights, both rigid and flexible, are considered. The response is evaluated for nominal payload weights and for twenty percent increase in payload weight.

A review of available analytical and experimental studies involving passive and active isolation systems indicates that in order to provide the desired degree of vibration isolation and displacement control, an electrohydraulic isolator is required. The isolator contains: (1) a narrow-band high gain network for the isolation of the discrete vibratory excitations; (2) and wide-band shaping network which, in combination with a flexible coupling, provides wide-band isolation; and (3) compensation networks to insure both system stability and displacement control.

Equations of motion are first derived for the rigid payloads. A digital computer program is developed to define the system frequency response, select appropriate linear flow gains, and select compensation networks to provide the desired degree of isolation, while insuring system stability. Once the gains are selected, the response to the step force at the payload is evaluated using an analog computer simulation of the system. It is shown that the linear gains which provide the desired degree of vibration isolation are not appropriate for limiting the displacements due to a step force at the payload to within 6 inches. Nonlinearities in the flow gains are then introduced such that the system provides the desired isolation during vibratory excitations, while limiting the displacement under combined vibratory and transient excitations to within 6 inches.

In all cases system open loop phase and magnitude gain margins are calculated to indicate the system stability. Flow and power requirements are also determined for each payload weight. The reliability and failure characteristic of the system is evaluated in terms of component characteristics. Finally, weight estimates are shown for each payload.

SECTION 1: INTRODUCTION

The isolation of equipment and/or personnel from the damaging effects and discomfort of dynamic loads such as shock and vibration has been the subject of numerous investigations. For a particular vibration and shock environment, it is usually possible to develop analytically an isolation scheme to significantly reduce the response of the item to be protected. However, in translating the results of analysis to physical hardware, additional criteria may be involved which compromise the design. These criteria include such things as hardware availability, the physical size and performance capability of the isolation system components, initial and operating costs, and reliability. Previous analytical and experimental studies indicate that active isolation systems: 1) do provide a degree of vibration isolation and displacement control which cannot be attained by passive systems; and 2) are both feasible and practical [Ref. 1-7]. Active isolators are particularly well suited for applications where vibration isolation is required at low frequencies during conditions of combined vibratory and transient excitations.

The subject of this investigation is an engineering study of active isolation systems suitable for protecting a range of payloads from dynamic inputs characterized by relatively large displacements. For the purposes of the study, dynamic loads and isolation system performance are defined in terms of the anticipated requirements associated with a high-speed tracked air cushion vehicle (TACV). These requirements are selected since they represent severe conditions from the point of view of the type and level of excitations, desired degree of vibration isolation, and maximum allowable dynamic displacements.

Passenger acceptance of any vehicle is dependent upon a comfortable ride. The subjective nature of ride comfort and the lack of applicable data makes it very difficult to define the

degree of vibration isolation which is required for any given dynamic environment. For TACV's, the precise level and frequency content of the excitations transmitted to the passengers are not known. Research vehicles presently under consideration by the Department of Transportation will allow definition of the excitations experienced by the passenger. Since it is anticipated that the air cushions alone will not provide the necessary degree of protection, the research vehicles include provision for testing various types of secondary suspension systems to reduce the transmitted excitations to acceptable levels. The investigation reported herein deals with the selection of isolation systems capable of providing a degree of isolation defined in terms of the maximum expected vertical excitations and conservative levels of allowable vertical passenger acceleration.

Passive and active systems, both linear and nonlinear, which have been successfully used in other applications are evaluated. It is shown that the postulated degree of desired isolation can be obtained by the combination of a static load support spring in parallel with a 0.2 Hz resonant frequency electrohydraulic isolation system. The latter provides isolation of both the discrete frequency and broad-band vibration excitations which reach the payload from the guideway through the air cushion. In addition, it limits the vertical deflection between the payload and the air cushion to within ±6 inches under conditions of combined discrete frequency and broad-band vibration excitations, and vertical transient force applied at the payload equal to one-half the nominal payload weight. The selected systems employ available components.

Rigid and flexible payloads of 1,000; 3,000 and 10,000 pounds per isolator are considered. Discrete frequency and broad-band excitations are defined for vehicle speeds of 50, 100, 200 and 300 mph and guideway span lengths of 50, 100 and 200 ft. The response of the selected isolation system to the

vibratory excitations is presented in terms of absolute and relative transmissibility values as a function of frequency. System stability is defined in terms of phase and gain margins. Response of the system to a force step at the payload is presented in terms of payload acceleration, and relative displacement between payload and the cushion. In all cases, the effect of increasing the payload weight by twenty percent is shown.

The response of systems employing linear gains in the feedback mechanisms is investigated first. Nonlinearities are introduced in such a manner so as to limit the deflections during transient conditions while insuring that the desired degree of vibration isolation is provided during vibratory excitations. The results indicate that the selected active isolation systems are capable of protecting a range of payloads from severe vibratory and transient dynamic loads. Estimates of flow and power requirements, and of system weight are shown for each case, as well as reliability and failsafe criteria considerations. Recommendations are made regarding extension of the techniques to provide isolation in the combined vertical and lateral directions.

The remaining sections of the report include:

Section 2: Definition of System Parameters
Section 3: Selection of Secondary Suspension System
Section 4: Response of Linear Feedback Active Isolation System
Section 5: Response of Nonlinear Feedback Active Isolation System
Section 6: Discussion of Results
Section 7: System Reliability and Weight Estimates
Section 8: Conclusions
Section 9: Recommendations

SECTION 2: DEFINITION OF SYSTEM PARAMETERS

Payload Characteristics

The selected system parameters are based on the anticipated requirements associated with the TACV secondary suspension system as being representative of severe ground transportation dynamic environments. Three payload weights per isolator were selected, namely: 1,000; 3,000; and 10,000 lbs, corresponding to different methods for partially supporting the total passenger compartment. The payloads were considered to be both rigid and flexible. The flexible payload was assumed to be a simple mass-spring-damper system having natural frequencies of 5 and 10 Hz and a damping ratio of 0.1. In all cases, the effect of a twenty percent increase in the payload mass was to be evaluated.

Dynamic Excitations

The dynamic excitations experienced by a TACV payload arise from guideway irregularities and deflections, and external forces acting on the vehicle. The guideway disturbances are essentially random in nature. However, they do contain harmonic components which are related to span lengths used in elevated guideway sections. External forces are a result of body aerodynamics, wind profiles at ground level, and disturbances produced by the necessity of the vehicle to follow the terrain upon entering or leaving a grade and rounding a curve. These excitations are both translational and rotational in all axes of the vehicle to varying degrees of severity. However, for the purposes of isolation system evaluation, vertical excitations only are considered.

The expected vertical excitations to the payload of a high speed track air cushion vehicle were assumed to be: discrete frequency sinusoidal and broad-band sinusoidal motions reaching the payload from the guideway through the secondary suspension system; and transient forces applied at the payload

as a result of aerodynamic and gust loadings.

Discrete Frequency Sinusoidal Excitations: The discrete vertical excitation was postulated to be a sinusoidal displacement resulting from the sag of the guideway between support columns as the weight of the vehicle traverses the span. For any given guideway construction, the amplitude of the vertical displacement is a function of the span length. The frequency at which it occurs is a function of the speed of the vehicle and the span length (wavelength); i.e., frequency = speed ÷ wavelength. Figure 1 shows the maximum expected peak-to-peak amplitude of the sinusoidal excitation to the secondary suspension system for span distances ranging from 50 to 200 ft, and speeds from 50 to 300 mph.

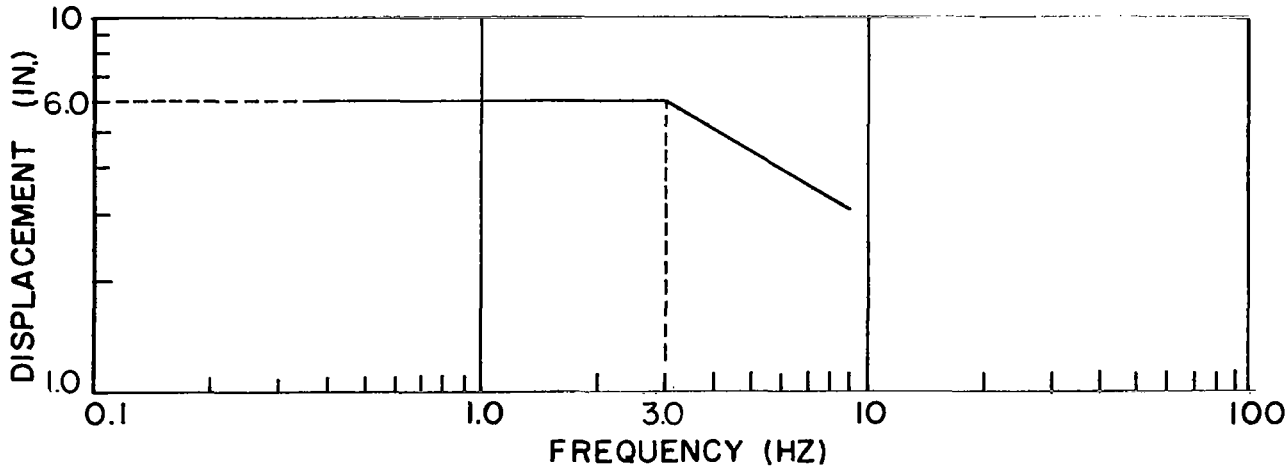

Figure 1. - Maximum expected peak-to-peak amplitude of vertical discrete sinusoidal excitation from guideway sag.

The lowest frequency (0.37 Hz) corresponds to the lowest speed (50 mph) and longest span (200 ft). Similarly, the highest frequency (8.8 Hz) corresponds to the highest speed (300 mph) and shortest span (50 ft). The maximum expected peak-to-peak amplitude is 6 inches up to 3 Hz, decreasing to 3 inches at 8.8 Hz.

Any one combination of speed and span length will give rise to a single discrete frequency sinusoidal excitation having a

displacement amplitude defined in Figure 1. Table I shows the discrete frequencies for combinations of the four speeds and three span lengths considered in the investigation. The corresponding displacement and acceleration amplitudes are shown in Table II.

TABLE I

SINUSOIDAL EXCITATION FREQUENCIES FOR THE VEHICLE SPEEDS AND SPAN LENGTHS CONSIDERED IN THE INVESTIGATION

Speed (mph)	Span Length (ft)		
	200	100	50
	Excitation Frequency (Hz)		
50	0.37	0.73	1.47
100	0.73	1.47	2.93
200	1.47	2.93	5.87
300	2.20	4.40	8.80

TABLE II

DISCRETE SINUSOIDAL DISPLACEMENT AND ACCELERATION AMPLITUDES

Excitation Frequency (Hz)	Displacement Amplitude (±in.)	Acceleration Amplitude (g peak)
0.37	3	0.04
0.73	3	0.16
1.47	3	0.62
2.20	3	1.50
2.93	3	2.75
4.40	2.35	4.60
5.87	1.95	7.00
8.80	1.50	13.50

Broad-band Sinusoidal Excitations: It is anticipated that the guideway will exhibit a random uneveness. The 3σ random level of the vertical displacement transmitted to the secondary suspension system at 300 mph, was selected in terms of an equivalent peak-to-peak sinusoidal displacement as shown in Figure 2. Wavelengths less than the length of a single air cushion (10 ft) were not considered since these shorter guideway irregularities would not be transmitted through to the secondary suspension system. Therefore, the highest frequency of the equivalent vertical sinusoidal excitation for a speed of 300 mph is 44 Hz. At 300 mph, the lowest frequency occurs for the longest span (200 ft).

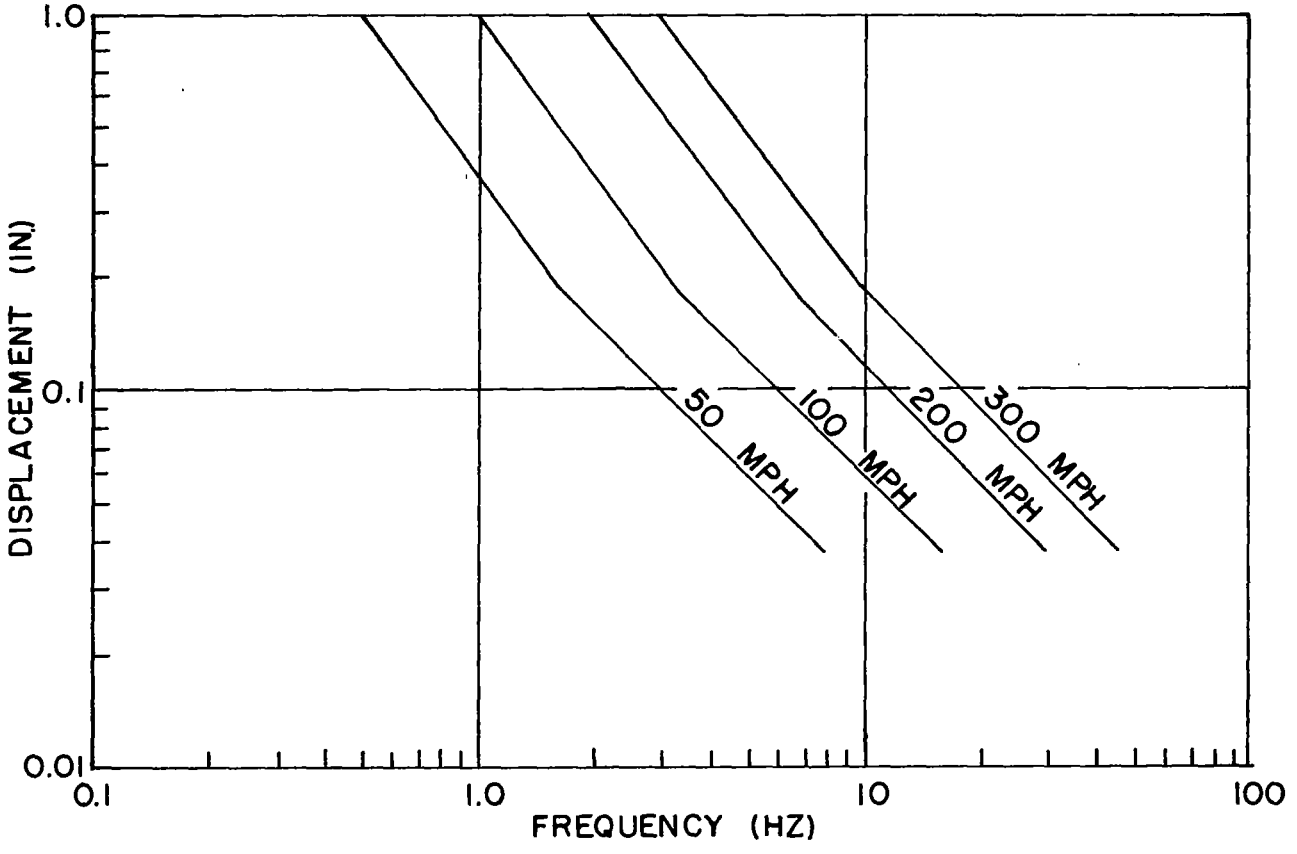

Figure 2. - Displacement amplitude of vertical broad-band sinusoidal excitation equivalent to a 3σ level of random guideway uneveness for four vehicle speeds.

The total peak-to-peak sinusoidal displacement equivalent to the 3σ level of random excitation is a constant regardless of speed. Therefore, the equivalent broad-band random vibration

excitation curves for 50, 100 and 200 mph exhibit the same values of displacement amplitude as the 300 mph curve except for a shift to lower frequencies proportional to the reduction in speed. Values of displacement amplitude as a function frequency for speeds of 50, 100, and 200 mph are also shown in Figure 2. The corresponding acceleration amplitudes for all four speeds are shown in Figure 3.

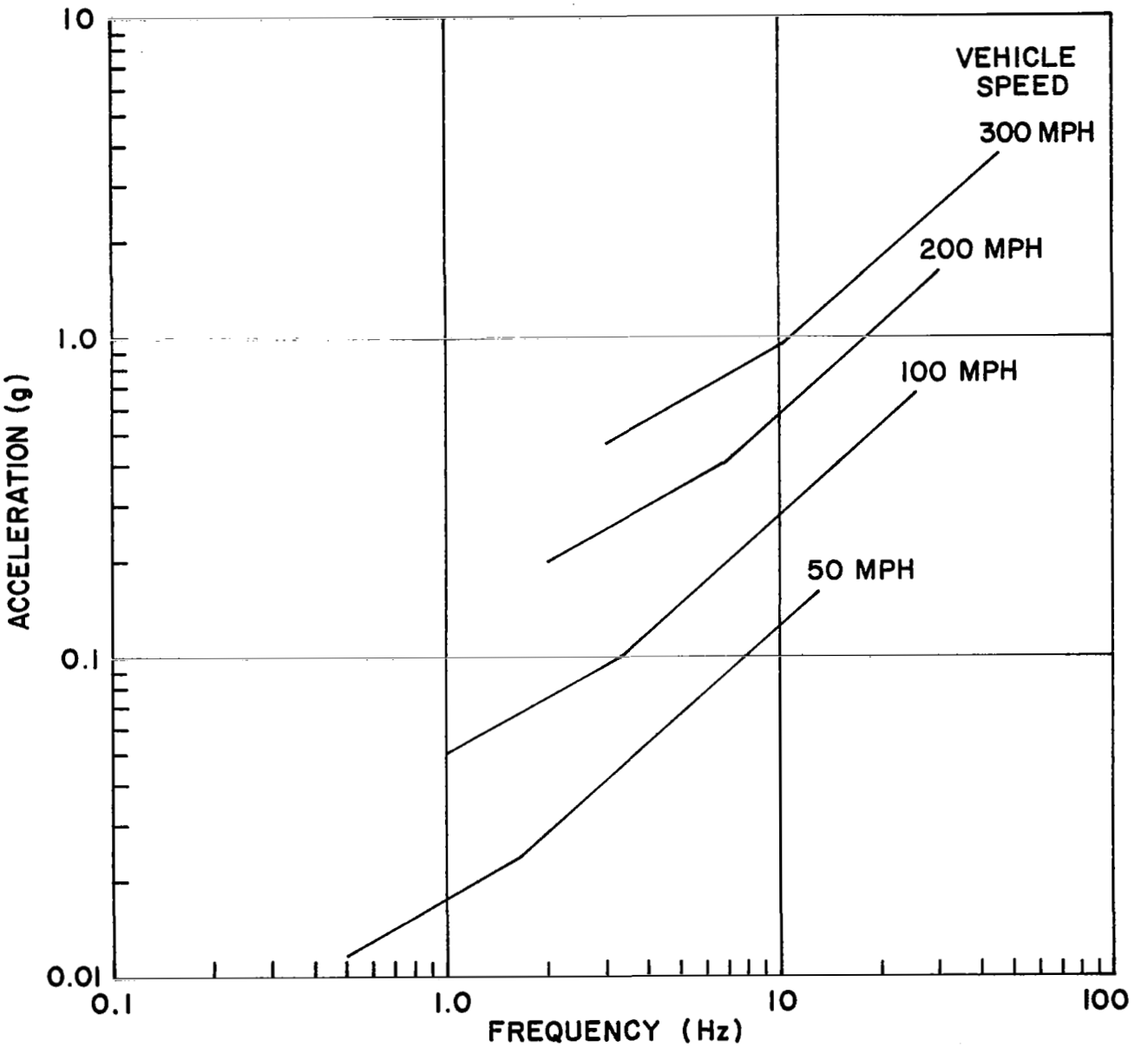

Figure 3 - Acceleration amplitude of vertical broad-band sinusoidal excitation equivalent to a 3σ level of random guideway uneveness for four vehicle speeds.

Transient Excitations: The effect of aerodynamic and gust loadings on the vehicle in the vertical direction was postulated to be equivalent to a step force applied at the payload. The magnitude of the transient force was set equal to one half the nominal weight (0.5W).

Desired Secondary Suspension System Performance

The vertical acceleration transmitted to the isolated payload during sinusoidal and random excitations was selected to be within the values shown in Figure 4. These values represent the desired output of the isolation system based on human comfort criteria [Ref. 8, 9].

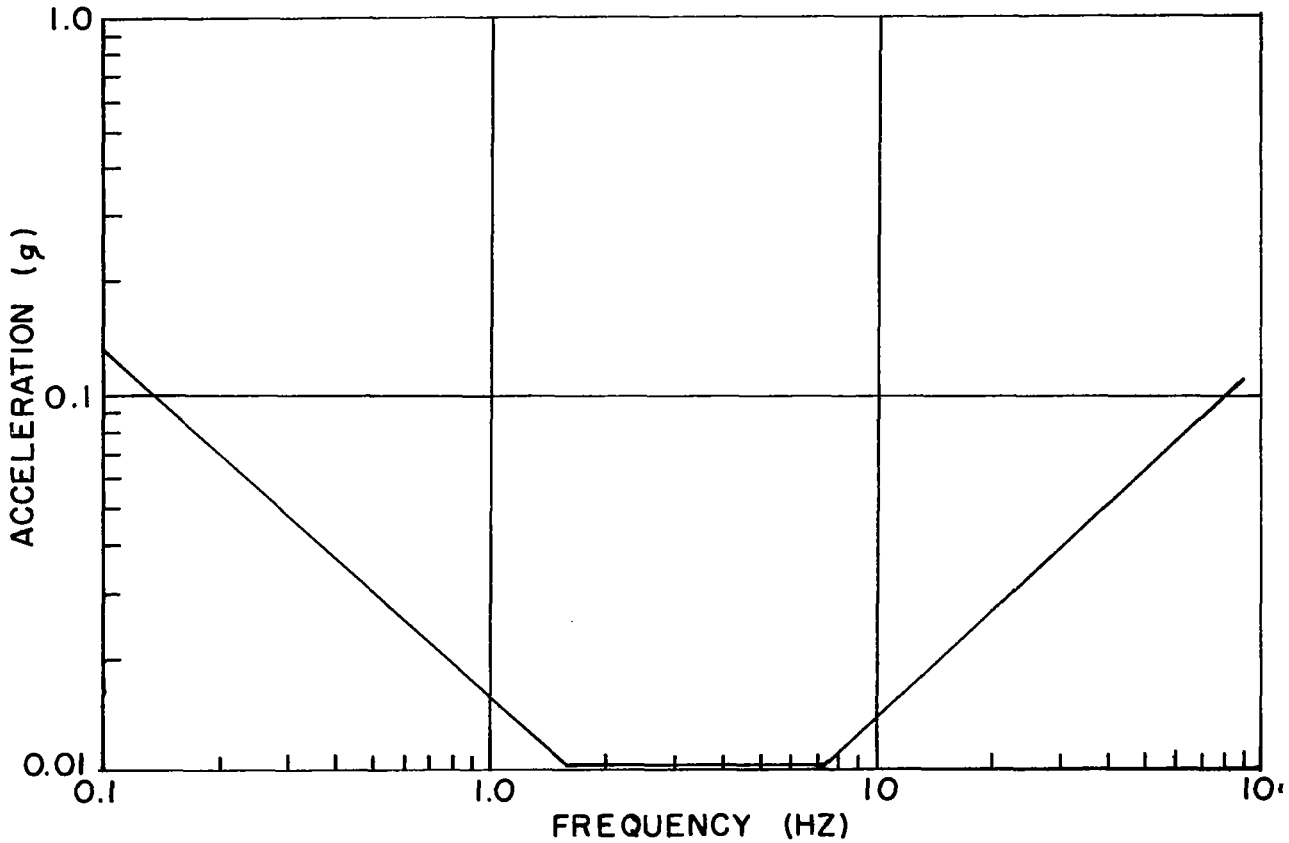

Figure 4. - Desired maximum acceleration of isolated payload for combined sinusoidal and random vibration excitations.

The vibration isolation requirements of the secondary suspension system can then be defined in terms of desired system transmissibility as a function of frequency. Transmissibility is the ratio of the peak payload acceleration to the peak expected acceleration excitation. Although the discrete frequency and broad-band sinusoidal excitations occur simultaneously, the transmissibility requirements for each are defined separately. For the discrete frequency sinusoidal excitations, the desired transmissibilities at each of the eight frequencies are calculated from the acceleration inputs listed in Table II and the desired payload acceleration shown in Figure 4. Desired transmissibilities at each of the eight excitation frequencies are listed in Table III.

TABLE III

DESIRED TRANSMISSIBILITY VALUES FOR DISCRETE FREQUENCY SINUSOIDAL EXCITATIONS

Excitation Frequency (Hz)	Desired Transmissibility
0.37	0.9000
0.73	0.1200
1.47	0.0170
2.20	0.0070
2.93	0.0037
4.40	0.0022
5.87	0.0015
8.80	0.0010

The level of broad-band excitation is a function of vehicle speed. Therefore, for each discrete frequency excitation, the associated level of the broad-band excitation should consider all the speeds that give rise to that particular frequency of discrete excitations. The speeds associated with each discrete frequency

are shown in Table I. The desired transmissibility for broad-band excitations associated with each discrete frequency were calculated from the broad-band excitation levels shown in Figure 3 and the payload accelerations indicated in Figure 4. The desired transmissibility as a function of vehicle speed is shown in Figure 5. Figures 6 and 7 show the desired transmissibilities for broad-band excitations for the eight discrete frequencies considered. In each case, the transmissibility values are calculated based on the maximum acceleration levels associated with the various speeds that give rise to that particular discrete frequency excitation.

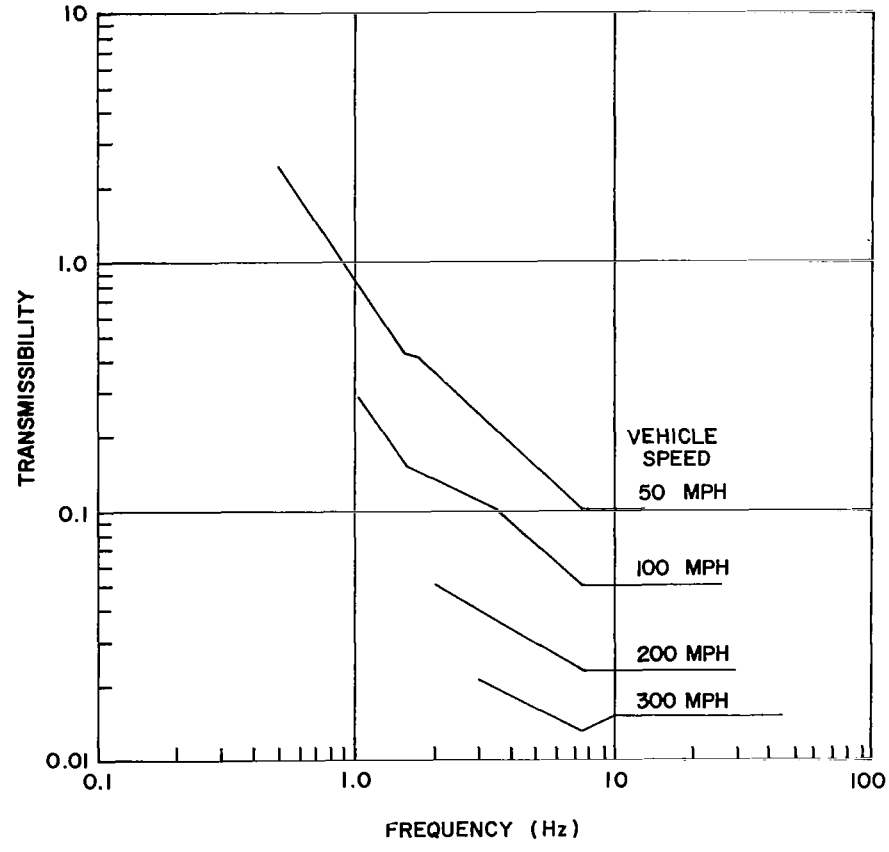

Figure 5. - Desired transmissibility based on broad-band sinusoidal excitation as a function of vehicle speed.

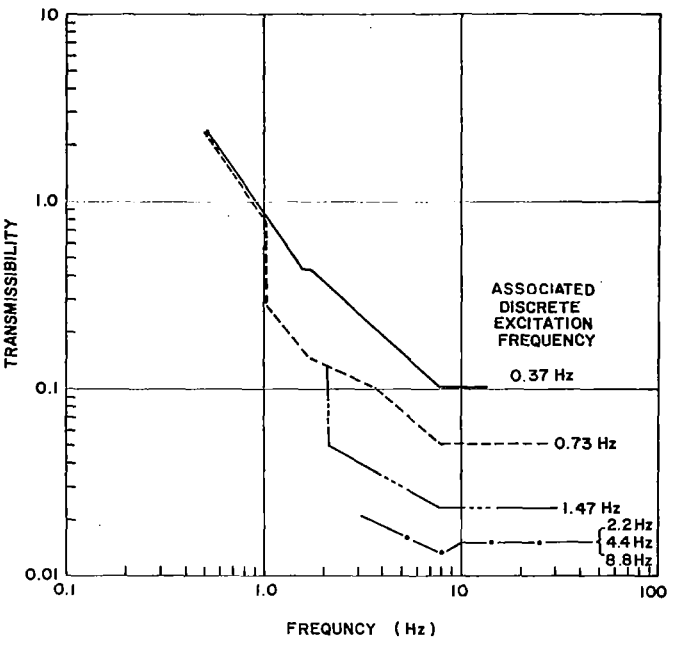

Figure 6. - Desired transmissibility based on broad-band sinusoidal excitations for conditions which give rise to discrete excitation frequencies of 0.37, 0.73, 1.47, 2.2, 4.4, and 8.8 Hz.

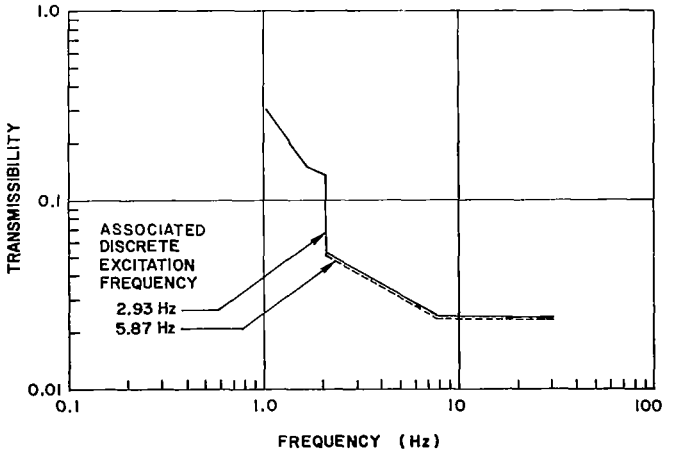

Figure 7. - Desired transmissibility based on broad-band sinusoidal excitations for conditions which give rise to discrete excitation frequencies of 2.93 and 5.87 Hz.

To summarize, the secondary suspension system should be capable of providing the degree of isolation listed in Table III at each of the discrete frequencies indicated. Simultaneously, it must provide the degree of broad-band isolation indicated in Figures 6 and 7. In addition, the total relative displacement for conditions of combined discrete frequency, broad-band, and transient excitations should not exceed ±6 inches.

The desired system performance, although based on postulated TACV requirements, can be considered to be representative of other applications in which the dynamic loads are characterized by large displacements, either at discrete frequencies or over a frequency range, and where combined vibratory and transient conditions exist. Since the study includes a range of payload weights and flexible as well as rigid payloads, the results can be used to evaluate equipment and/or personnel isolation needs under a variety of other similar environments.

SECTION 3: SELECTION OF SECONDARY SUSPENSION SYSTEM

Evaluation of Vibration Isolation Techniques

Vibration and shock isolation involves the insertion of an isolator having appropriate characteristics between the payload and the source of dynamic excitation so that, under specified conditions of vibration and shock excitations, the desired reduction in the level of payload dynamic response is achieved.

Vibration and shock isolation systems are generally categorized as linear or nonlinear, depending on whether or not their dynamic response is described by a set of linear time-invariant differential equations. They are further categorized as active or passive, depending on whether or not external power is required for the isolator to perform its function.

The intent of the investigation is to define the feasibility of providing the desired vertical vibration isolation and displacement control employing whenever possible proven techniques and readily available hardware. Therefore, various passive and active systems were evaluated on the basis of the expected excitations and performance requirements of a TACV. The most stringent isolation requirement occurs due to the discrete frequency excitations, where at 8.8 Hz, the required transmissibility is 0.001 (Table III). In order to provide the stated degree of isolation at 8.8 Hz, the system natural frequency should be approximately 0.05 Hz. Although less severe, isolation of the broad-band excitations must also be provided up to 44 Hz as shown in Figures 6 and 7. The isolation requirements of the broad-band excitations requires an isolation system natural frequency of approximately 0.2 Hz.

Passive Isolation Systems: The essential features of a passage isolator are a resilient load-supporting means (stiffness) and an energy dissipating means (damping). Typical passive isolators employ metallic springs, elastomers, fluidic springs,

wire cable, and combinations of these and other cushioning devices. Based on experience with actual hardware, the lowest practical natural frequency using passive isolators is approximately 1 Hz [Ref. 3]. One important limitation of passive isolation systems is that the static deflection varies as the inverse square of the natural frequency. The static deflection of a linear passive system having the required 0.05 Hz natural frequency would be over 30 feet. Even if the static deflection is eliminated by means of load support springs, the dynamic deflections of the system under a force step would exceed the maximum value of 6 inches. If nonlinearities are introduced in the isolator stiffness to limit the dynamic deflections to the desired level, the performance of the system would deteriorate since it would exhibit the vibration isolation characteristics of a stiffer system. Therefore, it is concluded that passive isolators cannot provide the desired degree of isolation and displacement control.

Active Isolation Systems: Active isolators are servo-mechanisms, power operated in accordance with a command signal derived from feedback control signals. They consist of excitation and/or response sensors, sensor signal processor and actuators. The sensors provide signals proportional to dynamic excitation or response quantities. The signal processors modify and combine sensor signals to create a command signal. And, the actuators apply forces or induce motions in accordance with the command signal.

Power is required to operate active isolator mechanisms, and, in some cases, power is also required for the signal processor. The requirement of externally supplied power is the primary distinguishing characteristic between active and passive isolation systems.

One main advantage of active isolators is that natural frequencies substantially lower than those realizable from passive isolators can be provided, with low dynamic deflections particularly under conditions of transient excitations. A wide variety of

excitation and response sensors can be employed to provide feedback signals and form a closed-loop active isolation system. For example, feedback signals can be developed which are a function of jerk, acceleration, velocity, displacement, time-integral of displacement, differential pressure or force. The signal processor may consist of an active network (e.g., electronic or fluidic) that performs amplification, attenuation, differentiation, integration, addition, and compensation functions. Alternately, the signal processor can be in the form of a passive mechanism (e.g., a mechanical linkage).

Types of actuators that may be used in active isolation systems include mechanical (e.g., ball screw or rack and pinion mechanisms), fluidic (e.g., pneumatic or hydraulic cylinders), variable resilience elements (e.g., electrically-active fluids), and electrodynamic force generators. By combining the various types of sensors, signal processors and actuators, active isolation systems can generally be classified as electromechanical, pure fluidic (pneumatic or hydraulic), mechanofluidic (mechanopneumatic or mechanohydraulic), electrofluidic (electropneumatic or electrohydraulic), electric-fluid (electrically conductive or magnetic fluids, and electrodynamic [Ref. 1].

Mechanofluidic and electrofluidic isolation systems represent the most practical active isolator mechanisms for the tracked air cushion vehicle application. Mechanofluidic isolator mechanisms are relatively uncomplicated, but provide limited servo-control capabilities because of restrictions on the types of mechanical feedback available [Ref. 3]. Electrofluidic isolator mechanisms are relatively complex, but provide considerable flexibility in servo-control capabilities [Ref. 1]. Consequently, initial selection was made of active isolator mechanisms with electronic feedback.

Linear analyses of electropneumatic and electrohydraulic isolation systems indicate that their performance is determined by

the same equations with suitable definitions of system parameters [Ref. 2 and 3]. This suggests that an engineering study could be performed on electrofluidic isolation systems and be applied to isolator mechanisms that employ either pneumatic or hydraulic actuators. Such a conclusion is not valid, however, since the actual dynamic characteristics of the pneumatic system are quite nonlinear compared to the hydraulic system. Furthermore, components (e.g., servovalve) for pneumatic and hydraulic systems are not interchangeable in general.

A listing of disadvantages associated with pneumatic control systems include temperature sensitivity of the gas (with consequent changes in pressure and effective feedback forces), nonlinear flow characteristics, compressibility effects, slow speed of response, limited standard hardware availability (servovalves, for example), size, and weight. The compressibility of the air and its effect on stability of the control system are an important consideration. The system can be stable for small motions about an operating point (i.e., essentially operation at constant volume); however, subjecting the system to any excitation which causes deflection away from the initial operating point could result in an unstable condition. The instability would be due to the rather severe changes which occur in the value of effective feedback gains with small changes in volume and, therefore, pressure. The compressibility of air places a definite restraint on the speed at which the feedback forces can be generated to achieve the desired response characteristics. Finally, power must be expended to compress the air and, for the relatively low pressures and high volume involved, components capable of handling large flows have to be employed. Therefore, even though it is recognized that pneumatic power may be readily available on air cushion vehicles, electrohydraulic isolation systems were selected for this investigation based on the stated disadvantages of electropneumatic systems.

Performance Characteristics of Electrohydraulic Isolators: A schematic diagram of a single-degree-of-freedom electrohydraulic isolation system is shown in Figure 8, where multiple electronic feedback signals are processed through a servoamplifier to create a command signal that controls the flow of a relatively incompressible fluid to and from a cylinder through a servovalve. Sensors are employed to provide acceleration and relative displacement feedback signals, which are modified in the servoamplifier such that the flow through the valve is made a function of acceleration, relative velocity, relative displacement, and the time-integral of relative displacement, where the effect of each feedback parameter may be independently controlled by adjusting its gain.

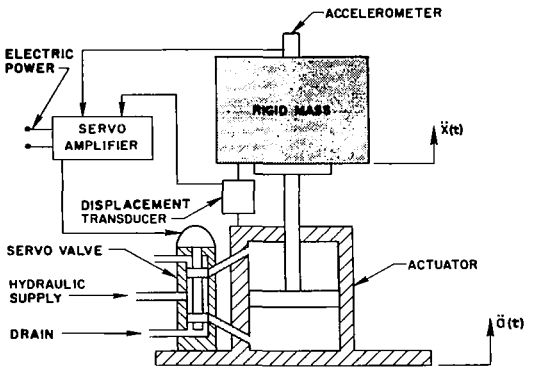

Figure 8. - Schematic diagram of electrohydraulic isolation system.

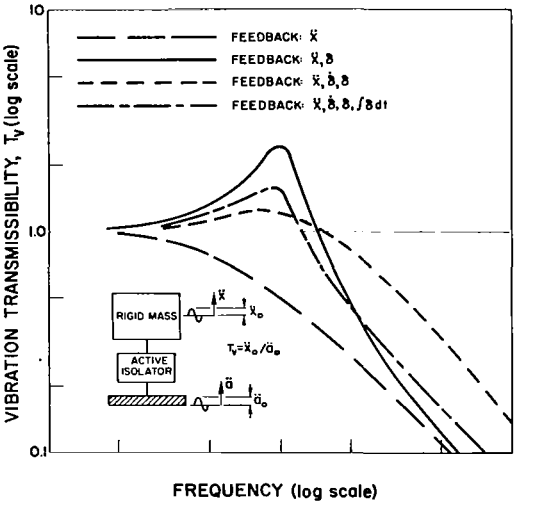

Figure 9. - Low-frequency vibration transmissibility characteristics of electrohydraulic isolation system.

Typical vibration transmissibility characteristics of the electrohydraulic isolation system with various combinations of feedback parameters are shown in Figure 9 [Ref. 1]. The analysis on which these results are based assumes unity transfer functions

for the sensors and servovalve and, therefore, is applicable in the low-frequency region where the effect of hydraulic component dynamics is negligible. Degradation of high-frequency vibration isolation occurs because of the effects of resonances, which are determined by the dynamic characteristics of the mechanical and hydraulic components and the electronic networks. This is illustrated by the "active" transmissibility curve in Figure 10, which indicates a low isolation system natural frequency (created electronically by selecting appropriate values of feedback gains), and a hydraulic resonance in the high-frequency region. The transmissibility generally exceeds a value of unity at the hydraulic resonance and, for higher frequencies, the isolation characteristics are those of a passive isolation system having a natural frequency associated with the hydraulic resonance condition.

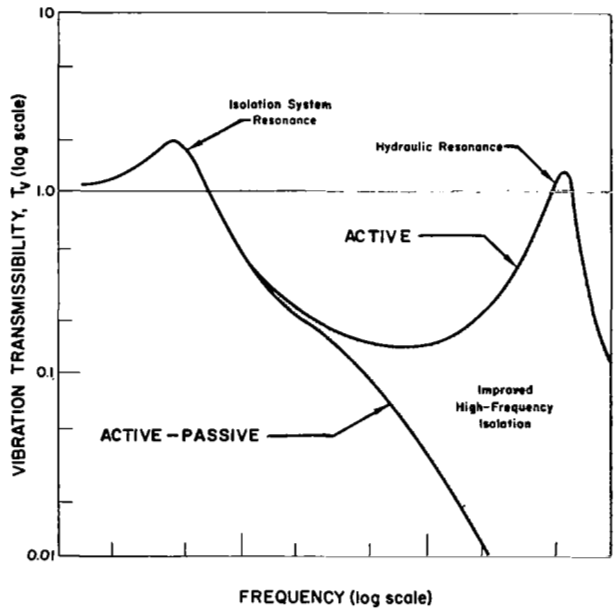

Figure 10. - Vibration transmissibility characteristics of electrohydraulic isolation systems with passive isolator (flexible coupling) in the servo loop.

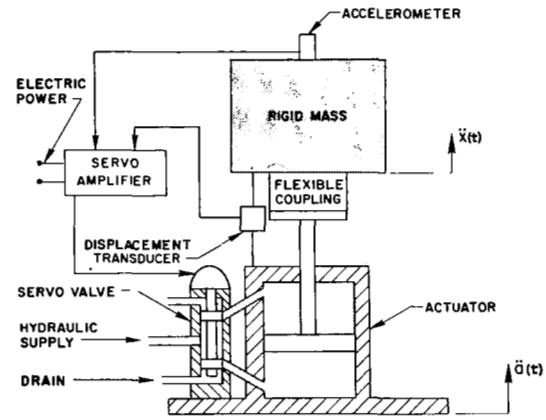

Figure 11. - Schematic diagram of electrohydraulic isolation system with passive isolator (flexible coupling).

Improved high-frequency isolation can be provided by introducing a suitable passive isolator in the form of a flexible coupling in the servo loop, as illustrated in Figure 11. The effect of the flexible coupling is to provide mechanical compensation which results in reshaping the high-frequency response characteristics. Analysis of the isolation system performance with the flexible coupling [Ref. 5] is similar to the analysis of the isolation of a flexible payload [Ref. 6]. As indicated by the "active-passive" transmissibility curve shown in Figure 10, broad-band isolation is provided with the combined active-passive isolator mechanism. Isolation of vibration is provided by active means in the low-frequency region where the passive isolator has a unity transfer function. The passive isolator provides isolation of high-frequency vibration, where the isolated body is effectively decoupled from the hydraulic actuator and the excitation frequency is beyond the frequency band over which the servo-control system is operative.

Experience indicates that proper selection of the various feedback parameter gains will result in a linear system which will exhibit the desired position control and transmissibility characteristics. In response to shock excitation, however, large dynamic deflections of the linear electrohydraulic isolation system will result because of the extremely low natural frequencies that can be achieved. To avoid this situation, nonlinear electronic compensation can be introduced into the acceleration and/or relative displacement feedback loops to substantially change the loop gain for relative displacements exceeding an established linear range of operation [Ref. 5]. This has the effect of providing a hardening stiffness characteristic with greatly increased feedback control operating to severely limit the relative displacement and rapidly reposition the isolator in its region of linear operation. Use of such nonlinear compensation will result in a higher acceleration being transmitted to the isolated body during severe shock excitation. However, the

isolation system will respond as a stiff system for only a limited time duration (because of the automatic return to initial position that is provided), after which the full degree of active vibration isolation is restored.

The transient response of the electrohydraulic isolation system subjected to an acceleration step is also a function of the feedback mechanisms employed. Pure acceleration feedback ($\ddot{x}$) provides excellent control of acceleration, but requires an infinite relative displacement. The combination of acceleration ($\ddot{x}$) and relative displacement (δ) feedback provides performance comparable to a conventional passive isolation system, with the capability of electronically creating an extremely low natural frequency. Additional system damping can be provided by use of relative velocity feedback. By introducing integral displacement feedback, excellent control of both acceleration and relative displacement response is provided with a high speed of response in eliminating the relative displacement, thereby providing vibration isolation during conditions of sustained acceleration. Nonlinear electronic compensation can be employed to provide even greater reduction of relative displacements [Ref. 5].

As an alternative to acceleration feedback, the force transmitted by the isolator can be employed as a primary sensor feedback signal. Comparable isolation characteristics are provided by use of either acceleration or force feedback; however, different effective isolator stiffness characteristics will result. For acceleration feedback, the isolator stiffness is essentially unilateral; that is, a very low stiffness is presented to the dynamic environment but a high stiffness is presented to forces acting on the isolated mass [Ref. 5]. Consequently, electrohydraulic isolation systems with acceleration feedback are relatively insensitive to payload dynamics. For force feedback in lieu of acceleration feedback, however, the isolator effective stiffness is bilateral; the isolator presents a very low

stiffness to both the environment and payload, and the isolation system is consequently more sensitive to payload dynamics and changes in payload weight [Ref. 2].

The feedback gains for acceleration and relative displacement determine the natural frequency (in a manner similar to the mass and stiffness in a passive system). The ability to select feedback gains over a very wide range (compared to the limited ranges for the mass and stiffness counterparts of these parameters in a passive isolation system) is the basis for being able to provide extremely low natural frequencies of electrohydraulic isolation systems that are independent of payload weight.

Experimental data on a single degree-of-freedom laboratory model, employing acceleration ($\ddot{x}$) and relative displacement (δ) feedback with various compensation schemes indicate the transmissibility characteristics which can be obtained in practice[Ref. 2].

Experimental transmissibility curves for broad-band isolation are shown in Figure 12(a) for the electrohydraulic isolation system with flexible couplings (passive isolators) employed to provide high-frequency vibration isolation. An electronic resonance was created at 0.5 Hz with a resonant transmissibility of 1.5. An elastomeric isolator was employed to achieve f_c = 10 Hz while a helical spring was used to achieve f_c = 3 Hz. The transmissibility curves demonstrate that lowering the stiffness of the flexible coupling improves high-frequency vibration isolation. In this case, isolation of vibration occurs for frequencies greater than 0.8 Hz, with greater than 75 percent isolation provided for frequencies greater than 2 Hz, and greater than 90 percent isolation provided for frequencies greater than 10 Hz.

Transmissibility curves for broad-band isolation are shown in Figure 12(b) for the electrohydraulic isolation system with a flexible coupling (f_c = 3 Hz), and various resonant frequencies created electronically. Changing the acceleration feedback gain provided resonant frequencies of 0.05, 0.1 and 0.5 Hz, respectively,

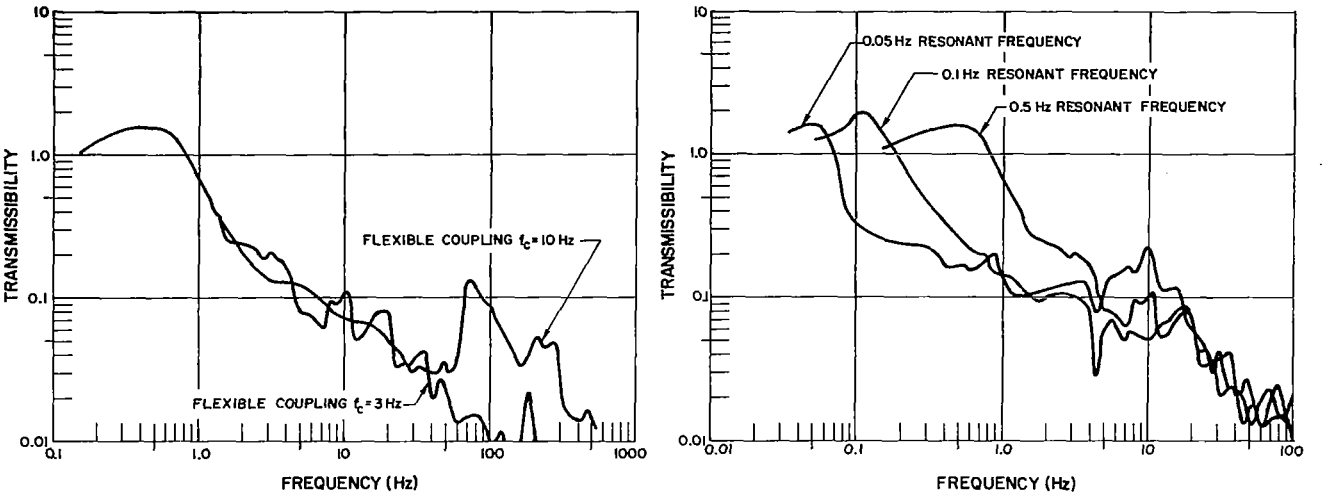

(a) Elastomeric (f_c = 10 Hz) and helical spring (f_c = 3 Hz) flexible couplings.

(b) Helical spring flexible coupling (f_c = 3 Hz).

Figure 12. - Experimental transmissibility curves for broad-band isolation systems.

with resonant transmissibilities ranging between 1.5 and 2.0. For frequencies greater than 15 Hz, the transmissibility is essentially the same for all three systems.

Transmissibility curves for broad-band isolation, with and without a single notch at 5 Hz, are shown in Figure 13 for the electrohydraulic isolation system with an elastomeric flexible coupling f_c = 10 Hz. An electronic resonance was created at 0.5 Hz with a resonant transmissibility of 1.5. The transmissibility characteristics of the broad-band isolation system were previously discussed with reference to Figure 12(a). The transmissibility curve providing combined notch and broad-band isolation characteristics is essentially the same as without the notch, except in the region of the notch frequency, at which greater than 99 percent isolation is provided.

The transmissibility curve shown in Figure 14 is for a three-notch isolation system. At the notch frequencies of 5, 7.5

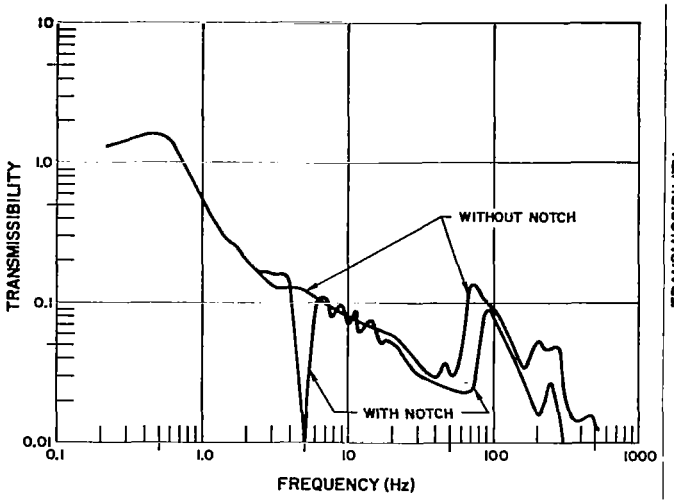

Figure 13. - Experimental transmissibility curves for broad-band and combined notch and broad-band isolation systems.

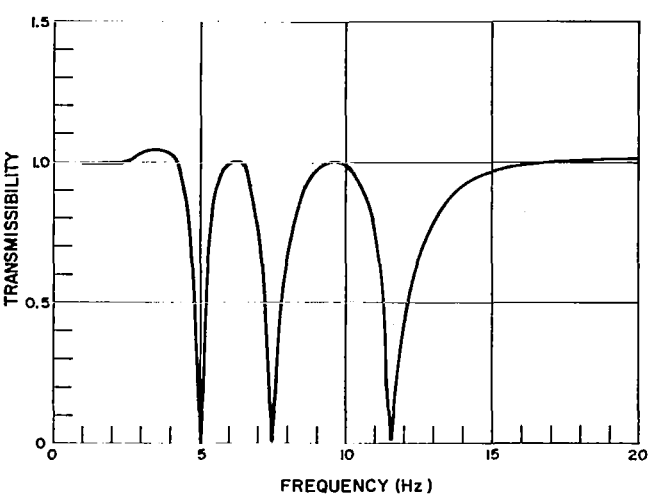

Figure 14. - Experimental transmissibility for a multiple-isolation system without flexible coupling.

and 11.5 Hz, greater than 99 percent isolation is provided. A resonance condition existed for this isolation system where the resonant frequency was 3.5 Hz and the resonant transmissibility was 1.05. A transmissibility of unity generally applies for excitation frequencies remote from the notch frequencies.

The notch isolation system can be made adaptive by automatically tracking variations in the excitation frequency. To

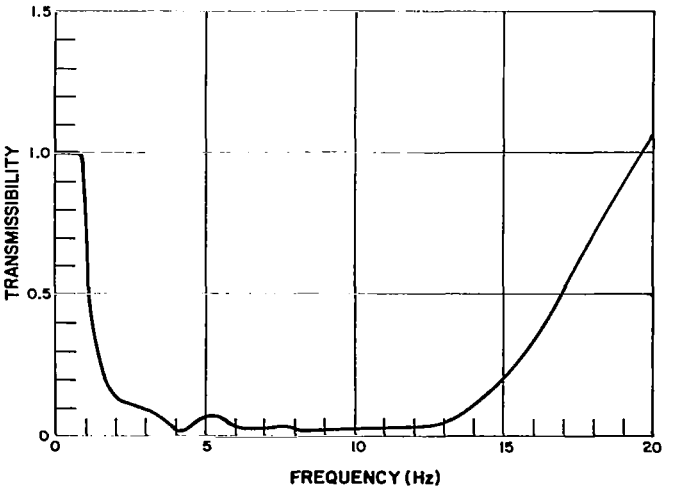

Figure 15. - Experimental transmissibility curve for a notch isolation system with automatic frequency tracking.

demonstrate this capability, tachometer feedback was employed to vary the notch frequency of a single-notch isolation system to obtain the experimental transmissibility curve shown in Figure 15. The tachometer was used to sense the frequency of vibration excitation imposed by a shaker, and the isolation system notch was automatically tracked to the excitation frequency in the range from 3 to 15 Hz.

Selection of System Configuration

The postulated vibration isolation and displacement control requirements can best be met by an electrohydraulic system employing a combination of the feedback mechanisms previously described. Although a broad-band electrohydraulic system having a resonant frequency of 0.05 Hz is realizable, Figure 12(b), and would provide the isolation required under both discrete frequency and broad-band isolation, high values of gain in the displacement feedback would be required to limit the displacements under a step force equivalent to fifty percent of the load (0.5W) to within the required ±6 inches. Such high gain values would reduce the phase and gain margins and severely affect the stability of the system.

The experimental results shown on Figures 13 and 14 indicate that isolation of discrete frequency excitations can be achieved by notches of isolation. If such a feedback mechanism is employed to isolate the TACV discrete frequency excitations, a separate wide-band shaping network, resulting in a resonant frequency of 0.2 Hz can then provide the required broad-band isolation. The gains associated with the higher frequency broad-band shaping network will allow acceptable margins of stability. The displacement with low frequency notches due to a transient excitation are smaller than the displacements of an equal natural frequency broad-band isolator. Therefore, the displacement gains required to limit the total displacement to within ±6 inches would be smaller and the over-all system margins of stability would be greater.

Finally, in order to limit the flow and power requirements of the system, a static load support spring can be added in parallel with the electrohydraulic actuator such that the actuator carries none of the static load.

To summarize, the selected configuration for the TACV suspension system consists of a static load support spring in parallel with an electrohydraulic isolator. The isolator contains: an actuator, flexible coupling, servovalve, servo-accelerometer, displacement transducer, and a servoamplifier. The servoamplifier will include a narrow-band high gain network (notch) for the isolation of the discrete vibration excitations; a wide-band shaping network which, in combination with the flexible coupling, provides wide-band isolation; and compensation networks to insure both system stability and displacement control. Automatic tracking of speed and span length will place the notches of isolation at the correct excitation frequencies.

Sections 4 and 5 present the analysis and response of such a system for the various load conditions and excitations selected for the investigation. Section 4 deals with a system with linear gains in the feedback networks; the finally selected system with nonlinear gains is discussed in Section 5.

SECTION 4: RESPONSE OF LINEAR FEEDBACK ACTIVE ISOLATION SYSTEM

Figure 16 shows schematic representations of the two configurations evaluated during the investigation. The first one consists of feedback control components isolating a rigid payload mass. The second one incorporates feedback control components to isolate a flexible payload represented as a rigid mass coupled to the active isolation system by a linear spring and a viscous damper in parallel.

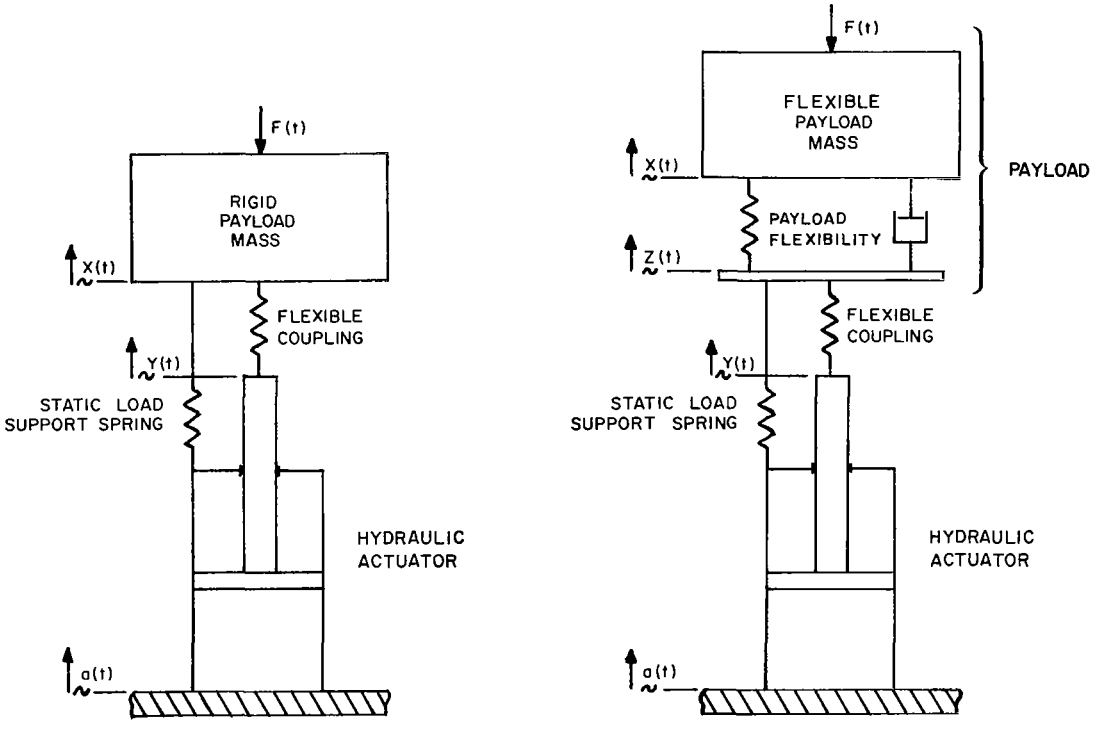

Figure 16. - Schematic diagram of actuator, static load support spring and flexible coupling with rigid and flexible payloads.

Rigid Payload

Description of Isolation System: A sketch of the components of the electrohydraulic vibration isolation system is shown in Figure 17. The design incorporates a static load support spring to carry the static weight of the payload, thus

allowing the use of a smaller diameter actuator and substantially reducing the flow and power requirements. The load support spring is a very slow acting feedback control system designed to carry the entire payload weight when the actuator is in its null or center position. This device consists of a fluidic actuator with integral force feedback such that the time average force applied to the actuator is zero (Appendix A). The force servo of the load support spring should have a very long time constant (in excess of 10 seconds) to minimize its flow and resulting power consumption. Therefore, the dynamics of the load support system may be neglected and the closed loop response of the entire isolation system can be calculated on the basis of representing the load support system as a linear spring (Appendix A).

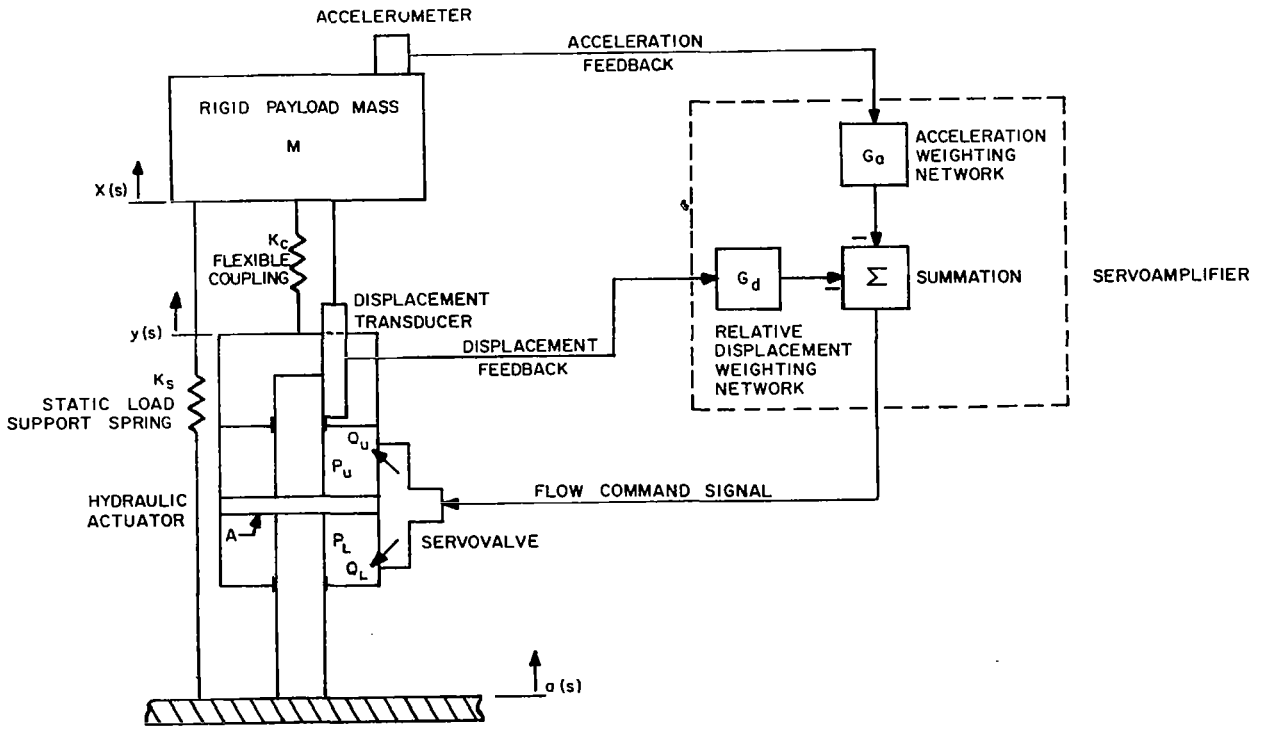

Figure 17. - Schematic diagram of electrohydraulic isolation system with rigid payload.

The hydraulic actuator consists of a double-acting, double-ended hydraulic cylinder rated for heavy duty operation at pressures up to 3000 psig. The actuator is coupled to the payload

through a passive undamped linear spring (flexible coupling), which is used both as a form of compensation required to stabilize the control system, and as a means of providing passive vibration isolation at frequencies above the bandwidth of the active portion of the electrohydraulic control system.

Two feedback transducers are used. A DC wideband accelerometer placed on the rigid payload mass senses the absolute acceleration of the payload mass. A linear displacement measurement device, such as a linear variable differential transformer, measures the relative displacement between the payload attachment point and the base excitation point.

The servoamplifier consists of electronic analog and digital components used to apply the proper weighting function on the two feedback signals as a function of excitation frequency and thereby generate the desired closed loop control functions. The output from the servoamplifier is fed to the torque motor of the servovalve.

The servovalve consists of an electric torque motor driving a single or double-stage hydraulic servomotor to locate the main valve spool in the desired position. The servovalve regulates the flow of hydraulic oil into and out of the upper and lower actuator chambers in proportion to the electrical command signal generated by the servoamplifier.

System Transfer Functions: In order to simplify the expressions for the system operation all of the equations presented in this section will be in the Laplace Operator Notation.

The flow $Q_u(s)$ out of the upper* actuator chamber is equal to the net actuator area, A, times the velocity of the actuator shaft relative to the cylinder walls, $\Delta_2(s) = Y(s) - a(s)$, less the quantity of oil stored by compression and the quantity of oil lost from leakage across the piston. Equation (1) presents

*The upper actuator chamber is defined as the one in which an increase of volume causes a downward motion of the payload.

the flow out of the upper actuator chamber, where s is the Laplace operator; V is the nominal volume of one of the actuator chambers; β is the bulk modulus of hydraulic oil; C_L is the leakage coefficient for the piston; $P_d(s)$ is the pressure drop across the piston where: $P_d(s) = P_L(s) - P_u(s)$; $P_L(s)$ is the pressure in the lower actuator chamber; and $P_u(s)$ is the pressure in the upper actuator chamber.

$$Q_u(s) = A\Delta_2(s)s + \frac{Vs}{\beta} P_u(s) - C_L P_d(s) \tag{1}$$

In the same manner, the flow of hydraulic oil into the lower actuator chamber is expressed as follows:

$$Q_L(s) = A\Delta_2(s)s - \frac{Vs}{\beta} P_L(s) - C_L P_d(s) \tag{2}$$

For a linear system analysis, the net flow to the system $Q_a(s)$ is taken as the average value of the flow to both the upper and lower actuator chambers

$$Q_a(s) = \frac{1}{2}\left[Q_u(s) + Q_L(s)\right] \tag{3}$$

The expression for the net flow output from the servovalve as a function of the actuator pressure drop and the relative velocity of the actuator shaft is given by

$$Q_a(s) = A\Delta_2(s)s - \left(\frac{Vs}{2\beta} + C_L\right)P_d(s) \tag{4}$$

The equation of motion for the rigid payload mass resting upon the flexible coupling is given by

$$Ms^2 X(s) + K_s\left[X(s) - a(s)\right] + K_c\left[X(s) - Y(s)\right] = 0 \tag{5}$$

where M is the mass of the rigid payload, K_s is the stiffness of the static load support spring, and K_c is the stiffness of

the flexible coupling. The actuator force output $F(s) = AP_d(s)$ is related to the system motions by the equation:

$$F(s) = K_c[X(s) - Y(s)] = AP_d(s) \tag{6}$$

The flow output from the servovalve $Q_v(s)$ is equal to the flow command signal from the servoamplifier weighted by the transfer function of the servovalve $G_{sv}(s)$. The flow command signal from the servoamplifier is composed of the summation of two signals: the first is the acceleration feedback signal $s^2X(s)$ weighted by a gain and shaping function $G_a(s)$; the second is the relative displacement signal $\Delta_1(s) = X(s) - a(s)$ also weighted by a gain and shaping function $G_d(s)$. Therefore, the flow command signal is given by:

$$Q_v(s) = -G_{sv}(s)\left[G_a(s)\ s^2\ X(s) + G_d(s)\ \Delta_1(s)\right] \tag{7}$$

The flow output from the servovalve $Q_v(s)$ is equal to the flow required by the actuator $Q_a(s)$ since there is no external leakage of hydraulic oil.

By combining equations (4) through (7) and setting $Q_v(s)$ equal to $Q_a(s)$, the solution for the system closed loop transfer function $X(s)/a(s)$ is formulated as shown below.

$$\frac{X(s)}{a(s)} = \frac{As\left(1 + \frac{K_s}{K_c}\right) + G_{sv}(s)G_d(s) + K_sA\left(\frac{Vs}{2\beta A^2} + \frac{C_L}{A^2}\right)}{As\left(1 + \frac{Ms^2 + K_s}{K_c}\right) + A\left(\frac{Vs}{2\beta A^2} + \frac{C_L}{A^2}\right)\left(Ms^2 + K_s\right) + G_{sv}(s)\left[G_a(s)\,s^2 + G_d(s)\right]} \tag{8}$$

The actuator stroke transfer function $\Delta_2(s)$ is calculated using equations (4) and (8).

$$\frac{\Delta_2(s)}{a(s)} = \frac{Q_v(s)}{As} - \frac{1}{s}\left\{Ms^2\ \frac{X(s)}{a(s)} + K_s\left[\frac{X(s)}{a(s)} - 1\right]\right\}\left(\frac{Vs}{2\beta A^2} + \frac{C_L}{A^2}\right) \tag{9}$$

The stability of the entire isolation system can be determined from the open loop transfer function of the electrohydraulic control system. The open loop transfer function $H(s)$ is obtained by setting the system excitation $a(s)$ to zero, opening the loop at the servovalve as shown on Figure 17 and replacing the valve output flow by a dummy flow term $V(s)$ at the actuator. The open loop transfer function is then equal to the ratio of the flow output of the servovalve $Q_v(s)$ to the dummy flow signal $V(s)$ and is given by

$$H(s) = \frac{1}{V(s)}\left[G_a(s)\ s^2\ X(s) + G_d(s)\ X(s)\right] G_{sv}(s) \tag{10}$$

The actuator response motions are related to the signal $V(s)$ through the expression [since $Q_v(s) = Q_a(s)$]:

$$V(s) = As\ Y(s) - \left(\frac{Vs}{2\beta} + C_L\right) P_d(s) \tag{11}$$

The expression for $X(s)$ as a function of $V(s)$ is obtained from equations (11) and (4) through (7) (with $a = 0$), and is given by

$$X(s) = \frac{Vs}{As\left(\frac{Ms^2 + K_s + K_c}{K_c}\right) + \left(\frac{Vs}{2\beta A} + \frac{C_L}{A}\right)\left(Ms^2 + K_s\right)} \tag{12}$$

Placing $X(s)$ of equation (12) into equation (10) gives the complete expression for the open loop transfer function.

$$H(s) = \frac{G_{sv}(s)\left[G_a(s)\ s^2 + G_d(s)\right]}{\frac{A}{K_c}\left[\left(Ms^2 + K_s + K_c\right)s + K_c\left(\frac{Vs}{2\beta A^2} + \frac{C_L}{A^2}\right)\left(Ms^2 + K_s\right)\right]} \tag{13}$$

Shaping Networks: The feedback control function $G_a(s)$ and $G_d(s)$ are generated by electronic weighting networks within the servoamplifier. The function $G_a(s)$ operates on the acceleration feedback signal to generate the principal control signal for active vibration isolation.

The acceleration weighting function consists of two basic types of circuits: a narrow-band high-gain network for the isolation of the sinusoidal vibration excitation, and a wide-band shaping network for the isolation of the broad-band vibration excitation. The basic narrow-band notch network consists of a second order undamped circuit, as shown in Figure 18, having the transfer function:

$$G(s)_{notch} = \frac{\omega_n^2}{s^2 + \omega_n^2} \tag{14}$$

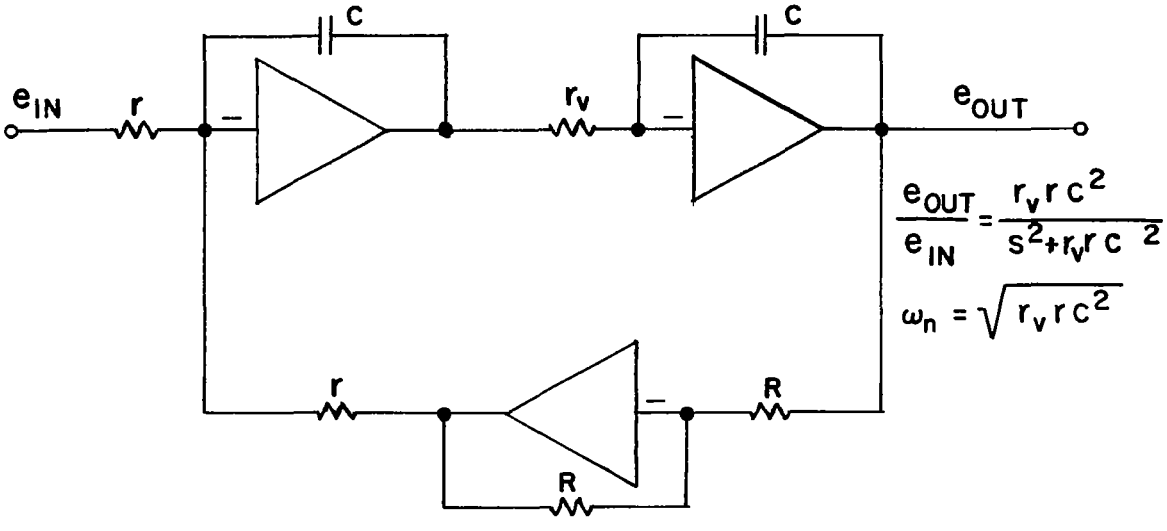

Figure 18. - Basic narrow-band notch circuit.

where ω_n represents both the resonant frequency of the circuit and the resulting notch frequency of the system. However, for the system under consideration, the frequency of sinusoidal excitation is not a constant and can vary from as low as 0.36 Hz to as high as 8.8 Hz. Figure 19 shows a modification of the notch circuit which enables the circuit to maintain the system notch frequency equal to the sinusoidal excitation frequency. Two analog multipliers are placed in the notch circuit as shown on the figure, and the multipliers are driven by a voltage proportional to the sinusoidal excitation frequency, $A_o\ \omega$. The transfer function for the tracking notch network, $G_{T\text{-notch}}(s)$, is given by

$$G_{T\text{-notch}}(s) = \frac{r_v r\ C^2\ A_o^2\ \omega^2}{s^2 + r_v r\ C^2\ A_o^2\ \omega^2} \qquad (15)$$

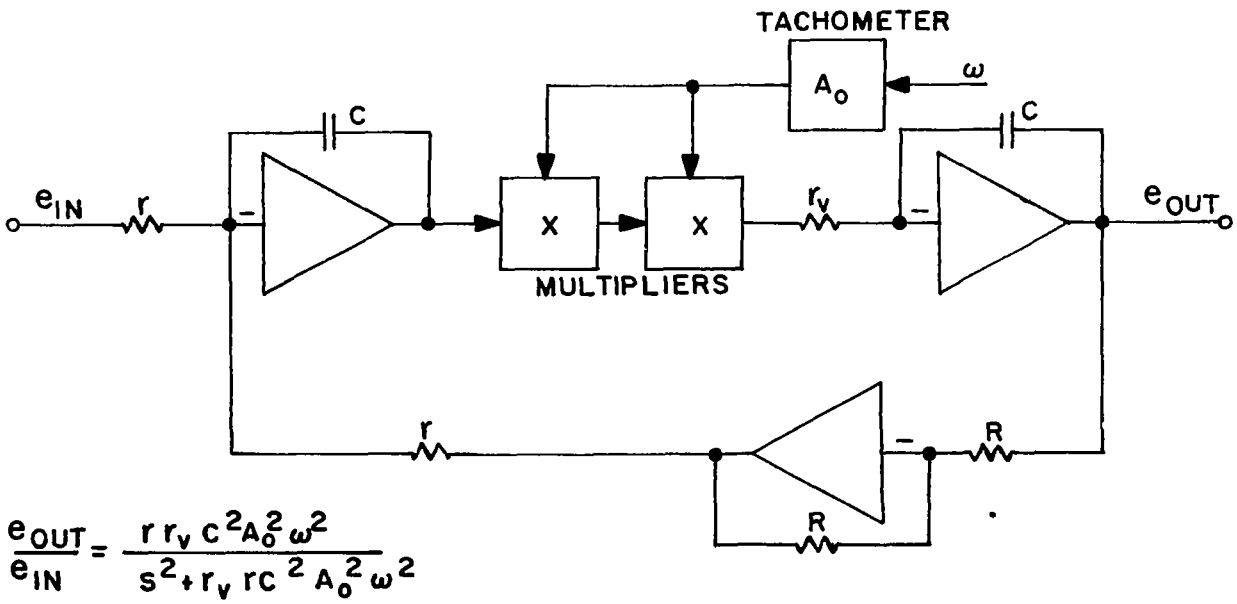

Figure 19. - Basic narrow-band tracking notch circuit.

Setting the frequency detector gain A_o equal to $\sqrt{1/r_v r\, C^2}$ results in a circuit which adapts its resonant frequency $\omega_n = \sqrt{r r_v C^2 A_o^2 \omega^2}$ to the excitation frequency ω. The resulting transfer function of the network with the frequency gain set as described above is:

$$G_{T\text{-notch}}(s) = \frac{\omega^2}{s^2 + \omega^2} \tag{16}$$

Use of such a tracking or adaptive notch circuit provides for the complete isolation of the sinusoidal excitation for frequencies within the tracking range of the circuit. This can be verified by replacing G_a in equation (8) with $G_{T\text{-notch}}(s)$ of equation (16) and letting $s = j\omega$. A digital study using equation (16) as the notch compensator and various functions for the wide-band acceleration compensation, indicated that the desired response could not be obtained for wide-band isolation due mainly to the 180° phase lag of the notch network at frequencies above its resonance. It is important, however, to maintain the notch mode of operation for isolation of the sinusoidal excitations, since only such a network can provide the very small transmissibilities desired using practical system gains.

The narrow-band compensation network used for the final parametric isolation analysis has the same magnitude response as the simple tracking notch of equations (14) and (16). However, by modulating the acceleration signal instead of directly weighting it, all phase information from the compensator is removed. Figure 20 shows a sketch of the phaseless notch (absolute notch) compensation network.

The absolute notch compensator operates in the following manner. The input signal e_{in} feeds into the tracking notch circuit as shown in Figure 20. The output of the notch circuit is then rectified by a precision full-wave rectifier, and the signal is then smoothed and averaged by a lag network. The resulting signal is an output DC voltage, which is equal to the average value of a fully rectified sine wave [i.e., $e_1(2/\pi)$] plus a low amplitud

ripple voltage at twice the excitation frequency. The ripple voltage amplitude is controlled by the time constant of a lag network set to give a ripple voltage of 10 percent of the DC average voltage $e_1(2/\pi)$ peak-to-peak for the worst case. The input voltage e_{in} is then modulated by a multiplier which is, in turn, driven by the output of the smoothing and averaging circuit. The resulting transfer function for the absolute notch network using the simple notch network of Figure 19 is given by

$$G_{A\text{-notch}}(s) = \frac{\omega_n^2}{|s^2 + \omega_n^2|} \tag{17}$$

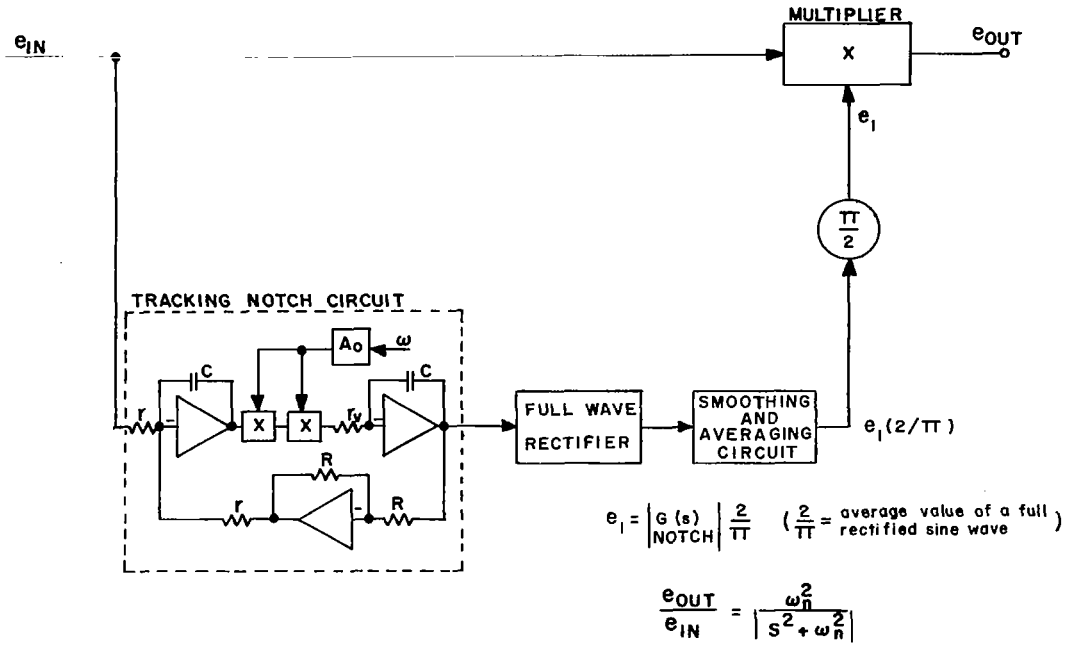

Figure 20. - Absolute narrow-band tracking notch circuit.

The compensation function of Equation (17) has a magnitude response which is identical to the simple notch compensator, but the phase angle of the network's transfer function is always zero. The zero phase lag of this type of notch compensator aids greatly in obtaining the desired system closed loop response. Therefore, the basic narrow-band shaping network in the parametric analysis uses the absolute notch network weighted by various gains

and compensation functions contained in the term $G_{NC}(s)$, and is given by

$$G(s)_{notch} = \frac{\omega_n^2}{|s^2 + \omega_n^2|} G(s)_{NC} \tag{18}$$

The isolation of the broad-band vibration excitation requires a wide-band linear gain term C_a, and a linear shaping network. The entire acceleration feedback network consists of the summation of the weighted wide-band and narrow-band network functions weighted in turn by additional shaping and compensation functions found essential by initial parametric search techniques. The acceleration feedback weighting function is given by

$$G_a(s) = \left(\frac{\tau_1 s}{1+\tau_1 s}\right)\left(\frac{1+\alpha_3\tau_3 s}{1+\tau_3 s}\right)\left[C_a\left(\frac{1+\alpha_2\tau_2 s}{1+\tau_2 s}\right) + K_a\omega_n\left(\frac{\omega_n^2}{|s^2+\omega_n^2|}\right)\left(\frac{\tau_5 s}{1+\tau_5 s}\right)\right] \tag{19}$$

The lead network having the transfer function $\frac{\tau_1 s}{1+\tau_1 s}$ is used to lower the gain of the entire acceleration feedback loop to zero at zero frequency. It can be shown that static system deflections resulting from sustained acceleration loading (such as gravity) can thus be eliminated [Ref. 7]. Improved resonance characteristics of the closed loop servo system can also be attained [Ref. 7]. The leak-lag network having the transfer function $\frac{1+\alpha_2\tau_2 s}{1+\tau_2 s}$, $(\alpha_2 > 1)$, in conjunction with the lead-lag network having the transfer function $\frac{1+\alpha_3\tau_3 s}{1+\tau_3 s}$, $(\alpha_3 < 1)$, forms a lead-lag, lag-lead network which enables the closed loop transmissibility of the electrohydraulic vibration isolation system to attenuate at a rate of 12 db per octave between the frequencies of 1 and 10 Hz for wide-band operation alone. The parameters C_a and K_a represent the acceleration static feedback flow gains for wide-band and narrow-band operational networks, respectively.

The lead network having the transfer function $\frac{\tau_5 s}{1+\tau_5 s}$ is used to lower the static loop gain of the narrow-band network at low frequencies. This lead network has a time constant inversely proportional to the resonant frequency of the notch network, $\tau_5 = \frac{1}{a\omega_n}$. The term $a\omega_n$ represents a gain which increases proportionally to the resonant frequency of the narrow-band notch network. The term "a" is a constant and ω_n is equal to the resonant frequency of the notch circuit. The gain adjustment proportional to frequency is required to adjust the bandwidth of the notch of isolation such that a reasonably wide bandwidth is provided at the level of sinusoidal transmissibility desired. The transfer function $\left| \frac{\omega^2 n}{s^2+\omega_n^2} \right|$ represents the absolute notch network described in previous paragraphs. Therefore, this network maintains nearly constant low frequency characteristics of the entire narrow-band network for all notch frequencies, and thereby provides for nearly constant resonant frequency characteristics in all cases.

The weighting function operating on the relative displacement feedback signal is given by

$$G_d(s) = \left(C_d + C_v s\right)\left(\frac{1}{1+\tau_4 s}\right)\left(\frac{1+\alpha_3 \tau_3 s}{1+\tau_3 s}\right) \qquad (20)$$

and consists of the relative flow gains C_d and C_v for relative displacement and relative velocity feedback respectively. The lag network having the transfer function $(\frac{1}{1+\tau_4 s})$ and the lag-lead network having the transfer function $(\frac{1+\alpha_3 \tau_3 s}{1+\alpha_3 s})$ are used to attenuate the relative feedback flow gains at high frequencies in order to obtain the desired high-frequency attenuation rate and a more stable system.

Dynamic Characteristics of Components: In order to calculate the response of the active isolation system, it is necessary to size the various components and estimate their dynamic response characteristics.

The actuator area is determined by the peak force which the actuator must deliver and the pressure drop across the actuator. The peak force is set equal to the total expected force applied to the actuator during operation; namely, the force exerted by the static load support spring when the actuator is in its extreme stroke positions; and the step transient force of one-half the nominal payload weight. The payload is isolated from vibrations, resulting in minimal steady-state dynamic loading of the actuator due to accelerations of the payload. Therefore, since the static load support system carries all sustained loads, no other significant forces are carried by the actuator.

The static load support spring consists of an active element having pressure feedback with a long time constant, such that zero static load is carried by the actuator. For the analysis, the support spring is considered as a linear spring having a stiffness $K_s = 0.1 \left(\frac{\text{weight}}{\text{stroke}}\right)$. The peak force generated by the spring is then equal to 10 percent of the payload weight, and it occurs at the full stroke position of the actuator. Since the static load support spring cannot react to sudden applied sources, the entire force loading of the step transient (i.e., one-half the nominal payload weight) will be carried by the actuator. Therefore, the total required peak force output of the actuator is equal to six tenths of the payload weight.

The selected actuator dimensions conform to Standard JIC specifications for heavy duty hydraulic cylinders. In some instances, oversize shaft diameters were selected in order to obtain the desired actuation area. The net actuation area for the 1000 pound payload was calculated as follows. The peak force loading applied to the actuator is equal to 600 pounds (500 pounds from the

transient force and 100 pounds from the static load support spring). The maximum pressure drop across the actuator piston is 2,000 psid, since the maximum supply pressure is 3,000 psi and a 1,000 psid drop is required across the servovalve. Therefore, the minimum actuator area which could be used for this case is equal to the peak load supported by the actuator (600 pounds) divided by the maximum pressure drop across the piston (2,000 psid), or $A_{min} = \frac{600 \text{ lb}}{2{,}000 \text{ lb/in}^2} = 0.3 \text{ in}^2$.

The minimum area calculated above is very small and probably could not be obtained in a practical design. Therefore, the area for the 1,000 lb. payload was selected on the basis of using the smallest JIC cylinder bore diameter and the largest practical diameter for the shaft. A cylinder having a 1-1/2 inch bore diameter and an oversize shaft having a diameter of 1-1/8 inches was chosen, resulting in a net actuation area of 0.673 in^2. The maximum pressure drop across the piston is equal to the peak load supported by the actuator (600 pounds) divided by the net actuation area (0.673 in^2), or 891.5 psig. Allowing for a 1,000 psi pressure drop across the valve, the system supply pressure was decreased to 1,890 psig.

The net actuation areas and supply pressures for the 3,000 and 10,000 pound payloads were calculated in the same manner. Results are shown on Table IV.

The stroke length of the hydraulic actuators were estimated based on the maximum displacement expected during vibratory and transient excitations. The relative transmissibility of the selected electrohydraulic isolation system over the frequency range from 0.37 to 45 Hz, is approximately 1. The maximum relative displacement between the payload and the air cushion is, therefore, equal to the summation of the displacements associated with the vibratory excitations and the deflections due to the transient step force at the payload. For the worst conditions, isolation of the sinusoidal excitation requires ±3.0 inches of travel. Based on the equivalent broad-band excitations, the 3σ displacement required

for isolation of the random excitations is ±0.65 inches. If ±2.35 inches are allowed for displacement due to transient excitations, then the total expected displacement of the actuator from its null position due to the combined excitations would be within the desired ±6 inches. As a safety provision, the actuators incorporate end cushions which require approximately one inch of displacement. Therefore, the actuator dynamic response for all cases is based on a total stroke of ±7 inches. Table IV lists a summary of the actuator characteristics for the three payload weights considered.

TABLE IV

SYSTEM SUPPLY PRESSURES AND ACTUATOR CHARACTERISTICS

Payload Weight	1,000 lb	3,000 lb	10,000 lb
Maximum Load	600 lb	1,800 lb	6,000 lb
Required Supply Pressure (P_s)	1892 psi	2833 psi	3000 psi
Required Pressure Drop (P_d)	891.5 psi	1883 psi	2005.3 psi
Minimum Net Area	0.3 $in.^2$	0.9 $in.^2$	3.0 $in.^2$
Bore Diameter	1.5 in.	1.5 in.	2.5 in.
Shaft Diameter	1.125 in.	1.00 in.	1.5625 in.
Net Actuation Area (A)	0.673 $in.^2$	0.982 $in.^2$	2.992 $in.^2$
Total Stroke (2L)	14.0 in.	14.0 in.	14.0 in.
Nominal Chamber Volume (V)	4.7 $in.^3$	6.9 $in.^3$	21 $in.^3$
Nominal Stiffness = $\frac{2\beta A^2}{V}$	38,457 lb/in.	56,114 lb/in.	170,971 lb/in.
Resonant Frequency = $\sqrt{\frac{2\beta A^2 g}{VW}}$	20 Hz	13.5 Hz	12.9 Hz
Percent of Critical Damping = $\frac{C_L W}{Ag}$	5	5	5

The actuator stiffness and natural frequency values shown in Table IV are based on a bulk modulus of hydraulic oil of $\beta = 200{,}000$ lb/in^2. The leakage coefficient is assumed to be $C_L = 1 \frac{(in^3/sec)}{(lb/in^2)}$

As indicated in Table IV the natural frequencies of the actuators range from approximately 13 to 20 Hz. Therefore, to maintain reasonable margins of stability, the broad-band shaping networks must attenuate the flow gains such that from approximately 10 Hz on, vibration isolation is provided by the flexible coupling only. The transmissibility requirements at frequencies higher than approximately 5 Hz can be met by introducing undamped flexible couplings within the active loop having natural frequencies of 2.5 Hz for the 1,000 lb. payload, and 2 Hz for the 3,000 and 10,000 lb. payloads.

The peak flow output from the servovalve for steady-state vibration isolation is estimated by the product of the net actuation area and the total peak excitation velocity. The peak excitation velocity for discrete frequency excitation occurs at 9 Hz (Figure 1) and is equal to 84 in/sec. The peak excitation velocity for the broad-band sinusoidal equivalent to random excitation occurs at a speed of 300 miles per hour and has an RMS magnitude of 6.335 inches per second. Frequencies above 10 cycles per second are not included in this calculation since, as mentioned in the previous paragraph, the servo gain should attenuate flow demands at higher frequencies. The total peak velocity is taken as the summation of the peak velocity due to discrete excitations and the 3σ magnitude of the equivalent broad-band velocity, and is equal to 103 in/sec. Table V lists the flow requirements of the servovalve, the valve type and its dynamic characteristics for each of the three payload weights selected. Valve characteristics were obtained from the manufacturer's catalog. In all cases, the valves are represented by a second order system.

TABLE V

ESTIMATED SERVOVALVE FLOW REQUIREMENTS

Payload Weight	1,000 lb	3,000 lb	10,000 lb
Required Peak Flow	69 in^3/sec	101 in^3/sec	308 in^3/sec
Servovalve (Moog Type)	35 (2-stage)	72 (2-stage)	79 (3-stage)
Maximum Available Flow @ 1000 psid	79 in^3/sec	231 in^3/sec	539 in^3/sec
Resonant Frequency (f_{sv})	100 Hz	63 Hz	90 Hz
Fraction of Critical Damping (ζ_{sv})	0.7	0.7	0.5

The accelerometers are represented by a second order system having a resonant frequency of 1000 Hz and a damping ratio of 0.10. The type selected is Kistler Type 305-A servoaccelerometer capable of responding from DC to frequencies above those of interest. The relative displacement signal is generated by a differential transformer having a transfer function equal to unity over the frequency range of interest.

Response to Vibratory Excitations: The system response to vibratory excitations was calculated using a digital computer program developed for the CDC 3600 time sharing computer. A listing of the program is shown in Appendix B.

Solutions were obtained using various values of gain for each of the feedback signals and for the time constants associated with the shaping networks. For each payload weight, values were selected from those initially tried in order to obtain the desired isolation characteristics while maintaining acceptable margins of system stability.

The response of the selected system is shown in terms of absolute and relative transmissibility curves as a function of

frequency. The absolute transmissibility $T_A(s)$ is given by Equation (8). The relative transmissibility $T_R(s) = T_A(s) - 1$. In addition, values of valve flow and actuator stroke were calculated from Equations (7) and (9), respectively. A separate computer program was used for automatic plotting of the system frequency response.

The magnitude and phase margins of the system open loop transfer function were calculated from Equation (13) using the CDC 3600 time sharing digital computer.

Results for 1,000 lb Payload

The system parameters for the 1,000 lb rigid payload are shown in Table VI. The gain of the notch network τ_s is set equal to $1/\omega_n$ where ω_n is the notch frequency corresponding to the discrete frequency excitation.

Figures 21 and 22 show the closed loop frequency response of the active system with 1,000 lb rigid payload for the eight values of notch frequency. The absolute transmissibility curves T_A indicate the vibration isolation provided by the system at each frequency. The degree of isolation attained at each notch frequency is well within the desired values for discrete frequency excitations listed in Table III. The minimum notch bandwidth at the desired level of isolation is 5 percent.

The desired levels of transmissibility for wide-band excitation, previously defined in Figures 6 and 7, are shown as dashed lines. In all cases, except for a notch frequency of 2.20 Hz (speed = 300 mph; span length: 200 ft.), the desired transmissibility requirements are met. For broad-band excitation associated with the 2.20 Hz discrete frequency, the calculated transmissibility exceeds the desired levels in the range from 2.5 to 10 Hz. The maximum deviation is approximately 17.5 percent at 7.5 Hz. The higher than desired values of transmissibility are due to the fact that the flexible coupling resonant frequency (2.5 Hz) coincides with this particular discrete excitation

TABLE VI

SYSTEM PARAMETERS FOR RIGID 1000 lb PAYLOAD

Parameter	Magnitude	Units
Payload Weight, W	1,000	lb
Payload Mass, M	2.5906	lb sec^2/in.
Load Support Spring Stiffness, K_s	14.29	lb/in.
Flexible Coupling Spring Stiffness, K_c	639.22	lb/in.
Servovalve Resonant Frequency, ω_{sv}	628.3	rad/sec
Servovalve Fraction of Critical Damping, ζ_{sv}	0.7	dimensionless
Net Actuation Area, A	0.673	$in.^2$
Bulk Modulus of Oil, β	200,000	lb/$in.^2$
Nominal Chamber Volume, V	4.711	$in.^3$
Piston Leakage Coefficient, C_L	0.000266	($in.^3$/sec)/(lb/$in.^2$)
Wide-band Acceleration Gain, C_a	0.337	($in.^3$/sec)/(in./sec^2)
Narrow-band Acceleration Gain, K_a	0.1343	($in.^3$/sec)/(in./sec^2)
Relative Displacement Gain, C_d	0.387	($in.^3$/sec)/(in.)
Relative Velocity Gain, C_v	0.202	($in.^3$/sec)/(in./sec)
Time Constants		
Acceleration, τ_1	8.63	sec.
Shaping, τ_2	0.053	sec.
Compensation, τ_3	0.053	sec.
Compensation, τ_4	1.27	sec
Shaping, τ_5	$1/\omega_n$	sec.
Constants		
Shaping, α_2	7.10	dimensionless
Compensation, α_3	0.24	dimensionless
Shaping, a	0.39788	dimensionless

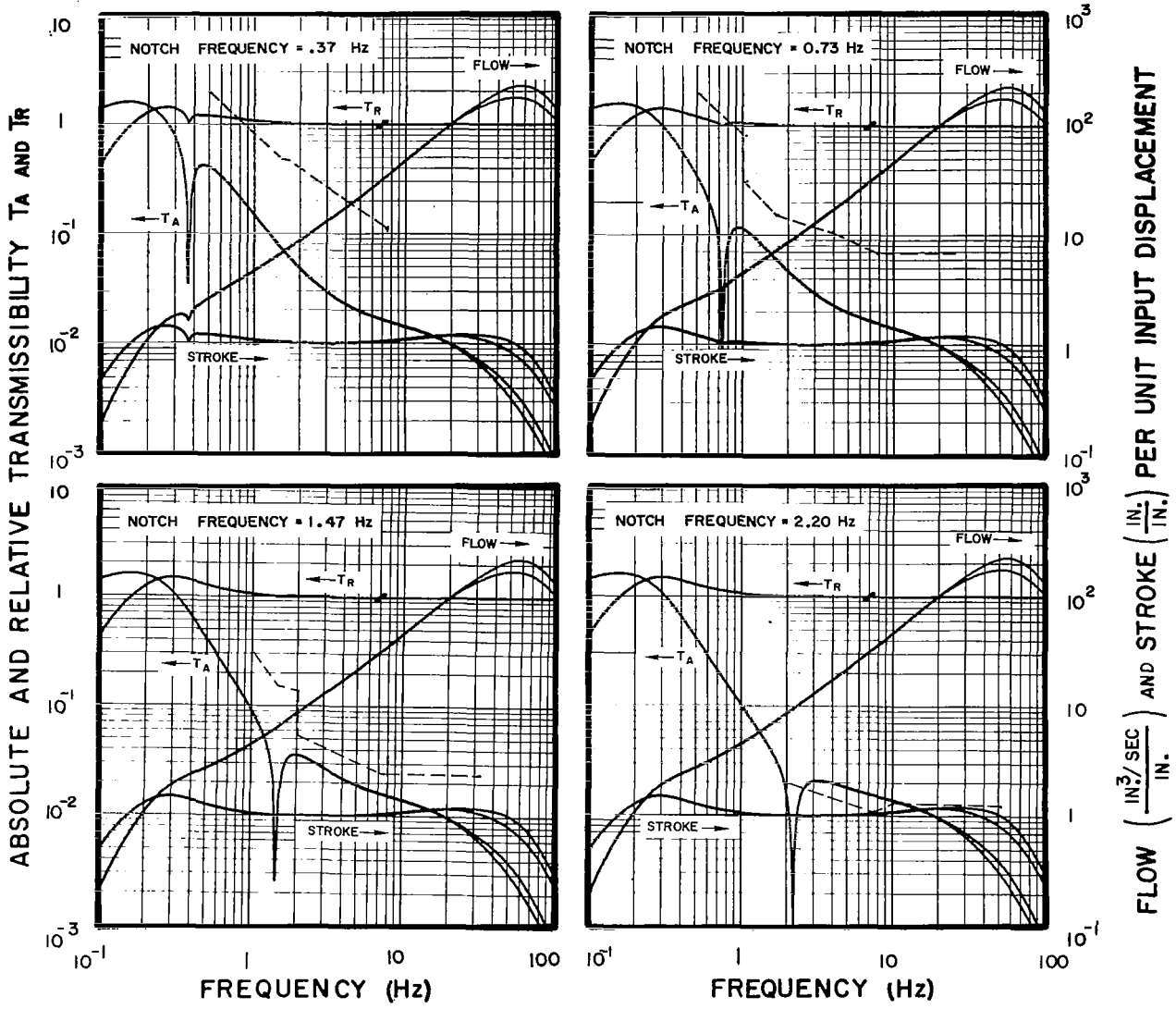

AT LOW FREQUENCIES, EACH CURVE APPLIES TO BOTH NOMINAL PAYLOAD AND A 20% INCREASE IN PAYLOAD. AT HIGH FREQUENCIES, THE UPPER CURVES APPLY TO THE NOMINAL WEIGHT AND THE LOWER CURVES TO THE INCREASED WEIGHT.

DASHED LINE REPRESENTS MAXIMUM ALLOWABLE ABSOLUTE TRANSMISSIBILITY FOR RANDOM INPUTS.

Figure 21. - System absolute and relative transmissibility, valve flow, and actuator stroke for 1,000 lb rigid payload. Notch frequencies: 0.37, 0.73, 1.47 and 2.20 Hz.

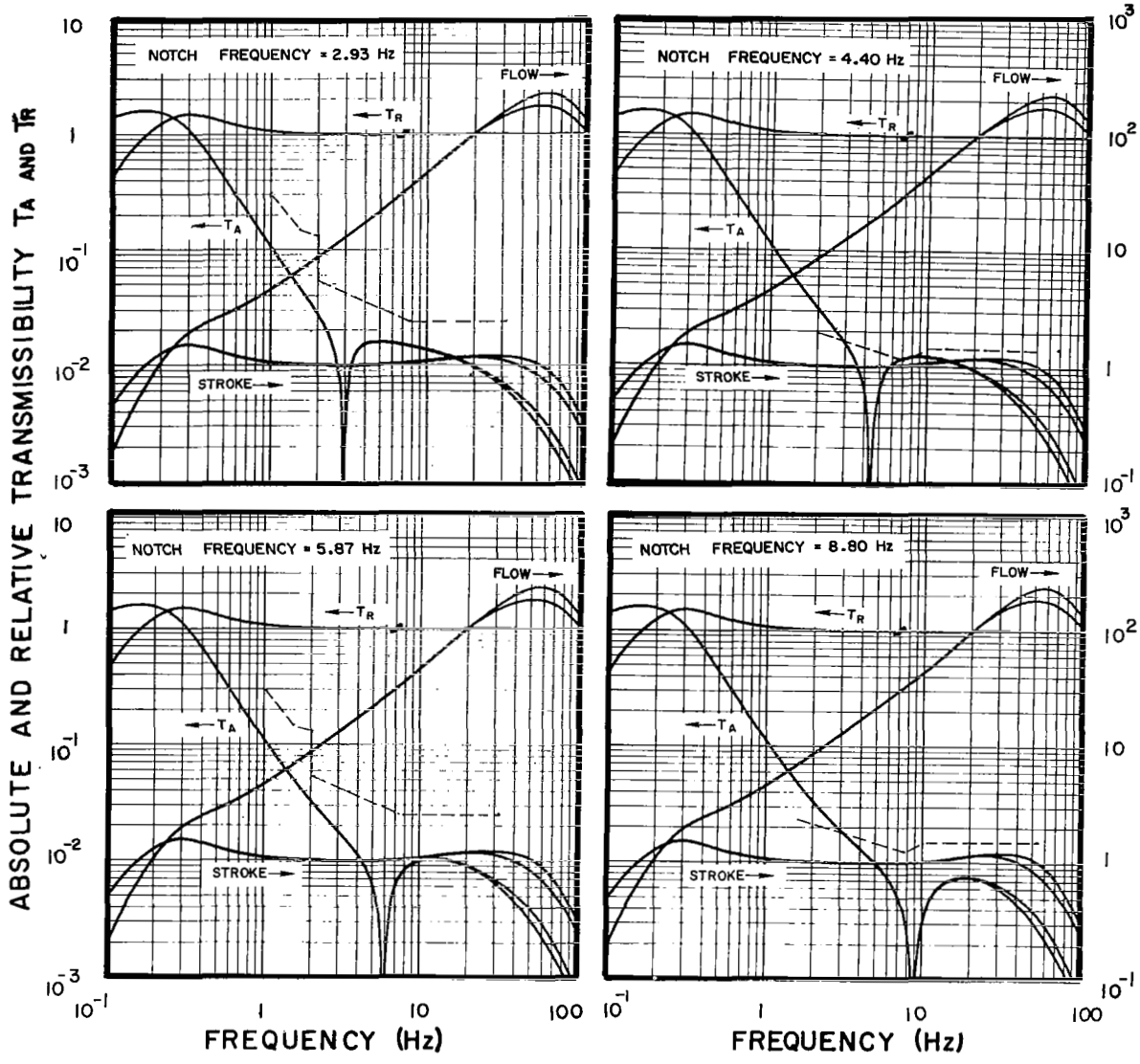

AT LOW FREQUENCIES, EACH CURVE APPLIES TO BOTH NOMINAL PAYLOAD AND A 20% INCREASE IN PAYLOAD. AT HIGH FREQUENCIES, THE UPPER CURVES APPLY TO THE NOMINAL WEIGHT AND THE LOWER CURVES TO THE INCREASED WEIGHT.

DASHED LINE REPRESENTS MAXIMUM ALLOWABLE ABSOLUTE TRANSMISSIBILITY FOR RANDOM INPUTS.

Figure 22. - System absolute and relative transmissibility, valve flow, and actuator stroke for 1,000 lb rigid payload. Notch frequencies: 2.93, 4.40, 5.87 and 8.80 Hz.

frequency. In the selection of gains for the 1,000 lb system, an attempt was made to arrive at the best performance for all conditions. Although a better performance than that shown for the 2.20 Hz notch could be obtained by selecting different values of gains, a deterioration in vibration isolation and a decrease in margins of stability would have resulted for the remaining notch frequencies.

The relative transmissibility curves (T_R) show that the relative displacement between the payload and the source of excitation is equal to the displacement excitation over the frequency range from 0.37 to 44 Hz. The curve labeled "stroke" represents the displacement of the piston within the actuator. The piston relative displacement (stroke) is approximately equal to 1 over the frequency range of interest. Above 10 Hz, the piston relative displacement (stroke) is higher than the payload relative displacement (T_R) since the cylinder must compensate for the deflections of the coupling. However, above 10 Hz, the excitation is considered to be random. Therefore, the rms displacement of the actuator piston would be approximately the same as the excitation rms displacement. Finally, the required servovalve flow as a function of frequency is shown for each case.

The effect of increasing the payload weight by 20 percent is indicated in each case. In the frequency range where the active portion controls the response of the system (< 20 Hz), increasing the payload weight has no effect on the system response. Above 20 Hz, the response is controlled primarily by the dynamics of the flexible coupling and of the actuator, since the valve flow gains are lagged. Increasing the payload weight reduces the flexible coupling resonant frequency and results in lower transmissibility values and reduced flow requirements at high frequencies.

Values of system open loop gain magnitude and phase margins and the crossover frequencies at which they occur are listed on Table VII for the rigid 1,000 lb nominal payload and for a payload

weight increase of 20 percent. For the 1,000 lb payload, the margins are approximately 11.5 db and 50 degrees for the gain magnitude and phase, respectively. Increasing the payload weight by 20 percent results in higher values of stability margins due to the decrease in flexible coupling and actuator resonant frequencies.

TABLE VII

OPEN LOOP GAIN MAGNITUDE AND PHASE MARGINS

FOR RIGID 1,000 LB PAYLOAD

Payload Weight (lb)	Notch Frequency (Hz)	Phase		Gain	
		Crossover Frequency (Hz)	Margin (degrees)	Crossover Frequency (Hz)	Margin (db)
1000	0.37	34.79	50.53	95.14	-11.65
	0.73	34.79	50.53	95.14	-11.65
	1.47	34.80	50.53	95.14	-11.65
	2.20	34.83	50.51	95.14	-11.65
	2.93	34.88	50.48	95.14	-11.65
	4.40	35.09	50.37	95.14	-11.64
	5.87	35.49	50.21	95.14	-11.62
	8.80	36.99	49.74	95.19	-11.57
1200	0.37	29.63	53.57	95.14	-13.23
	0.73	29.63	53.57	95.14	-13.23
	1.47	29.65	53.56	95.14	-13.23
	2.20	29.68	53.54	95.14	-13.23
	2.93	29.74	53.51	95.14	-13.23
	4.40	29.97	53.43	95.14	-13.22
	5.87	30.44	53.31	95.14	-13.21
	8.80	32.09	53.13	95.19	-13.15

Results for 3,000 lb Payload

The system parameters selected for the 3,000 lb payload weight are shown in Table VIII.

TABLE VIII

SYSTEM PARAMETERS FOR 3000 lb RIGID PAYLOAD

Parameter	Magnitude	Units
Payload Weight, W	3,000	lb
Payload Mass, M	7.772	lb sec^2/in.
Load Support Spring Stiffness, K_s	42.87	lb/in.
Flexible Coupling Spring Stiffness, K_c	1227.3	lb/in.
Servovalve Resonant Frequency, ω_{sv}	395.8	rad/sec
Servovalve Fraction of Critical Damping, ζ_{sv}	0.7	dimensionless
Net Actuator Area, A	0.982	$in.^2$
Bulk Modulus of Oil, β	200,000	$lb/in.^2$
Nominal Chamber Volume, V	6.874	$in.^3$
Piston Leakage Coefficient, C_L	0.000266	$(in.^3/sec)/(lb/in.^3)$
Wide-band Acceleration Gain, C_a	0.491	$(in.^3/sec)/(in./sec^2)$
Narrow-band Acceleration Gain, K_a	0.196	$(in.^3/sec)/(in./sec^2)$
Relative Displacement Gain, C_d	0.566	$(in.^3/sec)/(in.)$
Relative Velocity Gain, C_4	0.295	$(in.^3/sec)/(in./sec)$
Time Constants		
Acceleration, τ_1	8.63	sec
Shaping, τ_2	0.053	sec
Compensation, τ_3	0.053	sec
Compensation, τ_4	1.27	sec
Shaping, τ_5	$1/\omega_n$	sec
Constants		
Shaping, α_2	7.10	dimensionless
Compensation, α_3	0.24	dimensionless
Shaping, a	0.39788	dimensionless

Figures 23 and 24 show the frequency response of the 3,000 lb rigid payload. As for the case of the 1,000 lb payload, the isolation provided at the notch frequencies is well within the desired levels shown on Table III. The minimum notch bandwidth at the desired level is 4.8 percent. For the broad-band excitations, the isolation attained is within the desired levels except the case associated with the 2.2 Hz discrete frequency excitation. As for the 1,000 lb payload the interaction between the notch at this frequency and the flexible coupling resonant frequency (2.0 Hz) negates lowering the transmissibility values between 2.5 and 10 Hz. A comparison between the low frequency response of the 3,000 lb payload (Figures 23 and 24) and of the 1,000 lb payload (Figures 21 and 22) indicates that in all cases the relative and absolute transmissibilities and stroke are the same. In this frequency range the response is controlled by the active portion of the system and, since, the gains and compensation are identical, the response should be the same. The flow requirements are, as expected, proportionally higher for the 3,000 lb payload, since a larger area actuator is used.

Above 10 Hz, the response is controlled primarily by the dynamics of the flexible coupling and actuator. The absolute transmissibility values are lower for the 3,000 lb payload than for the 1,000 lb payload due to lower coupling and actuator resonant frequencies (2.0 and 13.5 Hz, respectively).

The effect of increasing the payload of the 3,000 lb system by 20 percent is similar to the one shown for the 1,000 lb system.

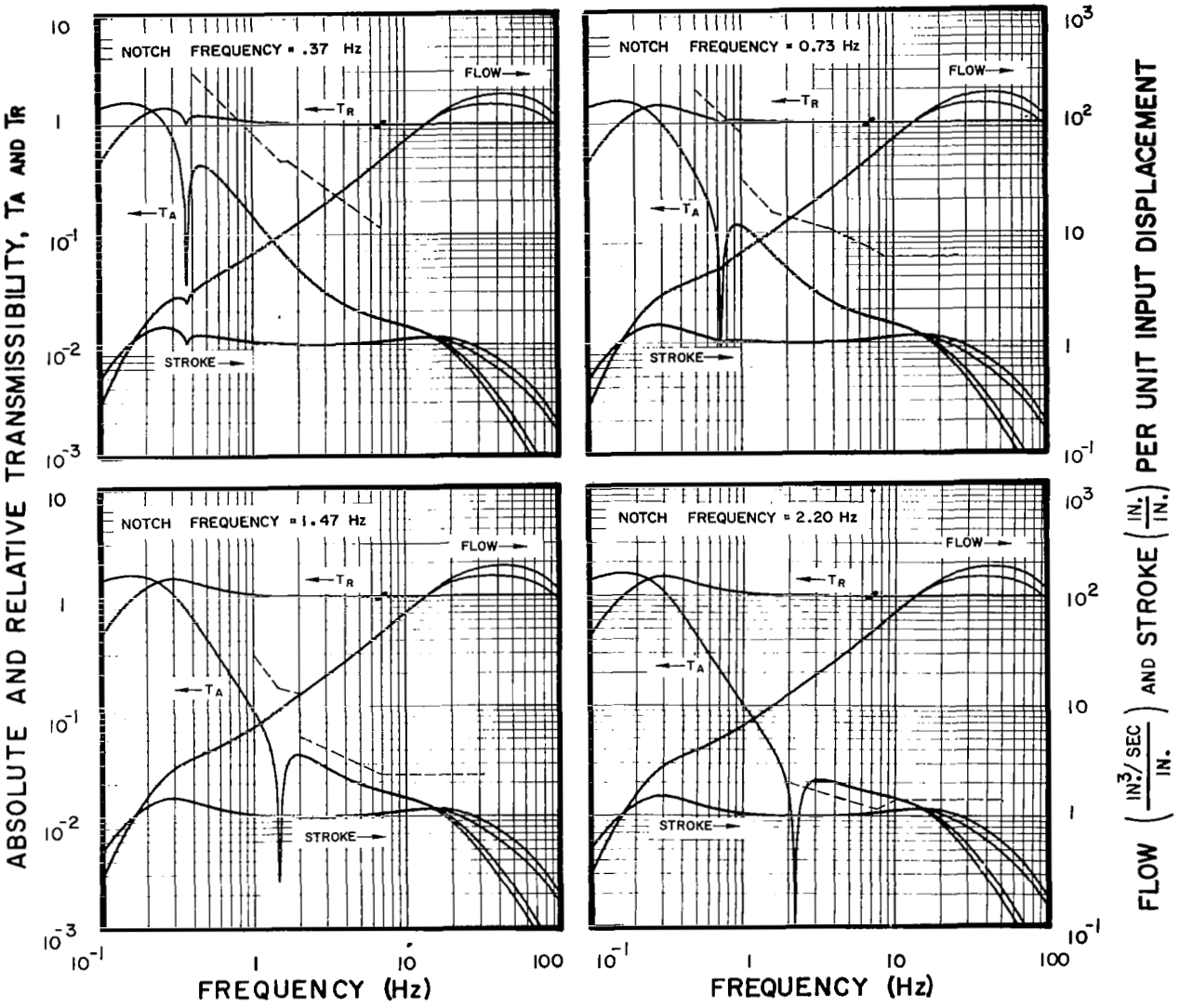

AT LOW FREQUENCIES, EACH CURVE APPLIES TO BOTH NOMINAL PAYLOAD AND A 20% INCREASE IN PAYLOAD. AT HIGH FREQUENCIES, THE UPPER CURVES APPLY TO THE NOMINAL WEIGHT AND THE LOWER CURVES TO THE INCREASED WEIGHT.

DASHED LINE REPRESENTS MAXIMUM ALLOWABLE ABSOLUTE TRANSMISSIBILITY FOR RANDOM INPUTS.

Figure 23. - System absolute and relative transmissibility, valve flow, and actuator stroke for 3,000 lb rigid payload. Notch frequencies: 0.37, 0.73, 1.47 and 2.20 Hz.

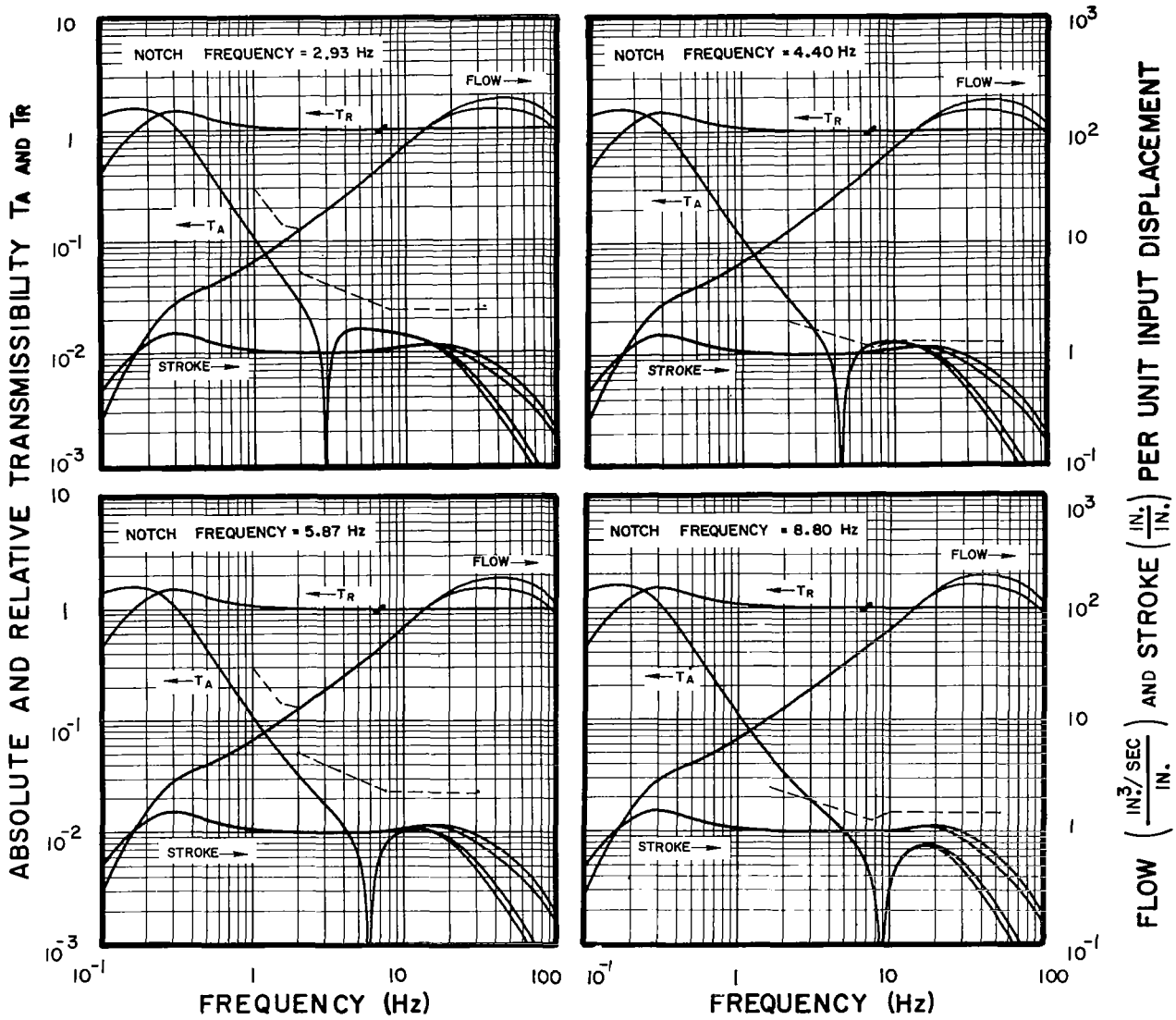

AT LOW FREQUENCIES, EACH CURVE APPLIES TO BOTH NOMINAL PAYLOAD AND A 20% INCREASE IN PAYLOAD. AT HIGH FREQUENCIES, THE UPPER CURVES APPLY TO THE NOMINAL WEIGHT AND THE LOWER CURVES TO THE INCREASED WEIGHT.

DASHED LINE REPRESENTS MAXIMUM ALLOWABLE ABSOLUTE TRANSMISSIBILITY FOR RANDOM INPUTS.

Figure 24. - System absolute and relative transmissibility, valve flow, and actuator stroke for 3,000 lb rigid payload. Notch frequencies: 2.93, 4.40, 5.87 and 8.80 Hz.

The open loop gain magnitude and phase margins and the cross-over frequencies at which they occur are shown on Table IX. For this payload, the margins are approximately 56 degrees and 15 db for the phase and gain magnitude, respectively. The values are higher than those for the 1,000 lb payload (Table VII). The lower resonant frequencies of the flexible coupling and actuator used with the 3,000 lb payload result in a more stable system.

TABLE IX

OPEN LOOP GAIN MAGNITUDE AND PHASE MARGINS

FOR RIGID 3,000 LB PAYLOAD

Payload Weight (lb)	Notch Frequency (Hz)	Phase		Gain	
		Crossover Frequency (Hz)	Margin (degrees)	Crossover Frequency (Hz)	Margin (db)
3,000	0.37	23.56	56.46	95.13	-15.57
	0.73	23.56	56.46	95.13	-15.57
	1.47	23.58	56.45	95.13	-15.57
	2.20	23.61	56.44	95.13	-15.57
	2.93	23.68	56.42	95.13	-15.57
	4.40	23.96	56.38	95.13	-15.56
	5.87	24.52	56.41	95.14	-15.55
	8.80	26.40	56.85	95.18	-15.49
3,600	0.37	20.29	57.69	95.13	-17.16
	0.73	20.29	57.69	95.13	-17.16
	1.47	20.30	57.68	95.13	-17.15
	2.20	20.35	57.67	95.13	-17.15
	2.93	20.43	57.65	95.13	-17.15
	4.40	20.77	57.66	95.13	-17.14
	5.87	21.36	57.84	95.14	-17.13
	8.80	23.37	58.85	95.18	-17.07

Results for 10,000 lb Payload

The system parameters selected for the 10,000 lb payload weight are shown in Table X.

TABLE X

SYSTEM PARAMETERS FOR 10,000 LB PAYLOAD

Parameter	Magnitude	Units
Payload Weight, W	10,000	lb
Payload Mass, M	25.907	lb sec^2/in.
Load Support Spring Stiffness, K_s	142.86	lb/in.
Flexible Coupling Spring Stiffness, K_c	4091.06	lb/in.
Servovalve Resonant Frequency, ω_{sv}	565.49	rad/sec
Servovalve Fraction of Critical Damping, ζ_{sv}	0.5	dimensionless
Net Actuator Area, A	2.992	$in.^2$
Bulk Modulus of Oil, β	200,000	lb/$in.^2$
Nominal Chamber Volume, V	20.944	$in.^3$
Piston Leakage Coefficient, C_L	0.000266	($in.^3$/sec)/(lb/$in.^2$)
Wide-band Acceleration Gain, C_a	1.495	($in.^3$/sec)/(in./sec^2)
Narrow-band Acceleration Gain, K_a	0.599	($in.^3$/sec)/(in./sec^2)
Relative Displacement Gain, C_d	1.725	($in.^3$/sec)/(in.)
Relative Velocity Gain, C_v	0.899	($in.^3$/sec)/(in./sec)
Time Constants		
Acceleration, τ_1	8.63	sec
Shaping, τ_2	0.053	sec
Compensation, τ_3	0.053	sec
Compensation, τ_4	1.27	sec
Shaping, τ_5	$1/\omega_n$	sec
Constants		
Shaping, α_2	7.10	dimensionless
Compensation, α_3	0.24	dimensionless
Shaping, a	0.39788	dimensionless

Figures 25 and 26 show the frequency response of the 10,000 lb rigid payload. Again the low frequency response for this payload is identical to the one previously shown for the 1,000 and 3,000 lb payloads. For this case, the minimum notch bandwidth at the desired level is 5.2 percent. For the conditions corresponding to the 2.2 Hz notch frequency, the desired broad-band transmissibility is exceeded between the frequencies of 2.5 and 10 Hz, with a maximum deviation of 21 percent at 7.5 Hz. At frequencies above 10 Hz, the response is almost identical to the 3,000 lb payload. Both the 3,000 and 10,000 lb systems use a 2.0 Hz resonant frequency coupling. Therefore, the only difference in the high frequency response is due to the effect of different resonant frequency actuators. Finally, the effect of increasing the payload by 20 percent is similar to the one shown for the previous payloads.

Table XI shows the open loop response phase and gain magnitude margins of stability for the 10,000 lb nominal payload and for a 20 percent weight increase. The phase and gain magnitude margins for the nominal payload are approximately 60 and 12 db, respectively. As for previous payloads, increasing the payload weight makes the system more stable.

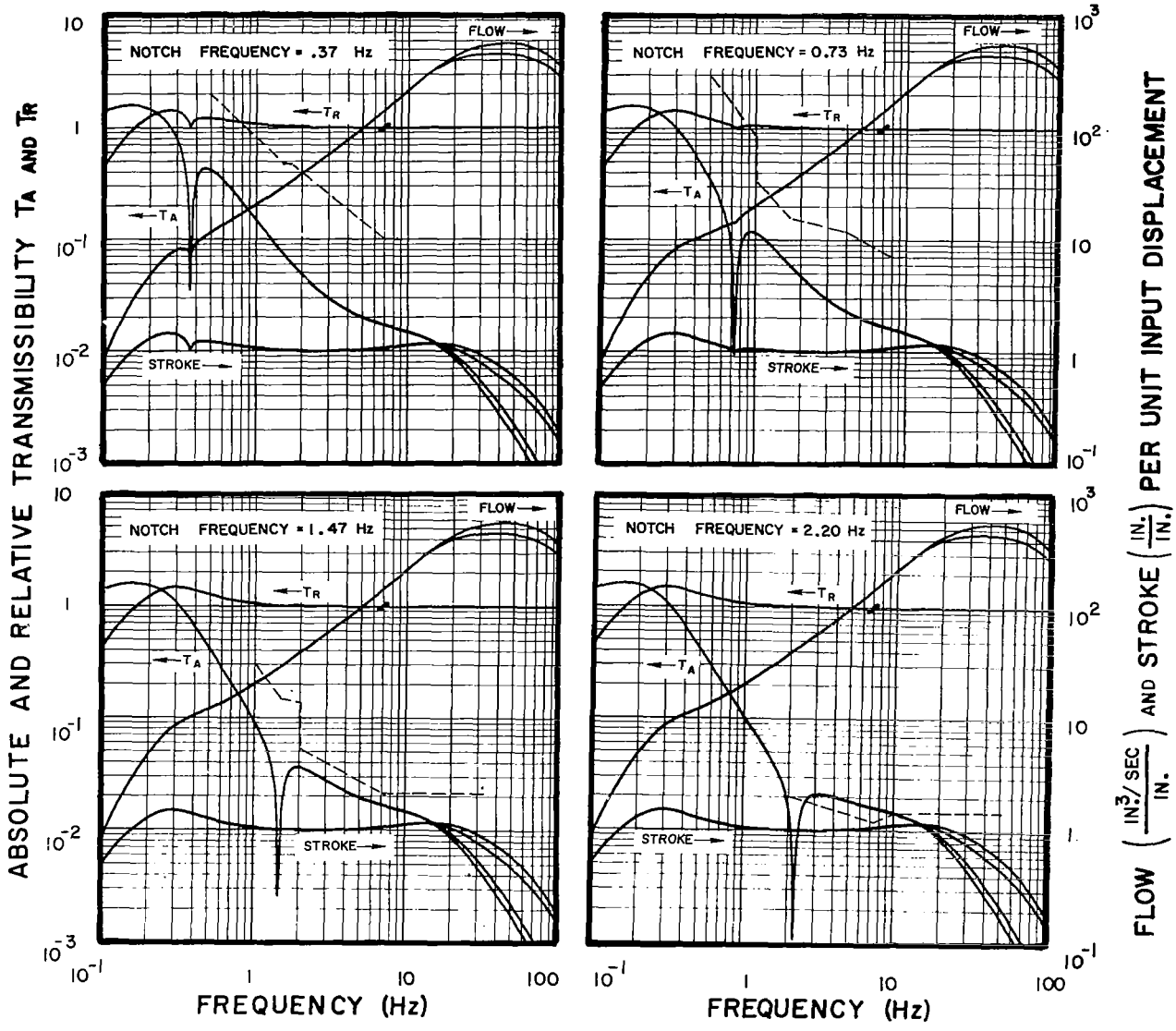

AT LOW FREQUENCIES, EACH CURVE APPLIES TO BOTH NOMINAL PAYLOAD AND A 20% INCREASE IN PAYLOAD. AT HIGH FREQUENCIES, THE UPPER CURVES APPLY TO THE NOMINAL WEIGHT AND THE LOWER CURVES TO THE INCREASED WEIGHT.

DASHED LINE REPRESENTS MAXIMUM ALLOWABLE ABSOLUTE TRANSMISSIBILITY FOR RANDOM INPUTS.

Figure 25. - System absolute and relative transmissibility, valve flow, and actuator stroke for 10,000 lb rigid payload. Notch frequencies: 0.37, 0.73, 1.47 and 2.20 Hz.

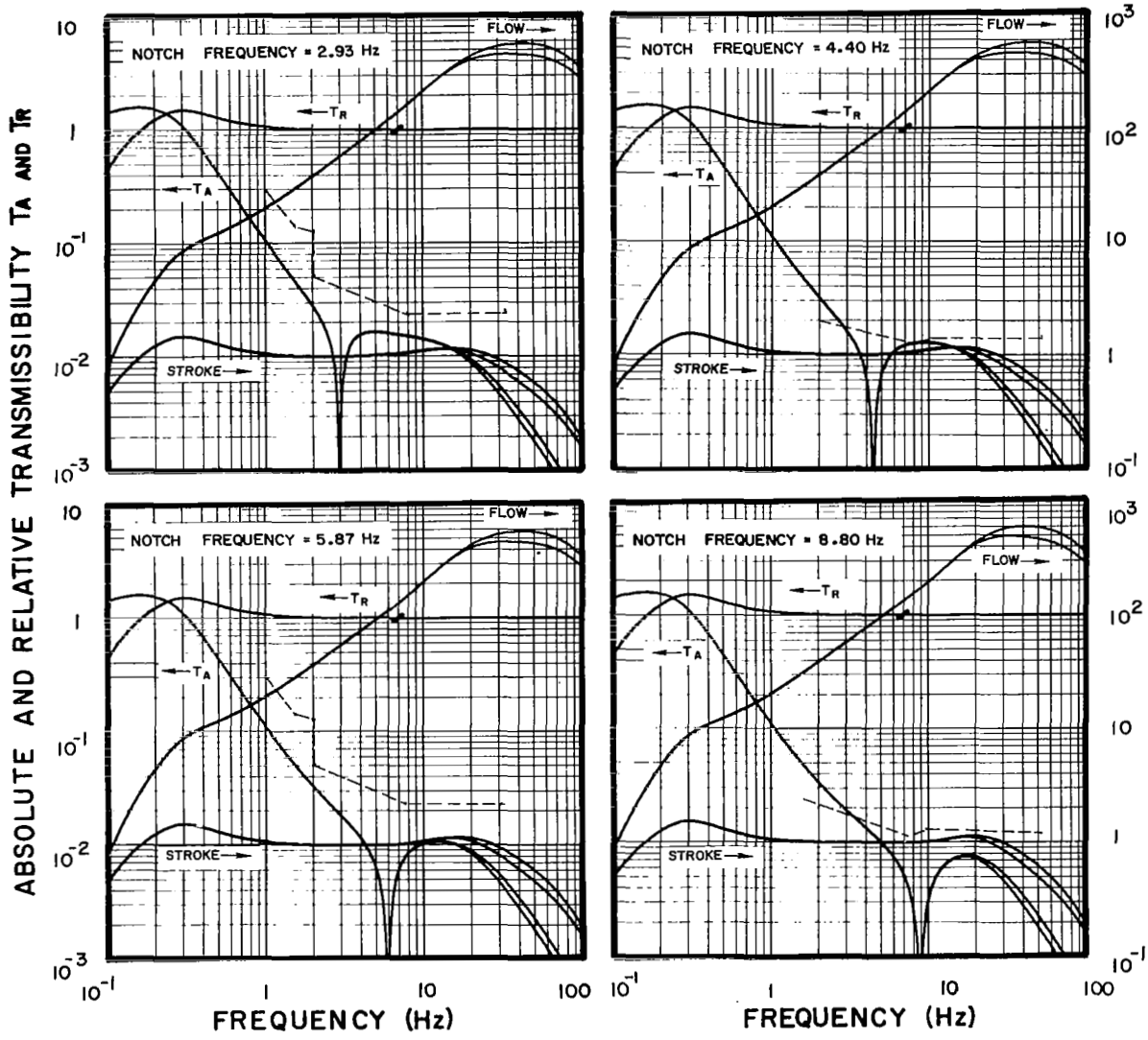

AT LOW FREQUENCIES, EACH CURVE APPLIES TO BOTH NOMINAL PAYLOAD AND A 20% INCREASE IN PAYLOAD. AT HIGH FREQUENCIES, THE UPPER CURVES APPLY TO THE NOMINAL WEIGHT AND THE LOWER CURVES TO THE INCREASED WEIGHT.

DASHED LINE REPRESENTS MAXIMUM ALLOWABLE ABSOLUTE TRANSMISSIBILITY FOR RANDOM INPUTS.

Figure 26. - System absolute and relative transmissibility, valve flow, and actuator stroke for 10,000 lb rigid payload. Notch frequencies: 2.93, 4.40, 5.87 and 8.80 Hz.

TABLE XI

OPEN LOOP GAIN MAGNITUDE AND PHASE MARGINS

FOR RIGID 10,000 lb PAYLOAD

Payload Weight (lb)	Notch Frequency (Hz)	Phase		Gain	
		Crossover Frequency (Hz)	Margin (degrees)	Crossover Frequency (Hz)	Margin (db)
10,000	0.37	24.21	59.74	86.53	-11.92
	0.73	24.21	59.74	86.53	-11.92
	1.47	24.23	59.73	86.53	-11.92
	2.20	24.27	59.72	86.53	-11.92
	2.93	24.35	59.70	86.53	-11.92
	4.40	24.66	59.68	86.53	-11.91
	5.87	25.22	59.73	86.53	-11.89
	8.80	27.20	60.22	86.57	-11.82
12,000	0.37	20.69	60.65	86.53	-13.51
	0.73	20.69	60.65	86.53	-13.51
	1.47	20.71	60.65	86.53	-13.51
	2.20	20.75	60.64	86.53	-13.51
	2.93	20.84	60.63	86.53	-13.50
	4.40	21.17	60.68	86.53	-13.50
	5.87	21.76	60.90	86.53	-13.48
	8.80	23.84	62.04	86.57	-13.41

Response to Transient Excitations: The transient excitation was defined as a step force applied at the payload equal to one-half the payload weight. The response of the system to transient excitations was calcualted using a GPS 240 high analog computer.

Analog Computer and Read-Out Equipment

Figure 27 shows the computer console. The patchboard which occupies a major portion of the upper right-hand side of the computer, allows connecting the various operating components to simulate the system under consideration. Directly below the analog patchboard is the potentiometer console containing forty high

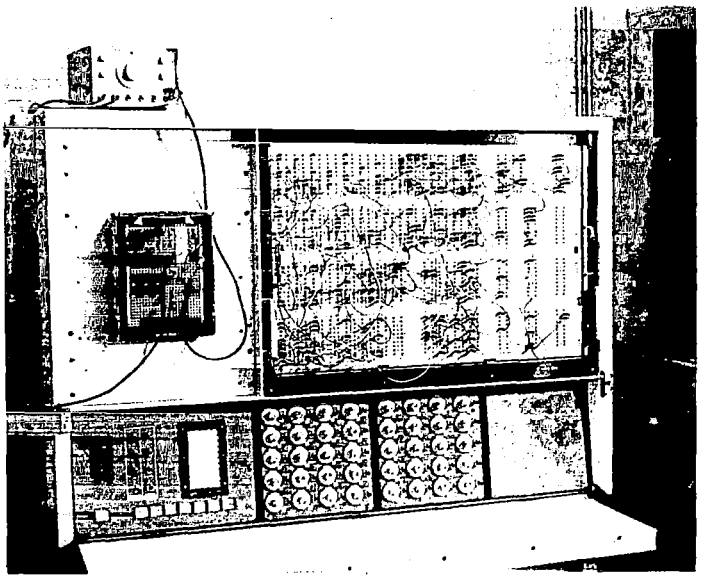

Figure 27: - Analog computer console

precision potentiometers. Associated with each potentiometer is a three-way switch, spring loaded to always return to the center, or compute, position. Deflecting the switch down connects a + 10. V D.C. signal to the input side of the potentiometer loaded as it is in the computer mode. The output of the potentiometer is connected to the digital voltmeter.

The left-hand side of the console consists of a small logic patch board which controls timing functions of the entire solution, generated by signals from the square wave output of a Wavetek function generator. Other connections determine integration time rates, on-off times of the comparitor units, and whether or not the multipliers are being used as multipliers or dividers.

Five types of operating components are available.

1. Summing amplifiers capable of summing four signals, two at a gain of 1.0, and two at a gain of 10.0.

2. Integrating-Summing amplifiers capable of integrating the sum of four signals, two at a gain of 1.0 and two at a gain of 10.0. By selected patching of the logic board each integrator may be set up to have one of four integra-

tion time constants 1.0, 0.1, 0.01, and 0.001 seconds. The integrators may be patched on the logic board in such a way that one integration time constant results from the "Rate 1" setting of the mode switch, and a different time constant from "Rate 2". This allows observation of the solution at high speed on "Rate 1", or at real time on "Rate 2".

3. Comparator components which allow the switching of any desired branch signal on and off as a function of any other branch signal.

4. Multiplying amplifiers which permit the multiplication of any branch signal by another branch signal. By patching on the logic board the multiplier may be converted to a divider.

5. Limiter amplifiers, the positive and negative output levels of which can be individually adjusted. By proper patching, the limiter can be made to have symmetrical limits set by one potentiometer. The limiters may also be patched to provide a dead-band having the same versatile limit settings.

6. Function generators which allow the construction of a ten-segmented output function of an input variable. The function consists of 10 straight line segments, the initial values and slopes of which can be set by 20 potentiometers contained in the unit.

The total number of components available is as follows: 30 summing amplifiers; 13 integrating-summing amplifiers; 6 comparators with associated electronic switches; 6 multiplier-dividers; 2 limiters; and 2 function generators.

Various readout devices were used to both monitor the solution and recording the various output variables. Figure 28 shows the output console which includes:

1. Hewlett-Packard Model 1401A, 8" x 10" screen dual trace oscilloscope. The oscilloscope has a flat response from D.C. to 450 K.C.

2. Tektronix Model 564 dual trace, 5-5/8" screen storage oscilloscope having a Model 2B67 calibrated time base. The oscilloscope has a flat response from D.C. to 250 K.C.

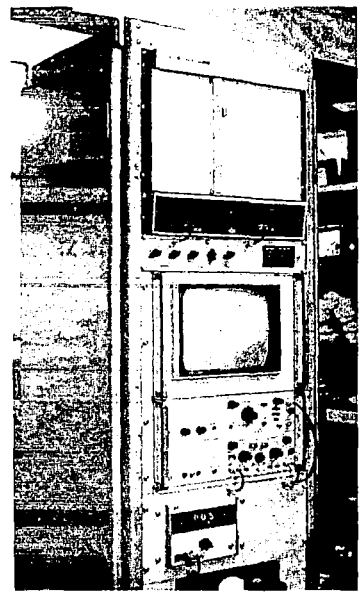

Figure 28. - Output read-out console.

3. Moseley Model 7005B, x-y recorder manufactured by Hewlett-Packard having an 11" x 17" plotting area. A Hewlett-Packard 17108B time base generator having calibrated rates of 0.5,1.0, 5.0, 10.0 and 50 seconds/inch is used in conjunction with the x axis of the plotter.

4. A Wavetek Model 110 function generator having continuously setable frequency ranging from 0.01 Hz to 1 M.C. and adjustable output voltage of from 0.0 to $\pm$ 6.0 volts for a sine, triangular and square wave.

Simulation of Active Isolation System

Figure 29 shows the schematic block diagram of the linear active isolation system with rigid payload. The transfer functions for each of the components and signal flow paths are also identified. Figures 30 and 31 show the corresponding scaled analog block diagram and an explanation of the symbols used in the analog diagram, respectively.

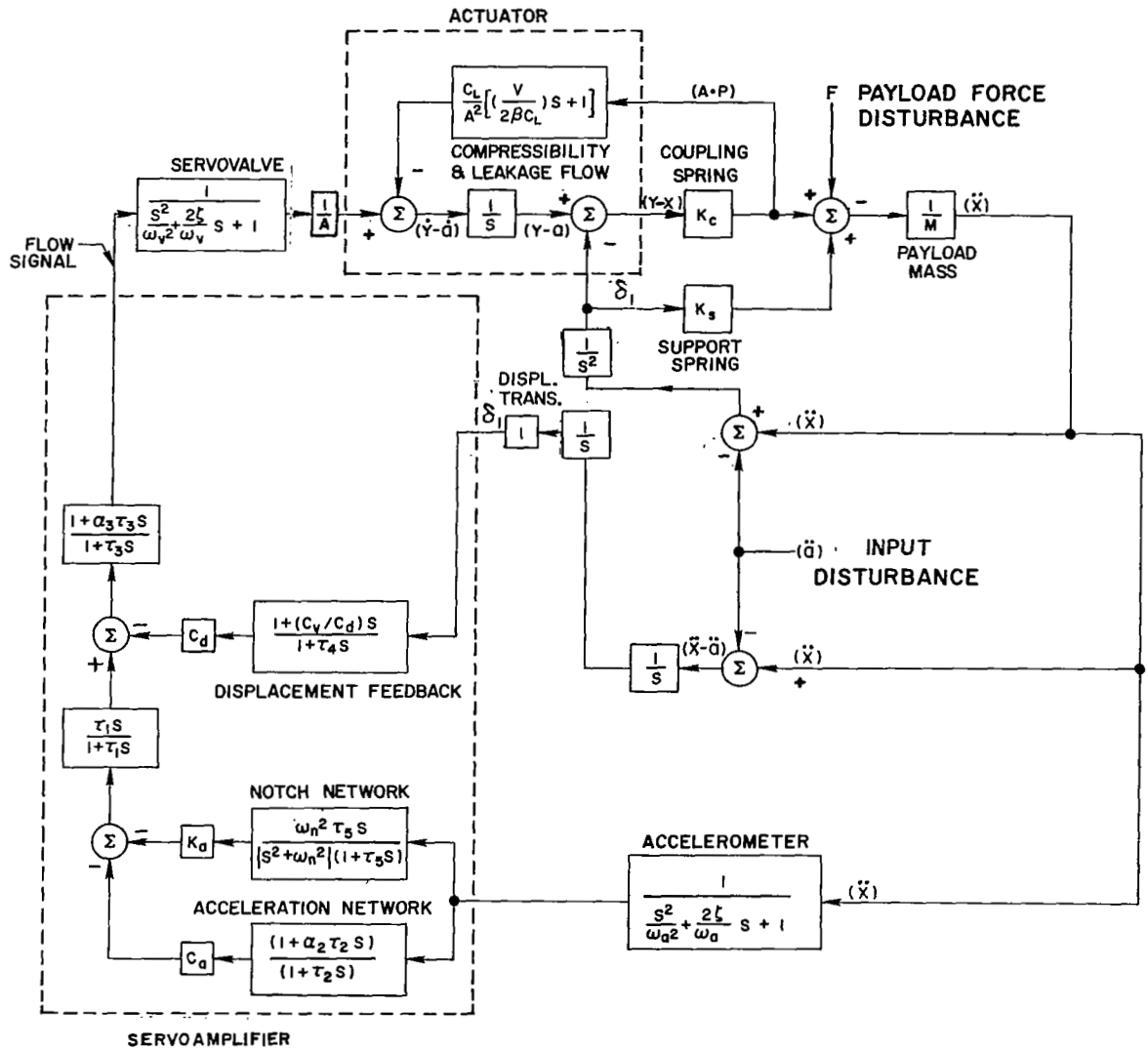

Figure 29. - Schematic block diagram of linear active isolation system with rigid payload.

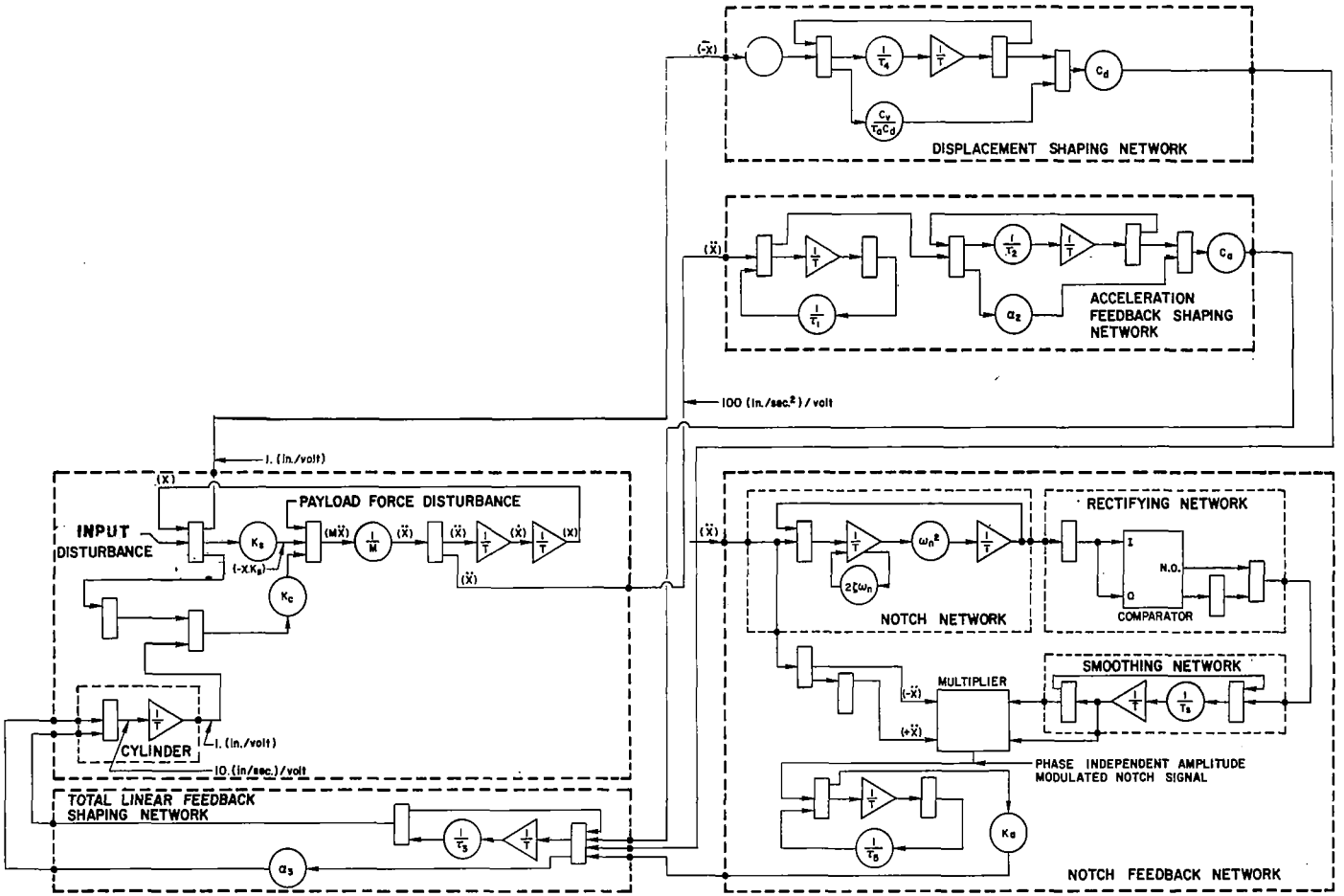

Figure 30. - Analog block diagram of linear active system with rigid payload.

SUMMING AMPLIFIER

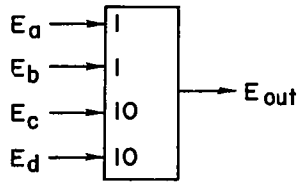

$$E_{out} = -(E_a + E_b + 10E_c + 10E_d)$$

INTEGRATING SUMMING AMPLIFIER

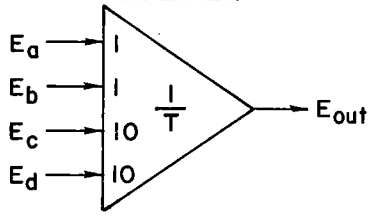

The integrator time constant T is controlled by the logic patchboard and the "Rate 1, Rate 2" mode switch. The available time constants are 1.0, 0.1, 0.01, and 0.001 seconds

$$E_{out} = -\left[\frac{1}{T}\int_0^t (E_a + E_b + 10E_c + 10E_d)\,dt\right]$$

COMPARATOR

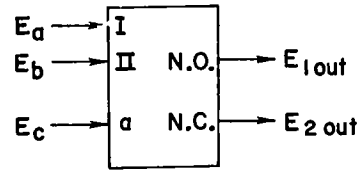

The comparator works in conjunction with an electronic switch on the logic patchboard. The operation of the comparator is defined by the following equations.

$E_a + E_b < 0;\ E_{1_{out}} = E_c,\ E_{2_{out}} = 0$

$E_a + E_b > 0;\ E_{1_{out}} = 0,\ E_{2_{out}} = E_c$

MULTIPLIER

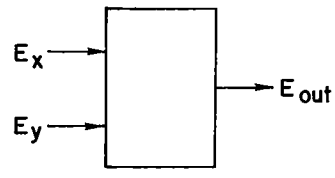

The multiplier may be made into a divider by patching the logic board to provide the divide mode. The expression governing the output for the divide mode is given by

$$E_{out} = -\left[(E_x)(E_y)/10\right]$$

LIMITER

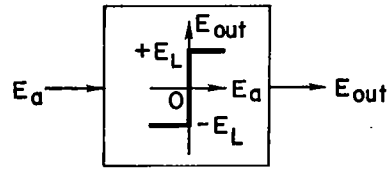

$E_{out} = E_a$ IF $E_{out} < \pm E_L$

$E_{out} = E_L$ IF $E_a > \pm E_L$

The limiter can be changed to a dead-band unit by proper patching on the analog board. The expressions governing the limiter output in this mode are given by

$$E_{out} = 0 \quad E_a < E_L$$
$$E_{out} = E_a \quad E_a > E_L$$

Figure 31. - Symbols used in analog computer diagram.

Rigid Payload Response

Solutions were obtained from the analog computer based on the block diagram shown in Figure 30. The response of the system to a step force applied at the payload equal to one-half the payload weight was defined in terms of four variables:

1. Vertical displacement of the payload relative to the source of vertical excitation; $\delta_1 = a-x$

2. Vertical displacement of hydraulic actuator piston; $\delta_2 = y-a$

3. Velocity of the actuator piston; $\dot{\delta}_2$

4. Vertical acceleration of the payload; $\ddot{x}$

Time histories of each of the variables were obtained from the response of systems using the gains and shaping networks previously selected to attain the desired vibration isolation with payload weights of 1,000; 3,000; and 10,000 lb (Tables VI, VIII, and X). It was found that, as expected, the transient response with 3,000 and 10,000 lb payloads were identical. The frequency response was shown to be identical (Figures 23-26) except for minor differences in the high frequency region due to the differences in actuator and servovalve resonant frequencies. Since the response to a step force at the payload is controlled primarily by the low frequency response of the system, no differences should be found between the response of 3,000 and 10,000 lb rigid payloads with a linear active system.

The initial parametric frequency response study also indicated that, in all cases, the response variables resulted in the highest values with a notch frequency of 8.8 Hz and the lowest values with a notch frequency of 0.37 Hz. The low frequency absolute transmissibility with the highest notch exhibits the highest value. It is to be expected that the response to a step will result in higher displacement for the highest notch frequency. Since the desired performance critieria is to limit the deflections to ±6 inches

in all cases only the response with the highest notch frequency is critical. However, in each case the response with the lowest notch frequency was calculated in order to define the effect of notch frequency on the response of the system.

Figures 32 through 35 show the payload displacement, actuator piston displacement, actuator piston velocity, and payload acceleration for a 1,000 and 10,000 lb nominal payload weight with the lowest and highest notch frequencies considered in the study. In each case the effect of increasing the payload weight by 20 percent is shown.

Table XII shows the peak values of the four transient response variables for the linear active system with 1,000 and 10,000 lb payload weights and notch frequencies of 0.37 and 8.8 Hz. In all cases the maximum relative displacement of the payload exceeds the desired six inch value. It was concluded that in order to limit the relative displacement of the payload, nonlinearities in the gains of the feedback mechanisms are required. Section 5 shows the selection of nonlinearities to meet the displacement criteria.

TABLE XII

PEAK RESPONSE OF LINEAR ACTIVE SYSTEM WITH RIGID PAYLOAD TO A 0.5 W FORCE STEP AT THE PAYLOAD

Payload Weight (lb)	Notch Frequency (Hz)	$(\delta_1)_{max}$ (in.)	$(\delta_2)_{max}$ (in.)	$(\dot{\delta}_2)_{max}$ (in./sec)	$\ddot{x}_{max}$	
					(in./sec^2)	(g)
1,000	0.37 8.8	9.0 9.4	8.2 8.8	9.2 9.8	31.0 30.5	0.080 0.082
1,200	0.37 8.8	8.4 8.8	7.6 8.0	8.4 8.6	29.0 29.8	0.050 0.077
10,000	0.37 8.8	10.6 12.0	10.4 11.0	11.2 12.0	36.0 39.0	0.093 0.101
12,000	0.37 8.8	10.7 11.0	9.6 10.0	11.8 13.4	39.0 36.5	0.101 0.094

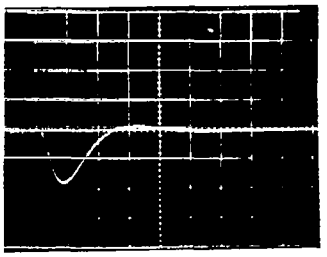

Payload relative displacement
δ_1; 5 in.per div.
t ; 2 sec per div.

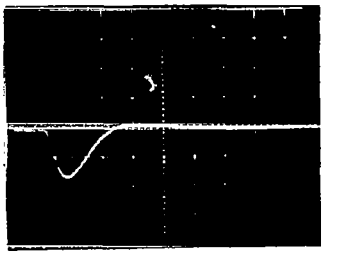

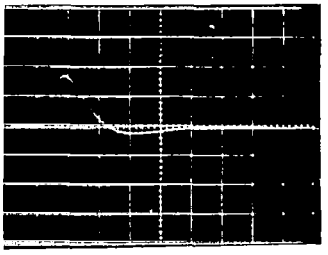

Actuator piston displacement
δ_2; 5 in.per div.
t ; 2 sec per div.

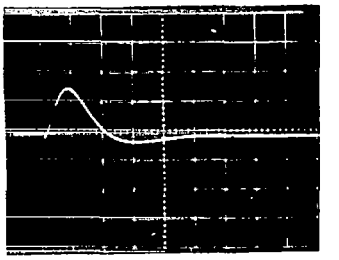

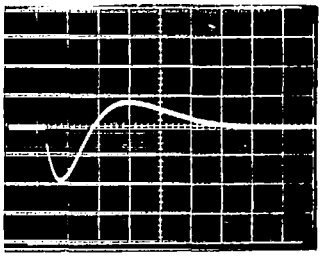

Actuator piston velocity
$\dot{\delta}_2$; 5 in./sec per div.
t ; 1 in./sec per div.

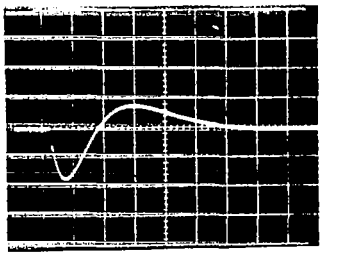

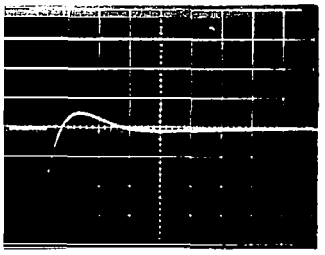

Payload Acceleration
$\ddot{x}$; 20 in./sec^2 per div.
t; 1 sec per div.

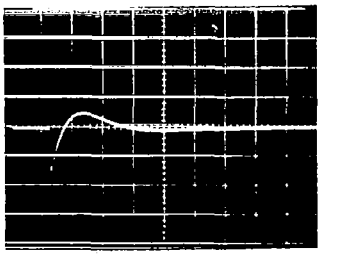

1,000 lb

1,200 lb

Figure 32: Response of linear active isolation system with 1,000 lb payload to a 0.5 W force step applied at the payload. Notch frequency: 0.37 Hz.

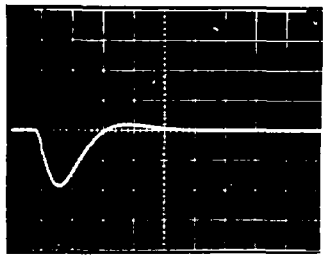

Payload relative displacement

δ_1; 5 in.per div.

t ; 2 sec per div.

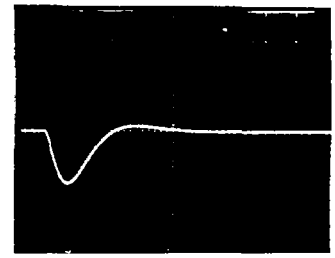

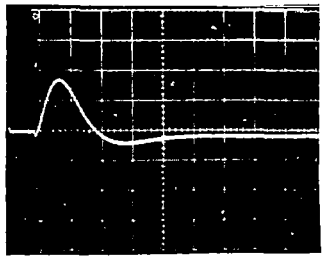

Actuator piston displacement

δ_2; 5 in.per div.

t ; 2 sec per div.

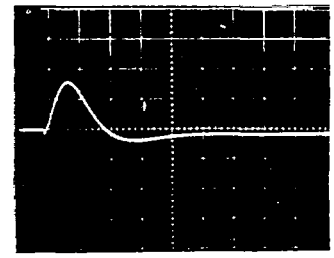

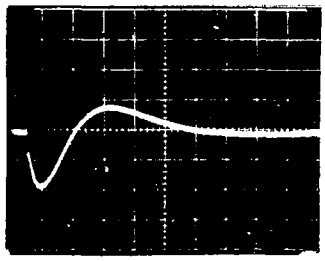

Actuator piston velocity

$\dot{\delta}_2$; 5 in./sec per div.

t ; 1 sec per div.

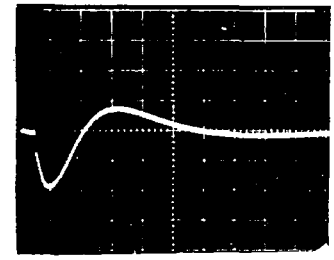

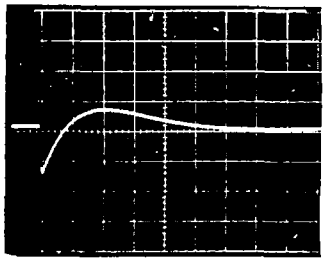

Payload Acceleration

$\ddot{x}$; 20 in./sec^2 per div.

t; 1 sec per div.

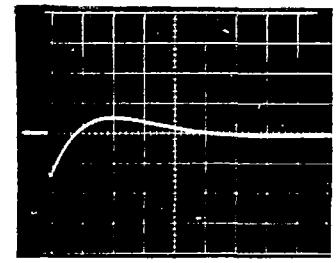

1,000 lb

1,200 lb

Figure 33: Response of linear active isolation system with 1,000 lb payload to a 0.5 W force step applied at the payload. Notch frequency: 8.8 Hz.

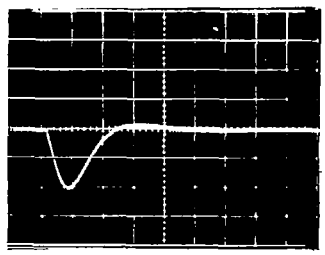

Payload relative displacement

δ_1; 5 in.per div.

t ; 2 sec per div.

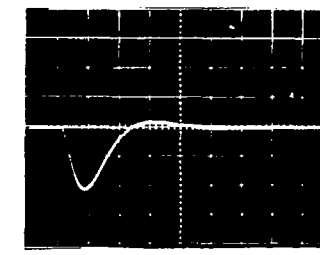

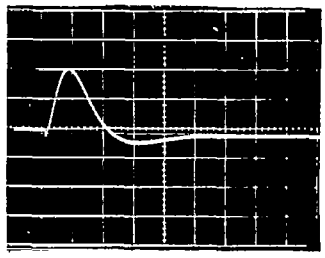

Actuator piston displacement

δ_2; 5 in.per div.

t ; 2 sec per div.

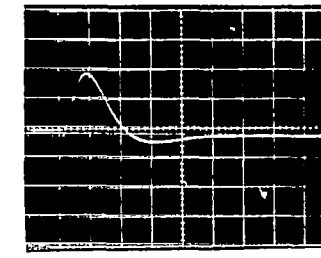

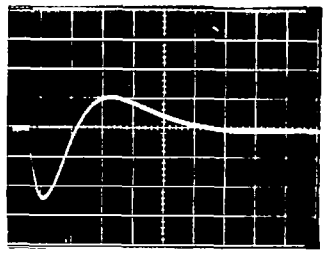

Actuator piston velocity

$\dot{\delta}_2$; 5 in./sec per div.

t ; 1 in./sec per div.

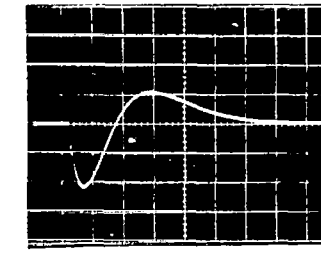

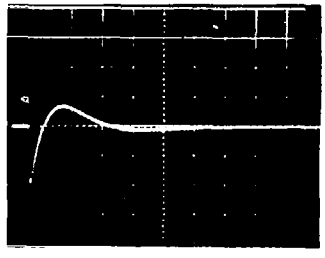

Payload Acceleration

$\ddot{x}$; 20 in./sec^2 per div.

t; 1 sec per div.

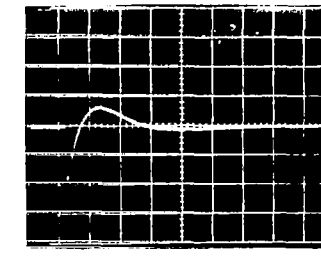

10,000 lb

12,000 lb

Figure 34: Response of linear active isolation system with 10,000 lb payload to a 0.5 W force step applied at the payload. Notch frequency: 0.37 Hz.

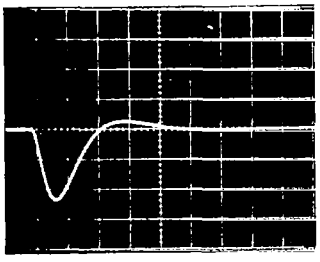

Payload relative displacement

δ_1; 5 in.per div.

t ; 2 sec per div.

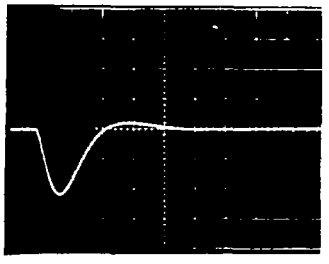

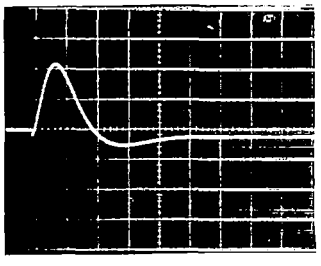

Actuator piston displacement

δ_2; 5 in.per div.

t ; 2 sec per div.

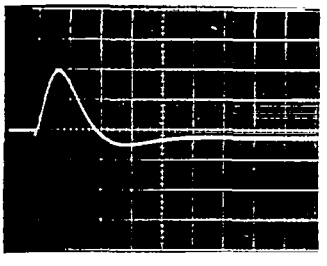

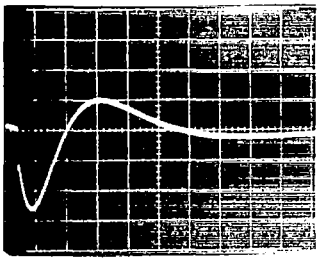

Actuator piston velocity

$\dot{\delta}_2$; 5 in./sec per div.

t ; 1 sec per div.

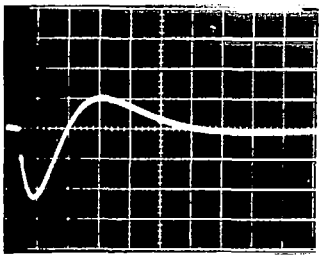

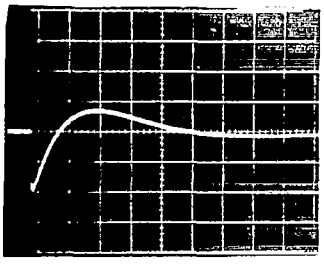

Payload Acceleration

$\ddot{x}$; 20 in./sec^2 per div.

t; 1 sec per div.

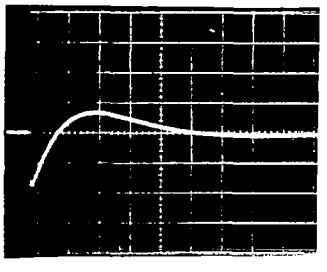

10,000 lb

12,000 lb

Figure 35: Response of linear active isolation system with 10,000 lb payload to a 0.5 W force step applied at the payload. Notch frequency: 8.8 Hz.

Flexible Payload

Description of Isolation System: A detailed sketch of the components of the electrohydraulic vibration isolation system with a flexible payload is shown in Figure 36.

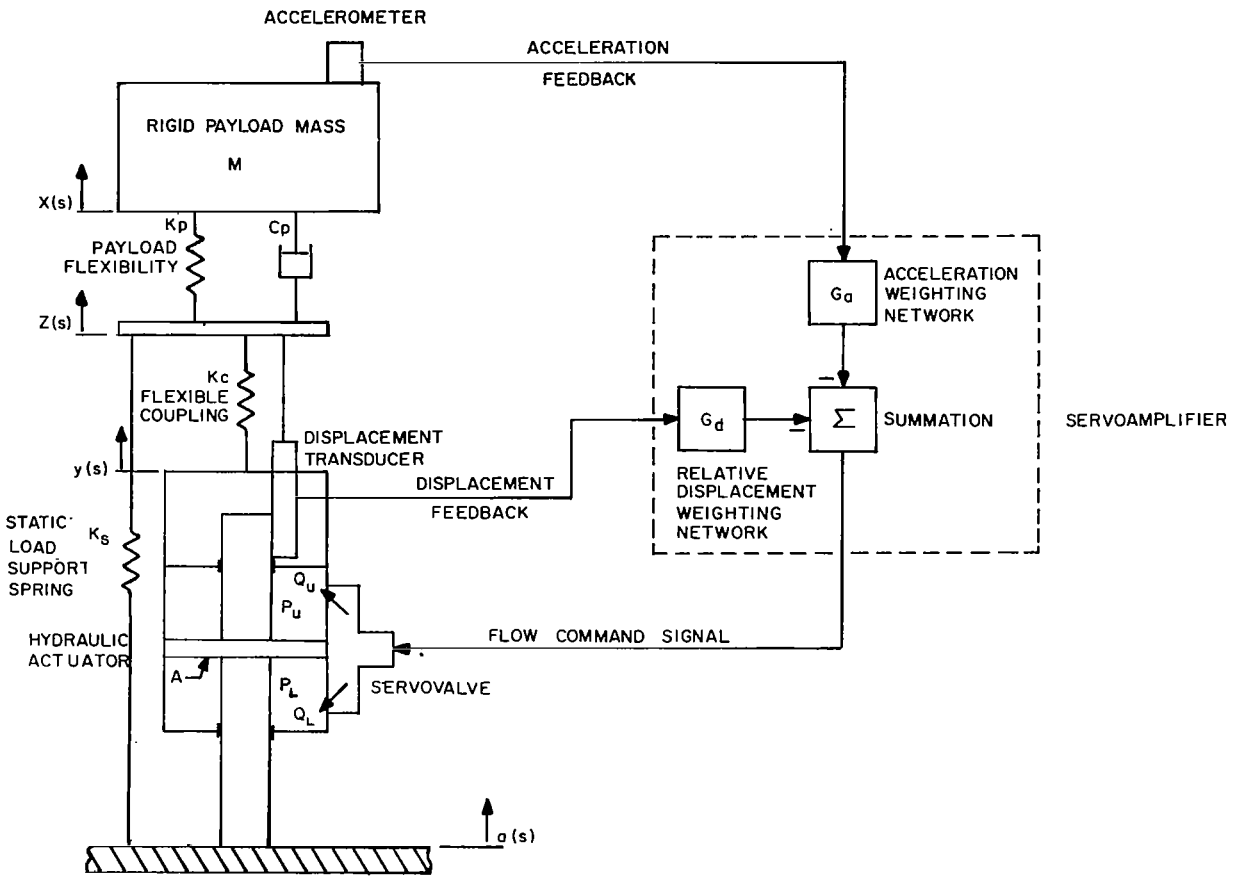

Figure 36. - Schematic diagram of electrohydraulic isolation system with flexible payload.

The components are identical to the ones shown in Figure 17 for the rigid payload. The only difference lies in the added payload stiffness and damping characteristics.

System Transfer Functions: The flow equations for the actuator and servovalve are developed in the same manner as those for the rigid payload. The net flow output from the servovalve $Q_a(s)$ as a function of the actuator pressure drop and the relative velocity of the actuator shaft is given by Equation (4). The expression for the flow command signal $Q_v(s)$ is similar to Equation (7) with the proper variables and is given by:

$$Q_v(s) = -G_{sv}(s) \left[G_a(s)\ s^2\ X(s) + G_d(s)\ (z - a)\right] \tag{21}$$

The equation of motion for the flexible payload is given by:

$$Ms^2\ X(s) + \left(K_p + C_p s\right)\left(X(s) - Z(s)\right) = 0 \tag{22}$$

where K_p is the payload stiffness and C_p is the coefficient of viscous damping for the payload. The actuator force output, $F = AP_d(s)$ is related to the system motion by the relationship

$$AP_d(s) = K_c\left[Z(s) - Y(s)\right] \tag{23}$$

The force continuity expression at the payload-coupling interface is given by

$$\left(K_p + C_p s\right)\left(X - z\right) = K_c\ \left(z - y\right) + K_s\ \left(z - a\right) \tag{24}$$

The system closed loop transmissibility transfer function $X(s)/a(s)$, obtained by combining Equations (4), (21), (22), (23), and (24), and setting $Q_v(s)$ equal to $Q_a(s)$, is given by

$$\frac{X(s)}{a(s)} = \frac{s\left(1 + \frac{K_s}{K_c}\right) + K_s\left(\frac{V_s}{2\beta A^2} + \frac{C_L}{A^2}\right) + \frac{1}{A}\, G_{sv}(s)\; G_d(s)}{D_1 + D_2 + D_3} \qquad (25)$$

where

$$D_1 = s\left[\frac{Ms^2}{K_c} + \left(1 + \frac{K_s}{K_c}\right)\left(\frac{Ms^2 + C_p s + K_p}{K_p + C_p s}\right)\right]$$

$$D_2 = \left[\frac{Vs}{2\beta A^2} + \frac{C_L}{A^2}\right]\left[Ms^2 + K_s\left(\frac{Ms^2 + C_p s + K_p}{K_p + C_p s}\right)\right]$$

$$D_3 = \frac{1}{A}\left[G_{sv}(s)\; G_a(s)\; s^2 + G_{sv}(s)\; G_d(s)\left(\frac{Ms^2 + C_p s + K_p}{K_p + C_p s}\right)\right]$$

The actuator stroke transfer function $\Delta_2(s)/a(s)$ is given by:

$$\frac{\Delta_2(s)}{a(s)} = \left[\frac{Ms^2}{K_c} + \left(1 + \frac{K_s}{K_c}\right)\left(\frac{Ms^2 + C_p s + K_p}{K_p + C_p s}\right)\right]\frac{X(s)}{a(s)} - \left(1 + \frac{K_s}{K_c}\right) \qquad (26)$$

The open loop transfer function is obtained in the same manner as was done for the rigid payload case, and is given by

$$H(s) = \frac{G_{sv}(s)\left[G_a(s)s^2\left(K_p + C_p s\right) + G_d(s)\left(Ms^2 + C_p s + K_p\right)\right]}{As\left\{\left(\frac{1}{K_c} + \frac{V}{2\beta A^2} + \frac{C_L}{A^2 s}\right)\left[Ms^2\left(K_p + C_p s\right) + K_s\left(Ms^2 + C_p s + K_p\right)\right] + C_p s + K_p\right\}} \qquad (27)$$

The electronic shaping networks for the flexible payload are identical to those employed with the rigid payload.

Response to Vibratory Excitations: The response of the linear active system with flexible payload to vibratory excitations was calculated using a digital computer in a manner similar to the

one used for the rigid payload. The flexible payload linear system employs the same values of gain as the rigid payload.

The response of the linear active systems with flexible payloads is defined in terms of absolute and relative transmissibility curves as a function of frequency. The absolute transmissibility $T_A(s)$ is calculated from Equation (25), and the relative transmissibility $T_R(s) = T_A(s) - 1$. Values of valve flow and actuator stroke were calculated from Equations (7) and (26), respectively.

The results for payload weights of 1,000; 3,000 and 10,000 lb with payload flexibilities defined in terms of 5 and 10 Hz resonant frequencies and 10 percent of critical damping are shown in Appendix C. The responses are identical to the ones previously shown for the rigid payload except at high frequencies. Below 10 Hz the active portion of the system controls the payload response. Above 10 Hz the response is controlled primarily by the flexible coupling dynamics. The flexibility of the payload has only a minimal effect on the high frequency response, since the resonant frequency of the coupling is no more than one-half the resonant frequency of the softest flexible payload.

The open loop phase and gain magnitude margins for the flexible linear system are listed in Appendix C. In all cases the system with the flexible payload is more stable than the system with rigid payload, due to the damping introduced into the system by the flexible payload.

Response to Transient Excitations: Figures 37 and 38 show the schematic and analog block diagrams of the linear active system with a flexible payload. The similarity between the frequency response of the linear active system with rigid and flexible payloads indicates that the response to a step force will also be similar. Since, as shown earlier, the rigid payload displacements due to 0.5W step force exceeded the desired values, it is expected that the response of the flexible payload will also be unsatisfactory. Therefore, the flexible payload response to transient excitations using a linear active system was not evaluated.

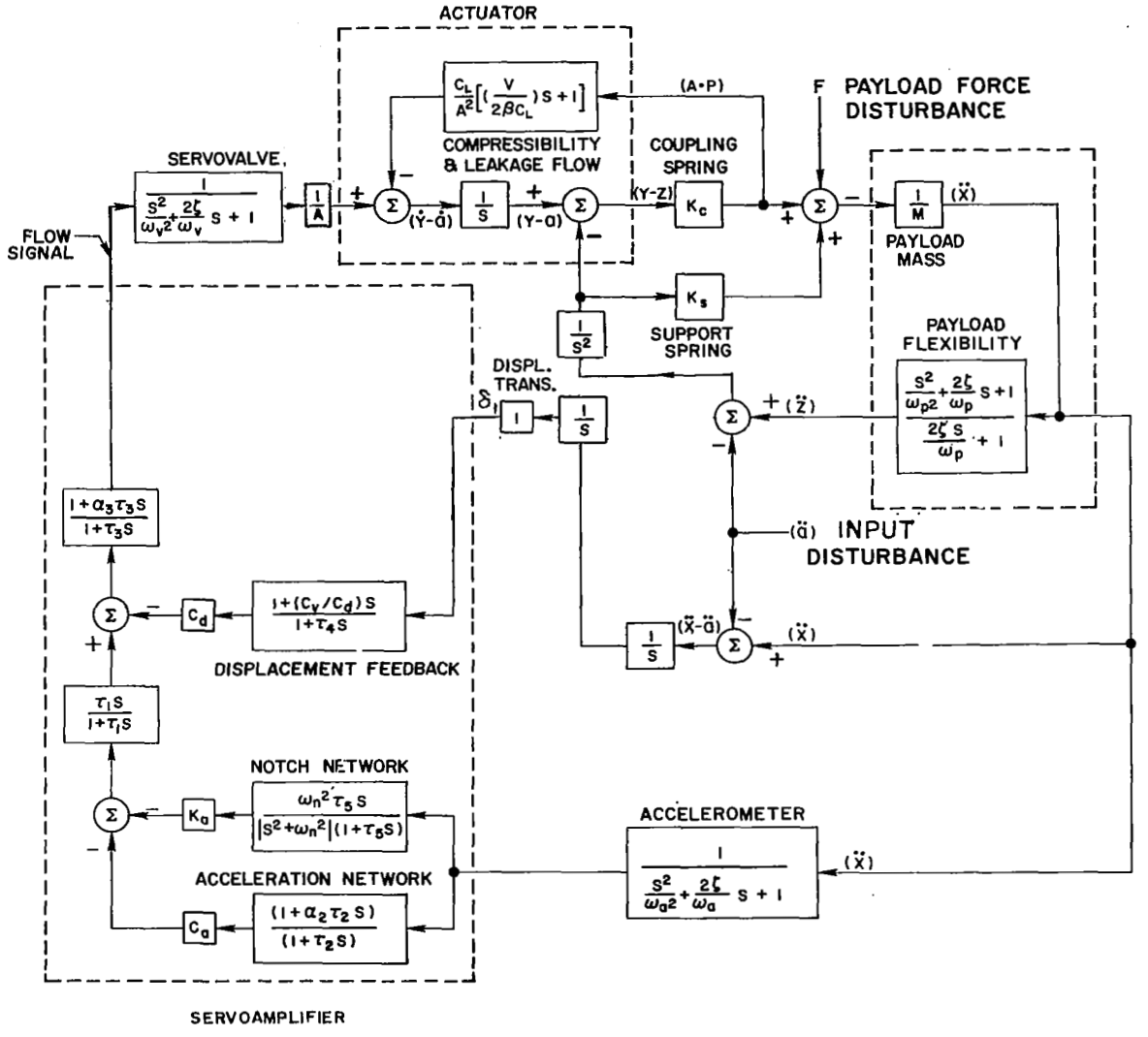

Figure 37. - Schematic block diagram of linear active isolation system with flexible payload.

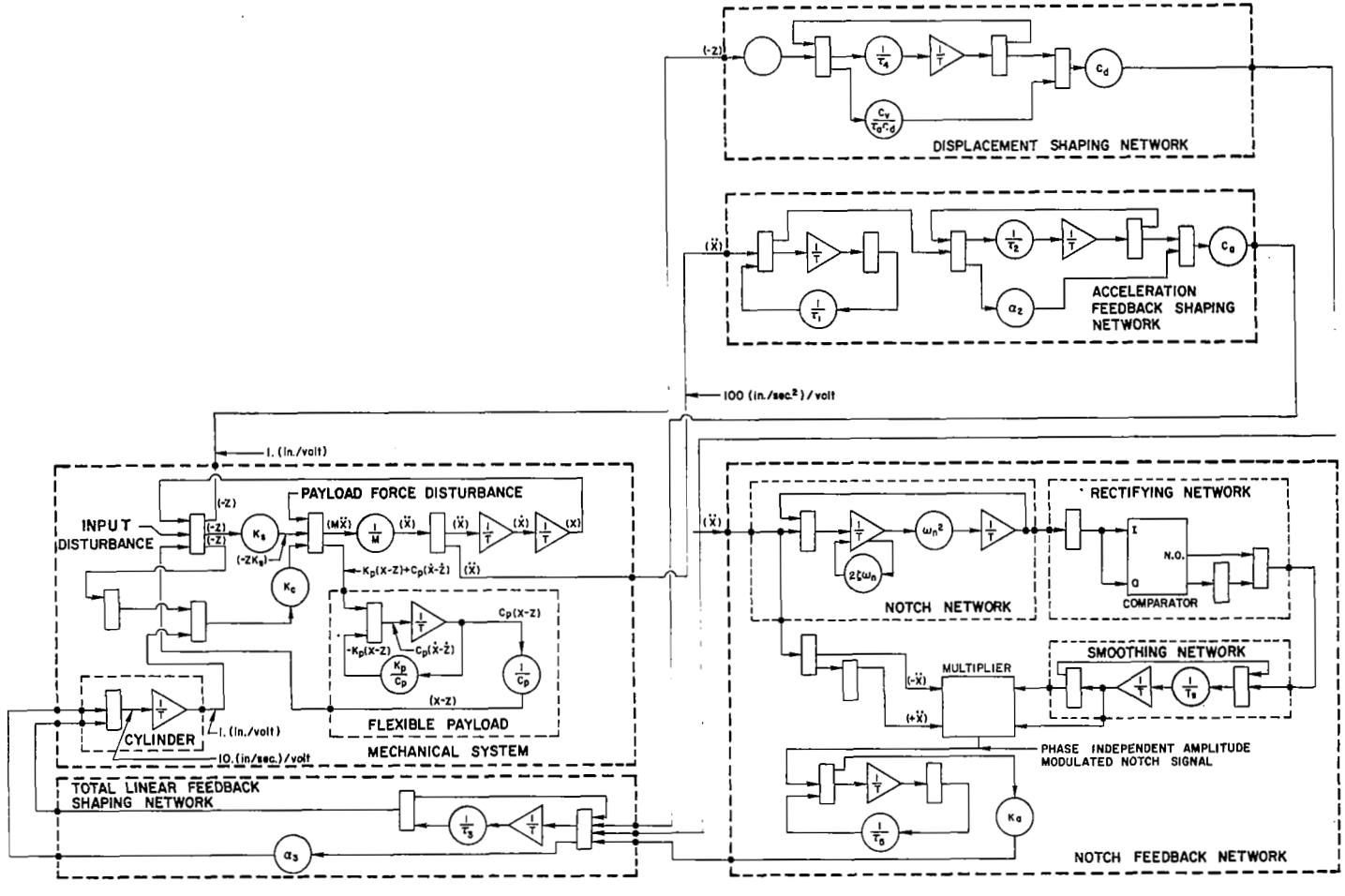

Figure 38. - Analog block diagram of linear active system with flexible payload.

SECTION 5: RESPONSE OF NONLINEAR FEEDBACK ACTIVE ISOLATION SYSTEM

The response of the active isolation system with linear feedback to a step force applied at the payload (Section 4) indicates that the relative displacement between the payload and the air cushion exceeds the desired 6 inches. In reality, the step force would be experienced while the vibratory excitations reach the payload from the air cushion. Therefore, the total displacement due to combined excitations is the sum of the displacements due to the discrete frequency sinusoidal excitation, broad-band sinusoidal excitation, and step force.

Introduction of nonlinearities in the feedback gains to limit the displacement introduces the problem of limiting the degree of isolation provided to the payload. In order to insure that vibratory excitations are isolated and the payload displacement is limited to ± 6 inches, the gains can be increased as a function of displacement. The response of the system to vibratory excitation is then controlled by the linear portion of the feedback, and the displacement control under the step force is achieved by the nonlinear portion.

Table XIII shows the maximum displacement of the payload under combined discrete frequency and broad-band vibratory excitations. If the relative displacement and velocity gains are increased whenever the relative displacement exceeds the maximum value expected during combined vibrations, the system will provide the vibration isolation indicated in Section 4 based on the linear system response. The procedure used for selecting both the values of nonlinear gains and displacement at which they occur is described in the following paragraphs. Values were selected based on a rigid payload; the response of the system with a flexible payload was then checked to demonstrate the effect of payload flexibility on system response.

TABLE XIII

MAXIMUM ISOLATED PAYLOAD RELATIVE DISPLACEMENT (δ_1) max DUE TO VIBRATORY EXCITATIONS

Notch Frequency (Hz)	Discrete Frequency (± in.)	Broad-Band 3 σ RMS (± in.)	Total (δ_1)max (± in.)
0.37	3.0	0.65	3.65
0.73	3.0	0.65	3.65
1.47	3.0	0.65	3.65
2.20	3.0	0.65	3.65
2.93	3.0	0.65	3.65
4.40	2.35	0.65	3.0
5.87	1.95	0.65	2.60
8.80	1.50	0.65	2.15

Rigid Payload

The transfer functions for the system with rigid payload and nonlinear gains are identical to those for the linear gain system shown in Equations (8), (9), and (13) except for the displacement loop gain $G_d(s)$. The nonlinear displacement loop gain $G_d'(s)$ is given by

$$G_d'(s) = G_d(s) + (C_d' + C_v's)(|\delta_1| - \delta_c) \qquad (28)$$

where $G_d(s)$ is the linear displacement loop gain given by Equation (20); C_d' and C_v' are the nonlinear relative displacement and velocity flow gains; and δ_c is the value of relative displacement at which the nonlinear gains are introduced.

Selection of Nonlinear Gains: Figures 39 and 40 show the schematic and analog block diagrams for the nonlinear feedback active system with rigid payload. The values of linear displacement and velocity flow gains C_d and C_v were set equal to those shown on Tables VI, VIII, and X for the 1,000; 3,000; and 10,000 lb payload weights, respectively.

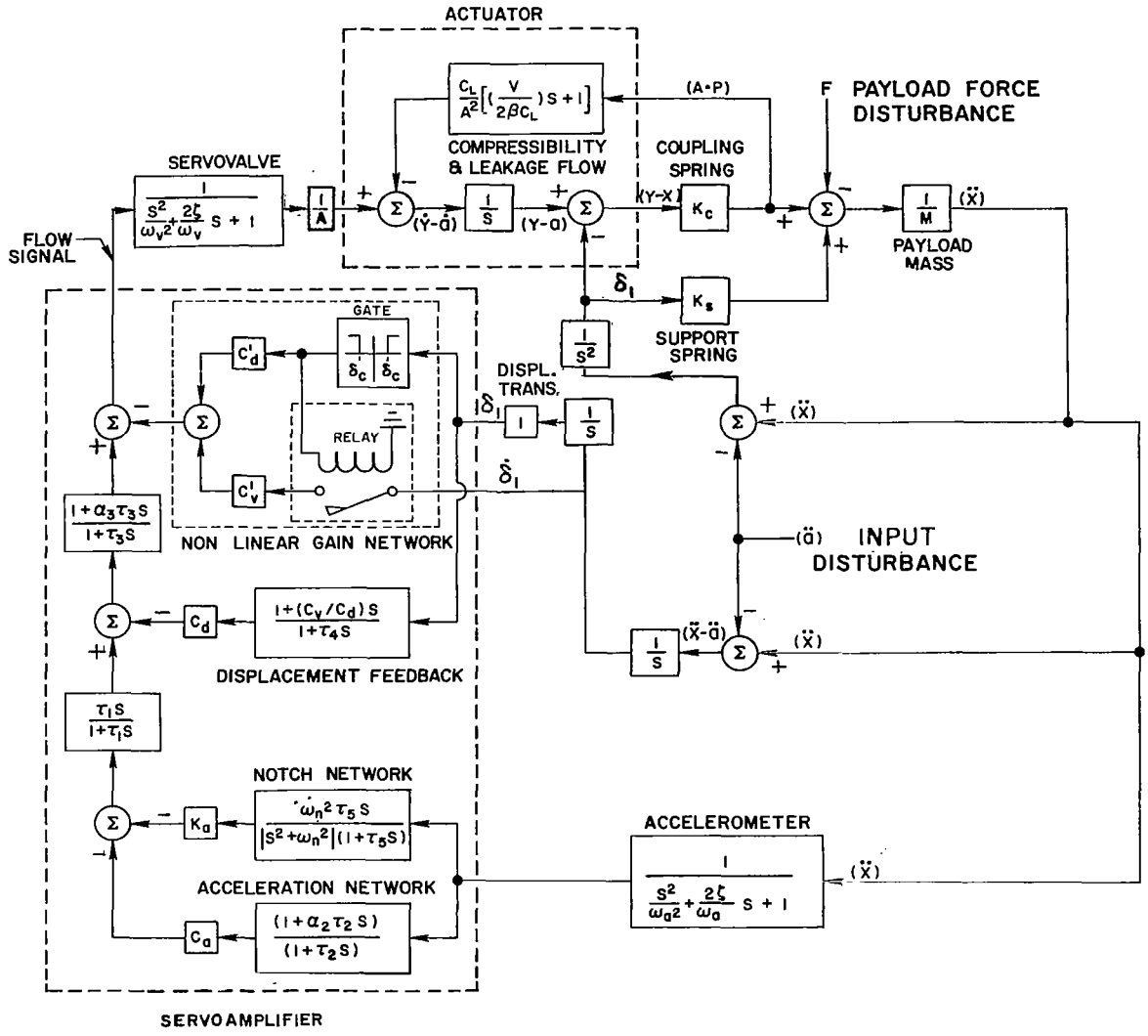

Figure 39 : Schematic block diagram of nonlinear active system with rigid payload.

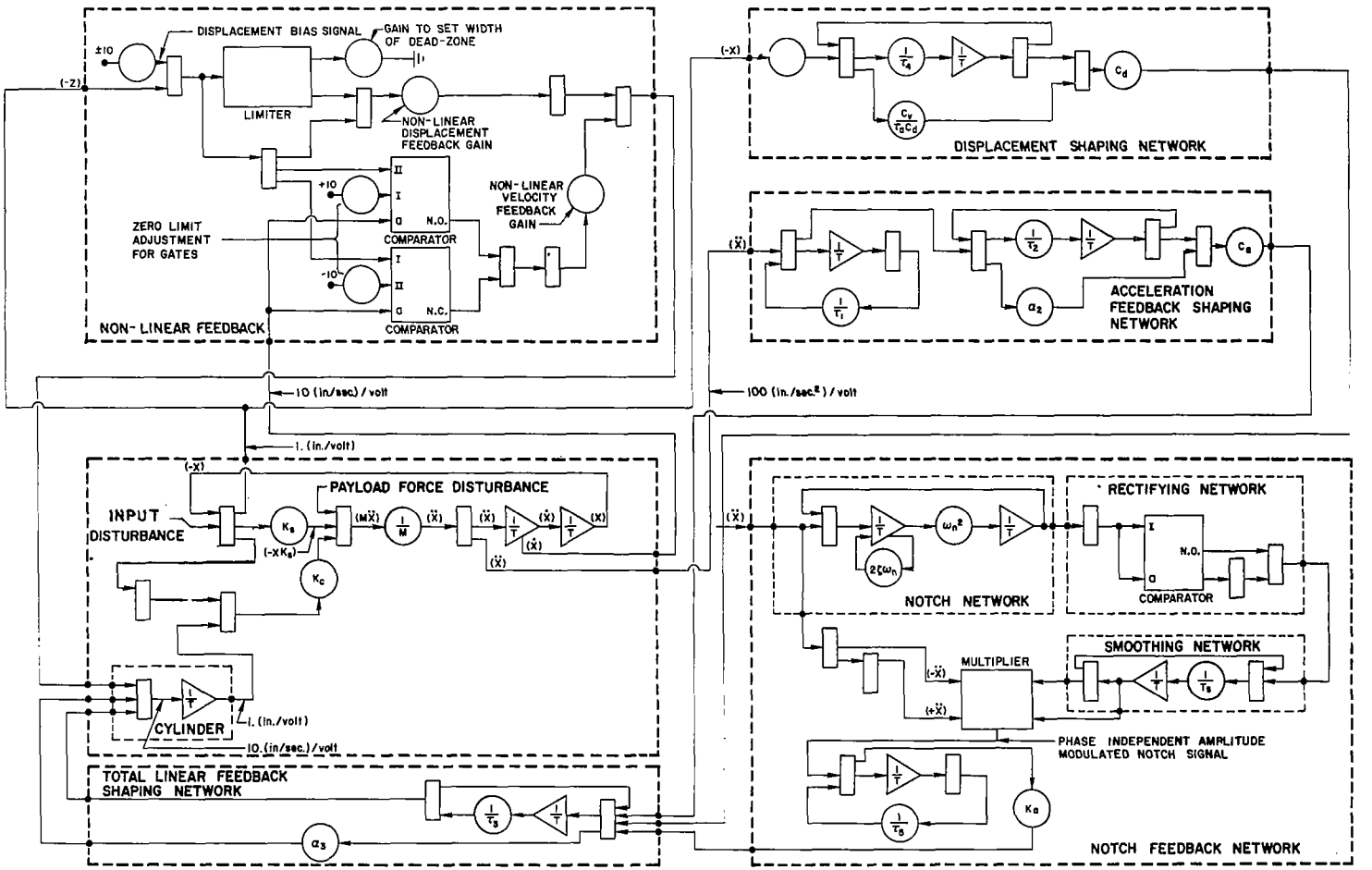

Figure 40: Analog block diagram of nonlinear active system with rigid payload.

Initially, only nonlinear velocity feedback was tried. Based on the response of the linear feedback system to the step force (Table XII), the largest displacement occurs for the 10,000 lb payload weight with a notch frequency of 8.8 Hz. A value of normalized flow gain $C_v'/A = 2.36$ $(in.^3/sec)/in./sec)/in.^2$ $\delta_1 > \delta_c$ (where $\delta_c = 5.0$ inches) was found to limit the value of δ_1 due to the step force to less than 6 inches for the 8.8 Hz notch frequency. The actual flow gain for the 10,000 lb payload is $C_v' = 7.08$ $(in.^3/sec)/in.sec)$. Figure 41 shows the time histories of the variables selected to define the system response.

Although the payload relative displacement due to the step force is less than 6 inches, the response of the system is very sluggish and the payload takes approximately 8 seconds to return to its null position. Moreover, the total displacement due to combined excitations would be in excess of ± 6 inches.

The system speed of response can be improved by the addition of nonlinear displacement flow gain C_d'. Since the desired maximum displacement criterion is based on the combined vibratory and transient excitations, it is necessary to select gains such that the total displacement does not exceed 6 inches. In order to simulate the response of the system to the combined vibratory and transient excitations, a displacement bias was introduced equal to the total displacement of the actuator resulting from the combined vibratory excitations alone. In each case, the displacement bias was set equal to the total displacement shown on Table XIII. The nonlinear gains C_d' and C_v' were introduced at a value of $\delta_c = 4.0$ inches, which is greater than the maximum expected displacement for combined vibratory excitations ($\delta_{1_{max}} = 3.65$ inches). The relative velocity of the payload at $\delta_{1_{max}}$ is zero. Therefore, the bias displacement simulates the payload entering the region where nonlinearities are introduced ($\delta_1 > 4.0$ inches) with velocity and acceleration corresponding to those experienced under combined vibratory excitations.

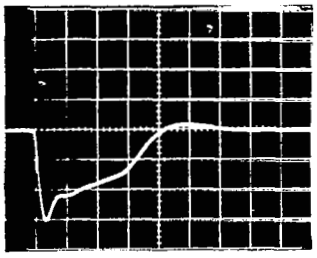

Payload relative displacement

δ_1; 2 in.per div.

t ; 2 sec per div.

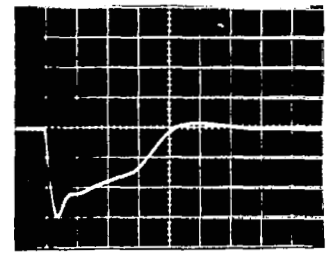

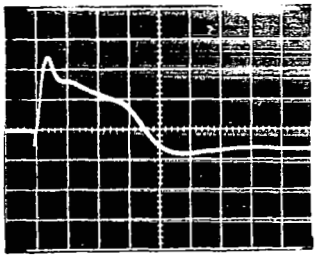

Actuator piston displacement

δ_2; 2 in.per div.

t ; 2 sec per div.

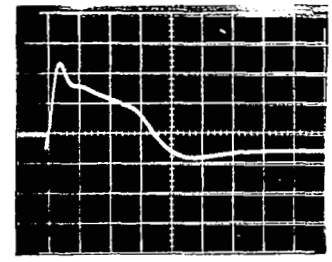

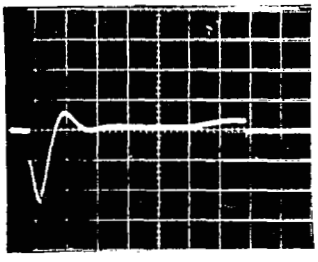

Actuator piston velocity

$\dot{\delta}_2$; 5 in./sec per div.

t ; 1 sec per div.

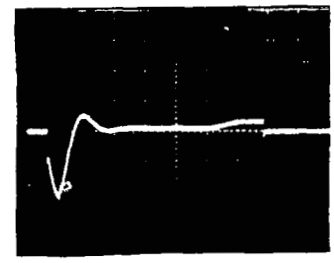

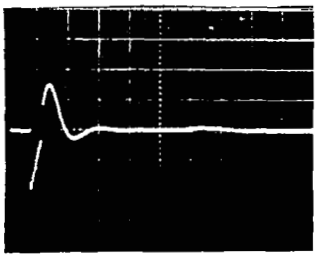

Payload Acceleration

$\ddot{x}$; 20 in./sec^2 per div.

t; 1 sec per div.

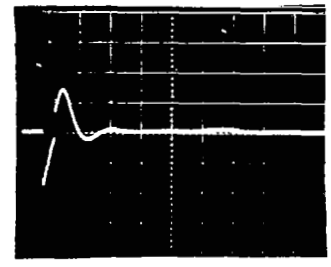

10,000 lb

12,000 lb

Figure 41: Response of nonlinear active system with 10,000 lb. rigid payload to a 0.5 W force step applied at the payload for 8.8 Hz notch frequency. Relative velocity gain increased at $|\delta_1|$ = 5.0 inches.

The largest displacement due to vibratory excitations occurs at notch frequencies below 2.93 Hz (Table XIII). As previously shown, the higher the notch frequency, the larger the displacement under the transient excitation. Therefore, the notch frequency of 2.93 Hz will give rise to the largest displacement under combined excitations. If values of nonlinear gains are selected for this case such that the total displacement is less than 6 inches, then the maximum displacement for all other cases will also be less than 6 inches.

Figure 42 shows the response of the nonlinear system with 10,000 lb rigid payload and 2.93 Hz notch frequency. The payload and actuator piston displacements are measured from a value of displacement equal to the bias displacement $\delta_c = 3.65$ inches. As indicated in the top traces, the peak displacement is 2.35 inches. Therefore, the total displacement under combined vibratory and transient excitations would be 6 inches. The values of normalized nonlinear flow gains are $C_v'/A = 4.82$ $(in^3/sec)/(in./sec)/in^2$ and $C_d'/A = 0.56$ $(in^3/sec)/in$. The actual nonlinear flow gains for the 10,000 lb payload are: $C_v' = 14.46$ $(in^3/sec)/in./sec)$ and $C_d' = 1.68$ $(in^3/sec)/in$. The nonlinear flow gains are introduced at $\delta_1 = 4.0$ inches. For $\delta_1 < 4.0$ inches, the gain values are as shown on Table XII for the linear system.

A comment should be made regarding the payload and actuator piston relative displacement time-histories shown on Figure 42. The displacement bias used to simulate the condition of combined vibratory excitations in the analog solutions, does give accurate values for the system peak response. However, it does not allow neither the payload nor the actuator piston to return beyond the point where the bias was introduced; namely, the zero displacement axis on the displacement time-histories. In the actual case, the system will enter to the linear gain region and return the payload to zero displacement.

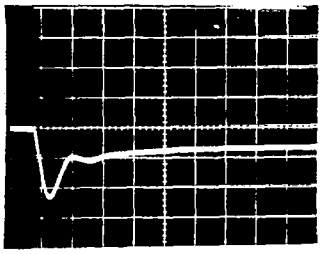

Payload relative displacement

δ_1; 1 in.per div.

t ; 1 sec per div.

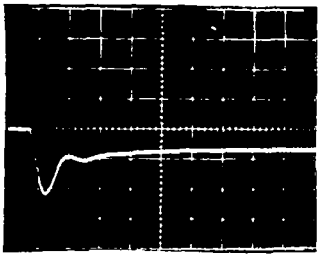

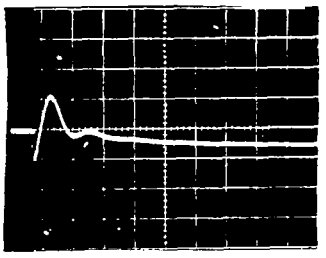

Actuator piston displacement

δ_2; 1 in.per div.

t ; 1 sec per div.

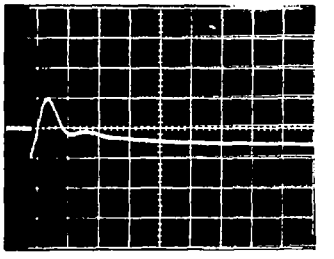

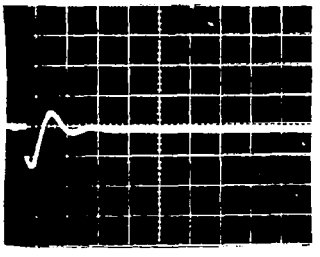

Actuator piston velocity

$\dot{\delta}_2$; 5 in./sec per div.

t ; 1 sec per div.

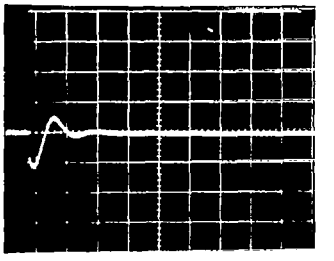

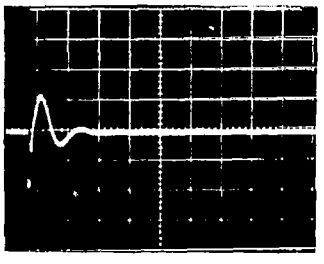

Payload Acceleration

$\ddot{x}$; 20 in./sec^2 per div.

t; 1 per div.

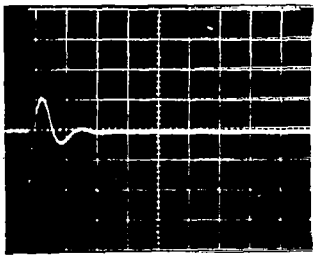

10,000 lb

12,000 lb

Figure 42: Response of nonlinear active isolation system with 10,000 lb. rigid payload to a 0.5 W force step applied at the payload for 2.93 Hz notch frequency. Relative displacement and velocity gains increased at $|\delta_1|$ = 4.0 inches with displacement bias at δ_1 = 3.65 inches.

Response to Vibratory Excitations: The maximum expected displacement under combined vibratory excitations for the system with linear gains is ± 3.65 inches. The nonlinear flow gains C_d' and C_v' are introduced at ± 4.0 inches. Therefore, the response of the system with rigid payload and nonlinear flow gains to discrete frequency and broad-band vibratory excitations, is identical to the response with linear gains shown in Section 4.

Response to Transient Excitations: Figures 43 through 48 show the payload displacement, actuator piston displacement, actuator piston velocity and payload acceleration for the nonlinear system with 1,000 and 10,000 lb rigid payload and notch frequencies of 0.37, 2.93 and 8.8 Hz. In each case, the values of C_d and C_v are listed in Tables VI (for the 1,000 lb payload) and X (for the 10,000 lb payload). the Values of C_d' and C_v' selected for the 2.93 Hz notch frequency are introduced at $\delta_1 = 4.0$ inches.

As shown in the displacement time-histories, the payload remains in the nonlinear gain region ($\delta_1 > 4.0$ inches) for approximately one second. During this time the transmissibility of the system would not meet the desired values.

Table XIV shows the peak values of the four transient response variables for the nonlinear active system with 1,000 and 10,000 lb rigid payloads and notch frequencies of 0.37, 2.93 and 8.8 Hz. The response with 3,000 lb rigid payload is identical to the 10,000 lb payload since the same values of normalized flow gains are used. In all cases the peak displacement is within 5.2 inches.

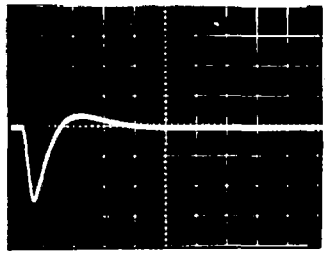

Payload relative displacemen
δ_1; 2 in.per div.
t ; 2 sec per div.

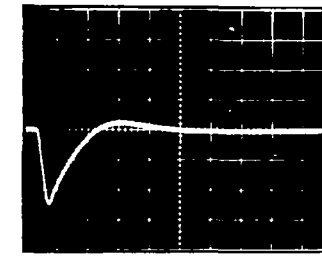

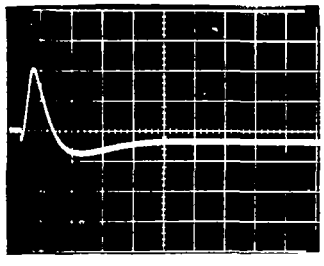

Actuator piston displacement
δ_2; 2 in.per div.
t ; 2 sec per div.

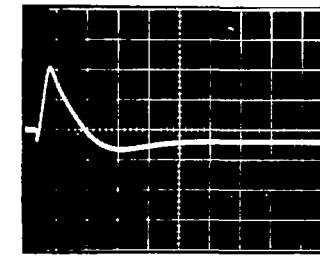

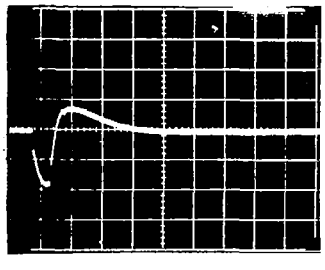

Actuator piston velocity
$\dot{\delta}_2$; 5 in./sec per div.
t ; 1 sec per div.

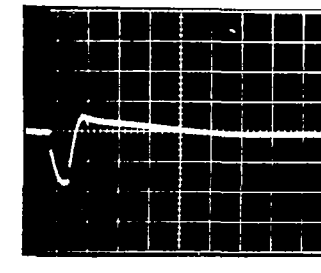

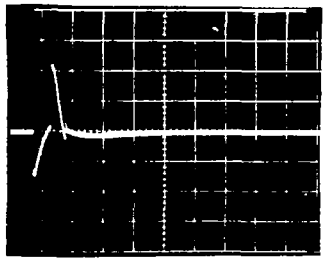

Payload acceleration
$\ddot{x}$; 20 in./sec^2 per div.
t; 1 sec per div.

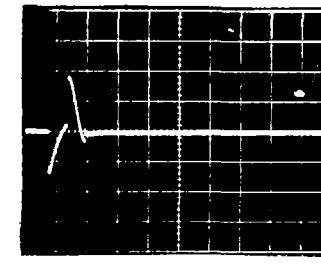

1,000 lb

1,200 lb

Figure 43: Response of nonlinear active isolation with 1,000 lb. rigid payload to a 0.5 W force step applied at the payload for 0.37 Hz notch frequency. Relative displacement and velocity gains increased at $|\delta_1|$ = 4.00 inches.

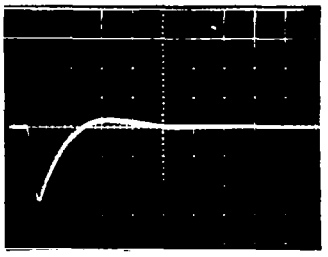

Payload relative displacement

δ_1; 2 in.per div.

t ; 2 sec per div.

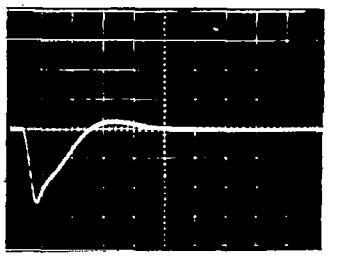

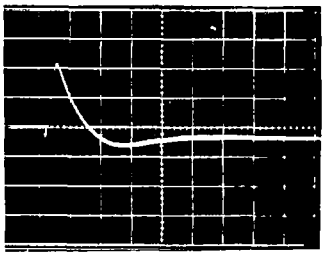

Actuator piston displacement

δ_2; 2 in.per div.

t ; 2 sec per div.

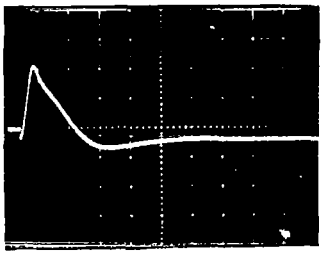

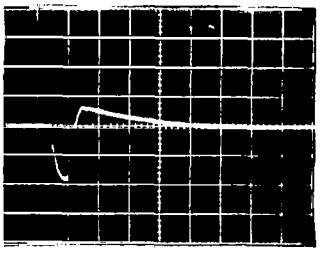

Actuator piston velocity

$\dot{\delta}_2$; 5 in./sec per div.

t ; 1 sec per div.

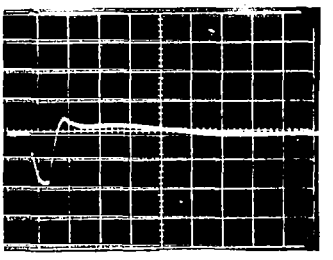

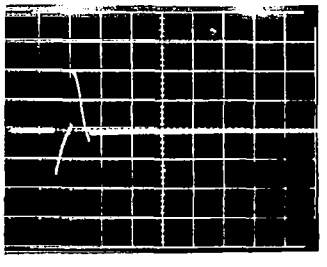

Payload acceleration

$\ddot{x}$; 20 in./sec^2 per div.

t; 1 sec per div.

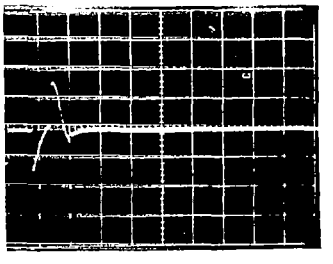

1,000 lb

1,200 lb

Figure 44: Response of nonlinear active isolation with 1,000 lb. rigid payload to a 0.5 W force step applied at the payload for 2.93 Hz notch frequency. Relative displacement and velocity gains increased at $|\delta_1|$ = 4.00 inches.

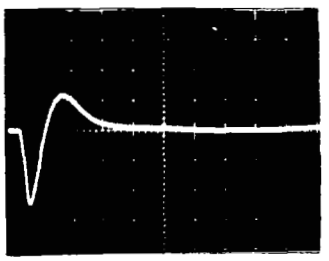

Payload relative displacement
δ_1; 2 in.per div.
t ; 2 sec per div.

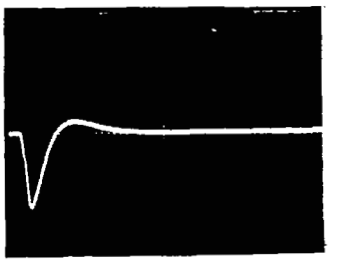

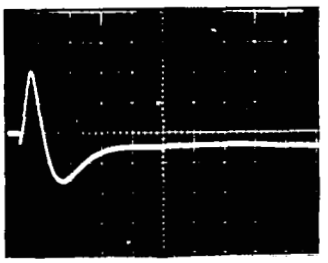

Actuator piston displacement
δ_2; 2 in.per div.
t ; 2 sec per div.

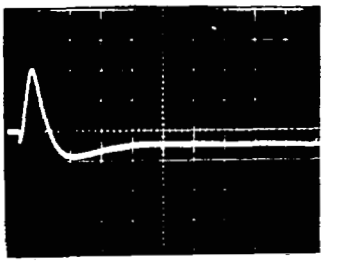

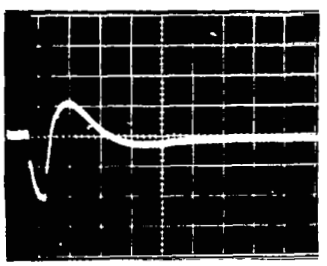

Actuator piston velocity
$\dot{\delta}_2$; 5 in./sec per div.
t ; 1 sec per div.

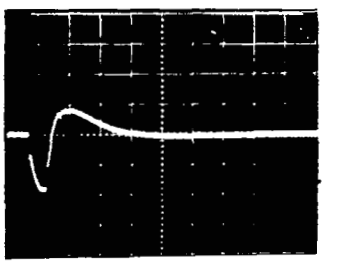

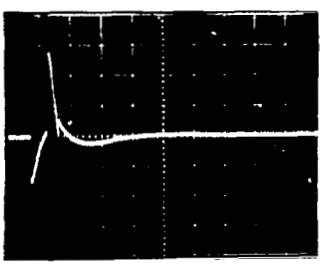

Payload acceleration
$\ddot{x}$; 20 in./sec^2 per div.
t; 1 sec per div.

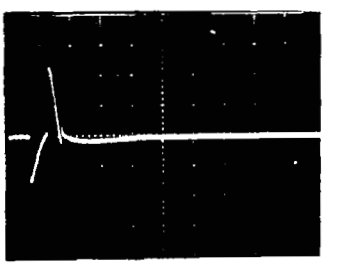

1,000 lb

1,200 lb

Figure 45: Response of nonlinear active isolation with 1,000 lb. rigid payload to a 0.5 W force step applied at the payload for 8.8 Hz notch frequency. Relative displacement and velocity gains increased at $|\delta_1|$ = 4.00 inches.

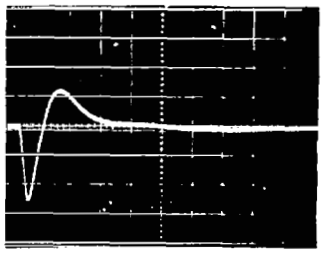

Payload relative displacement

δ_1; 2 in.per div.

t ; 2 sec per div.

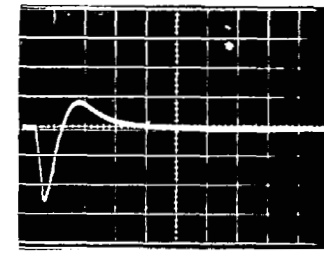

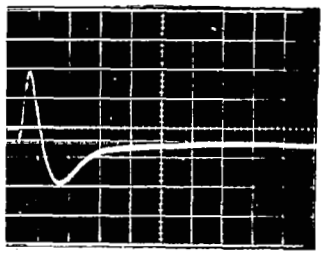

Actuator piston displacement

δ_2; 2 in.per div.

t ; 2 sec per div.

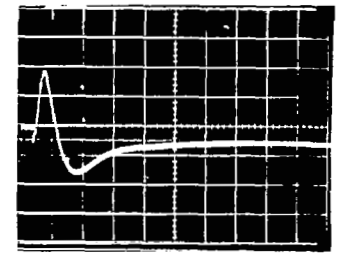

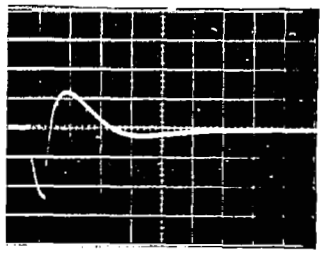

Actuator piston velocity

$\dot{\delta}_2$; 5 in./sec per div.

t ; 1 sec per div.

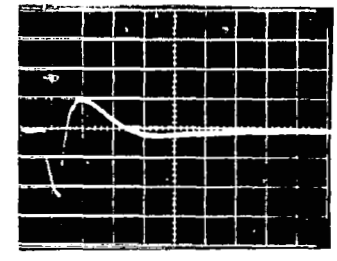

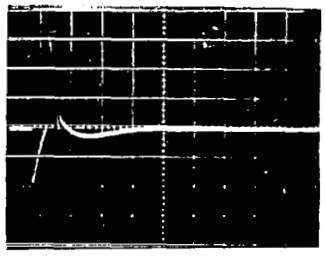

Payload acceleration

$\ddot{x}$; 20 in./sec^2 per div.

t; 1 sec per div.

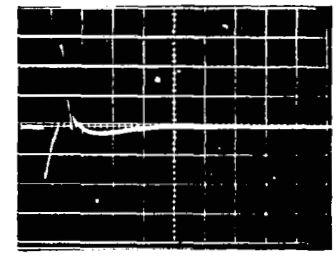

10,000 lb

12,000 lb

Figure 46: Response of nonlinear active isolation with 10,000 lb. rigid payload to a 0.5 W force step applied at the payload for 0.37 Hz notch frequency. Relative displacement and velocity gains increased at $|\delta_1|$ = 4.00 inches.

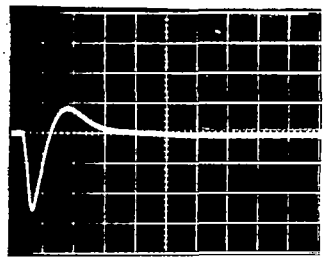

Payload relative displacement
δ_1; 2 in.per div.
t ; 2 sec per div.

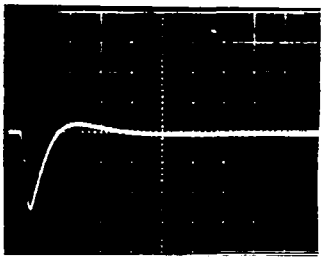

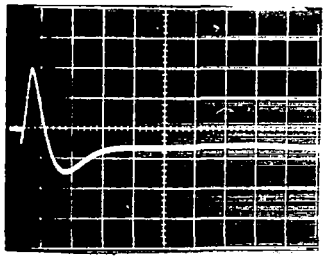

Actuator piston displacement
δ_2; 2 in.per div.
t ; 2 sec per div.

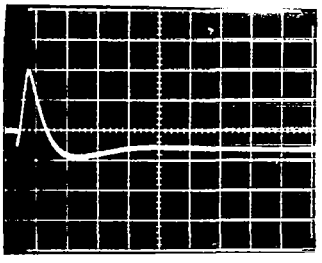

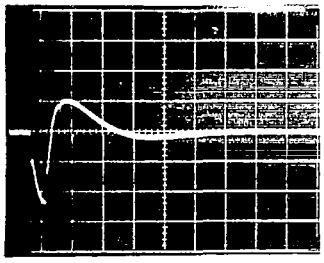

Actuator piston velocity
$\dot{\delta}_2$; 5 in./sec per div.
t ; 1 sec per div.

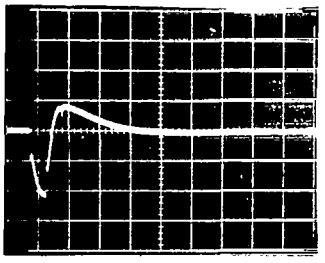

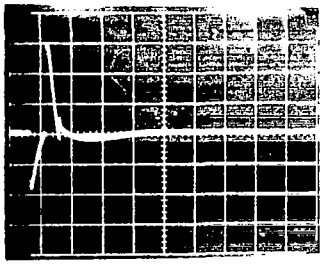

Payload acceleration
$\ddot{x}$; 20 in./sec^2 per div.
t; 1 sec per div.

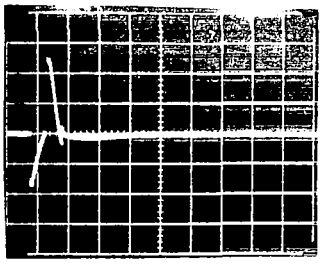

10,000 lb

12,000 lb

Figure 47: Response of nonlinear active isolation with 10,000 lb. rigid payload to a 0.5 W force step applied at the payload for 2.93 Hz notch frequency. Relative displacement and velocity gains increased at $|\delta_1|$ = 4.00 inches.

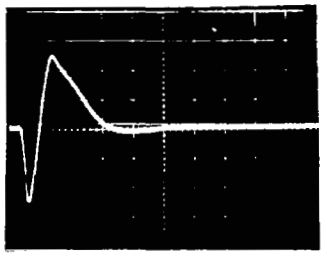

Payload relative displacement
δ_1; 2 in.per div.
t ; 2 sec per div.

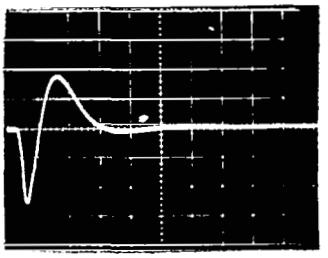

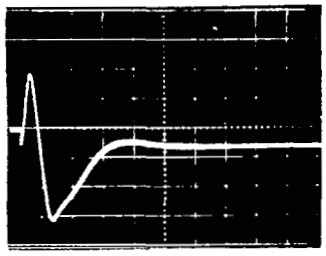

Actuator piston displacement
δ_2; 2 in.per div.
t ; 2 sec per div.

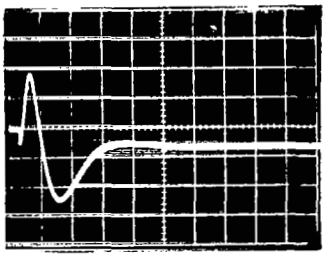

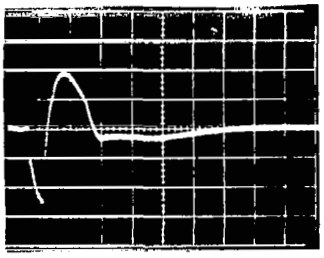

Actuator piston velocity
$\dot{\delta}_2$; 5 in./sec per div.
t ; 1 sec per div.

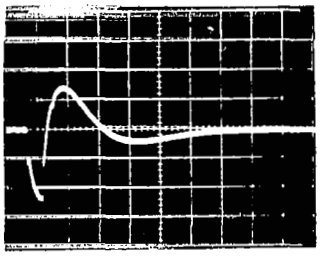

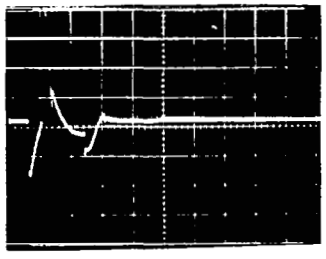

Payload acceleration
$\ddot{x}$; 20 in./sec^2 per div.
t; 1 sec per div.

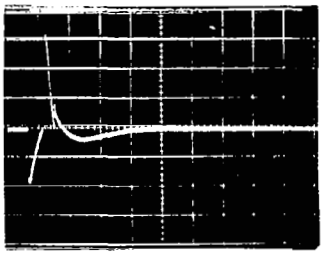

10,000 lb

12,000 lb

Figure 48: Response of nonlinear active isolation with 10,000 lb. rigid payload to a 0.5 W force step applied at the payload for 8.8 Hz notch frequency. Relative displacement and velocity gains increased at $|\delta_1|$ = 4.00 inches.

TABLE XIV

PEAK RESPONSE OF NONLINEAR ACTIVE SYSTEM WITH RIGID PAYLOAD TO A 0.5 W STEP FORCE AT THE PAYLOAD

Payload Weight (lb)	Notch Frequency (Hz)	$(\delta_1)_{max}$ (in.)	$(\delta_2)_{max}$ (in.)	$(\dot{\delta}_2)_{max}$ (in./sec)	$\ddot{x}_{max}$ (in./sec^2)	(g)
1,000	0.37	4.9	4.1	9.0	44	0.114
	2.93	5.1	4.3	9.6	40	0.103
	8.8	4.9	4.0	9.5	49	0.127
1,200	0.37	5.0	4.2	8.8	35	0.091
	2.93	5.2	4.4	8.8	34	0.088
	8.8	5.0	4.2	9.2	42	0.109
10,000	0.37	5.1	3.9	11.8	60	0.155
	2.93	5.2	4.0	11.0	57	0.151
	8.8	5.0	5.2	13.0	67	0.174
12,000	0.37	5.0	3.8	11.0	53	0.137
	2.93	5.2	4.0	10.0	50	0.129
	8.8	5.0	4.9	11.0	60	0.155

Response to Combined Vibratory and Transient Excitations:

Figure 42 shows the response of the 10,000 lb rigid payload with a 2.93 notch frequency and nonlinear gains to the simulated combined vibratory and transient excitations. The same technique was used to calculate the response for the remaining payloads and notch frequencies. In each case a bias displacement was introduced at the corresponding value of maximum displacement under vibratory conditions. The nonlinear gains C_d' and C_v' were introduced at $\delta_1 = 4.0$ inches.

The results are shown in Figures 49 through 53. Again it should be indicated that the displacements shown are measured from the bias displacement equivalent to that associated with the combined vibratory conditions. The total peak displacements of

the rigid payloads are shown on Table XV and are calculated by adding the peak displacements shown in Figures 42 and 49 through 53 to the corresponding bias displacements. The largest displacement of $\delta_{1_{max}} = 6.0$ inches is exhibited by the 10,000 lb payload with 2.93 notch frequency, which was the case used to select values of nonlinear gains.

Peak values of the actuator piston displacement, piston velocity, and payload acceleration for all cases are shown on Table XVI. The peak values for the nonlinear system with a displacement bias, which was used to simulate the response to combined excitations, are lower than the peak values without the displacement bias. Under the transient step force the system without bias starts with zero velocity at zero displacement and enters the nonlinear gain region ($\delta_1 = 4.0$ inches) with a finite velocity. With the displacement bias, the system starts with zero velocity at the bias displacement. The velocity with which it enters the nonlinear region is therefore lower, and the peak values of response variables are smaller.

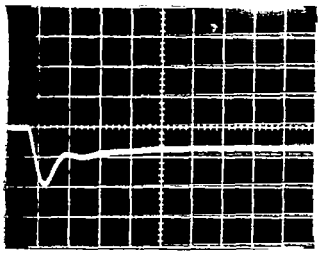

Payload relative displacement
δ_1; 1 in.per div.
t ; 1 sec per div.

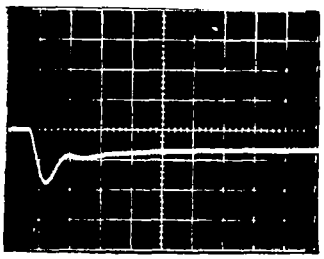

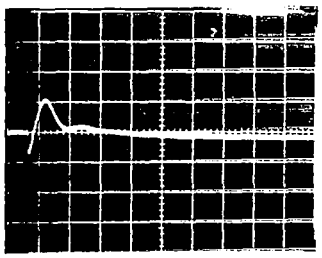

Actuator piston displacement
δ_2; 1 in.per div.
t ; 1 sec per div.

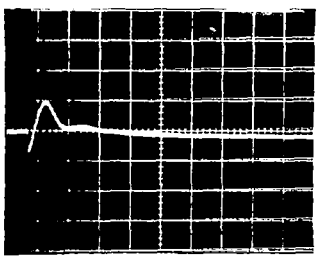

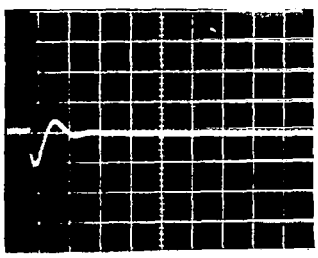

Actuator piston velocity
$\dot{\delta}_2$; 5 in./sec per div.
t ; 1 sec per div.

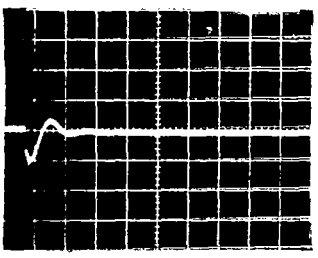

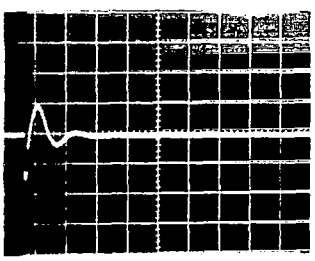

Payload acceleration
$\ddot{x}$; 20 in./sec^2 per div.
t; 1 sec per div.

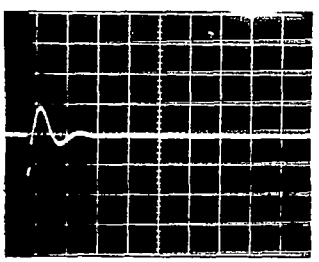

1,000 lb

1,200 lb

Figure 49: Response of nonlinear active isolation system with 1,000 lb. rigid payload to a 0.5 W force step applied at the payload for 0.37 Hz notch frequency. Relative displacement and velocity gains increased at $|\delta_1|$ = 4.0 inches with displacement bias at δ_1 = 3.65 inches.

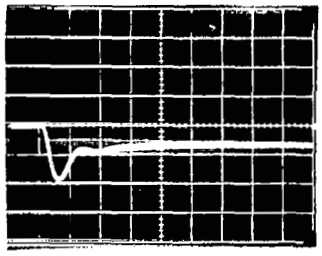

Payload relative displacement
δ_1; 1 in.per div.
t ; 1 sec per div.

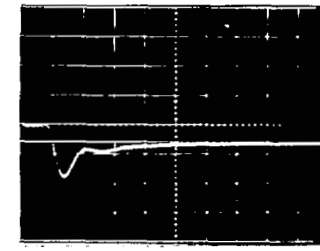

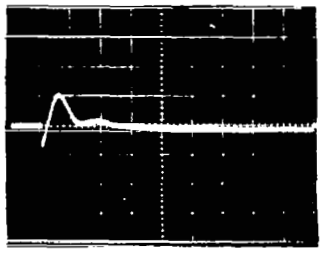

Actuator piston displacement
δ_2; 1 in.per div.
t ; 1 sec per div.

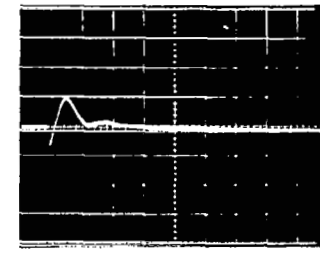

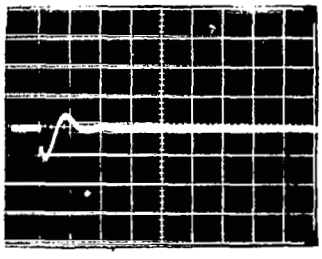

Actuator piston velocity
$\dot{\delta}_2$; 5 in./sec per div.
t ; 1 sec per div.

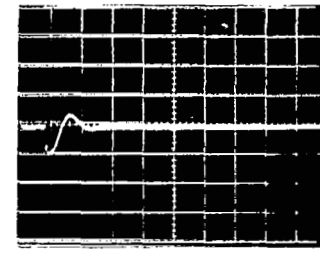

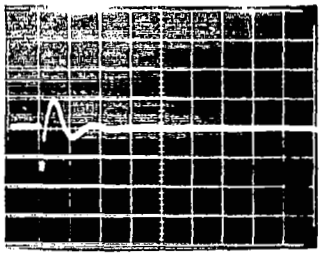

Payload acceleration
$\ddot{x}$; 20 in./sec^2 per div.
t; 1 sec per div.

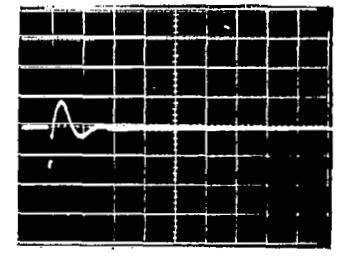

1,000 lb

1,200 lb

Figure 50: Response of nonlinear active isolation system with 1,000 lb. rigid payload to a 0.5 W force step applied at the payload for 2.93 Hz notch frequency. Relative displacement and velocity gains increased at $|\delta_1| = 4.0$ inches with displacement bias at $\delta_1 = 3.65$ inches.

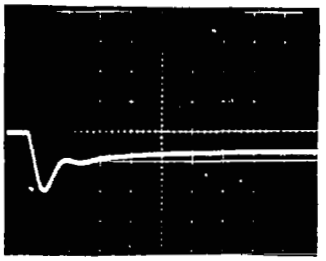

Payload relative displacement
δ_1; 1 in.per div.
t ; 1 sec per div.

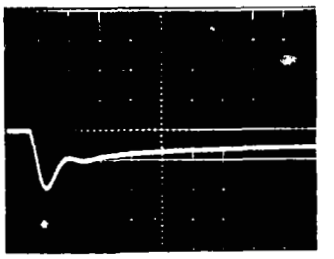

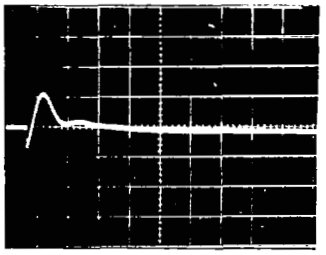

Actuator piston displacement
δ_2; 1 in.per div.
t ; 1 sec per div.

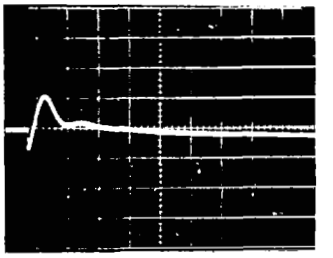

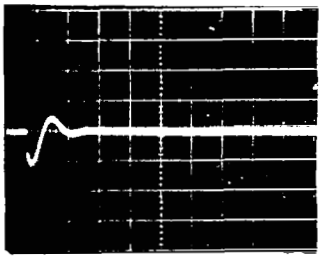

Actuator piston velocity
$\dot{\delta}_2$; 5 in./sec per div.
t ; 1 sec per div.

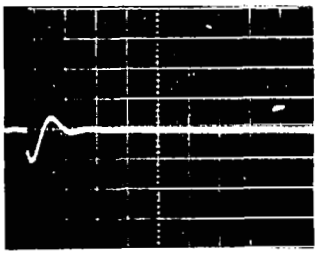

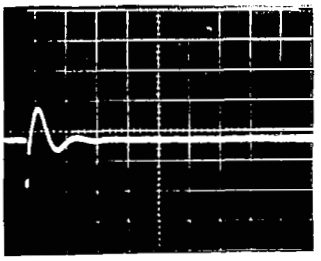

Payload acceleration
$\ddot{x}$; 20 in./sec^2 per div.
t; 1 sec per div.

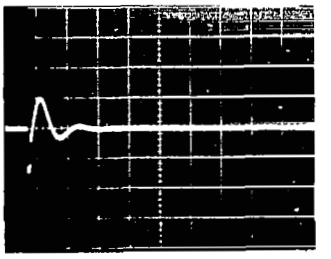

1,000 lb

1,200 lb

Figure 51: Response of nonlinear active isolation system with 1,000 lb. rigid payload to a 0.5 W force step applied at the payload for 8.8 Hz notch frequency. Relative displacement and velocity gains increased at $|\delta_1|$ = 4.0 inches with displacement bias at δ_1 = 2.15 inches.

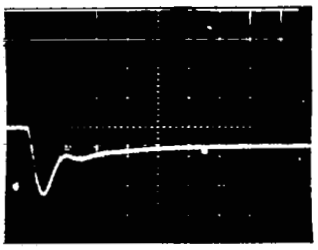

Payload relative displacement

δ_1; 1 in.per div.

t ; 1 sec per div.

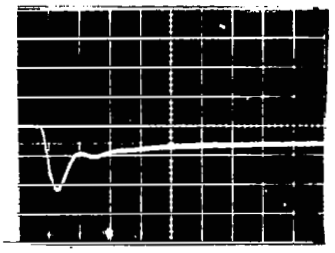

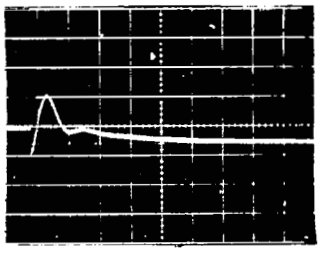

Actuator piston displacement

δ_2; 1 in.per div.

t ; 1 sec per div.

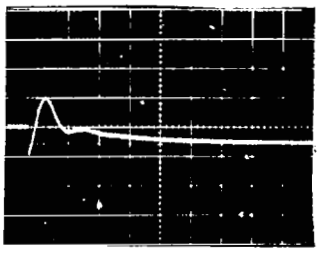

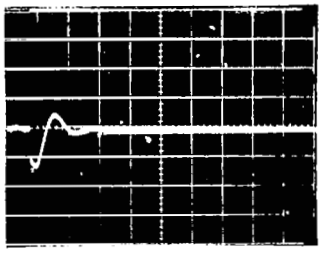

Actuator piston velocity

$\dot{\delta}_2$; 5 in./sec per div.

t ; 1 sec per div.

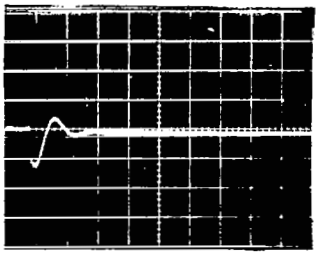

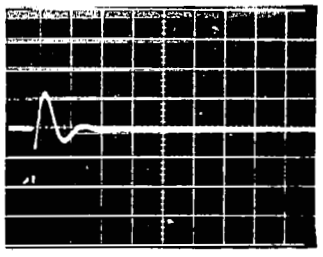

Payload Acceleration

$\ddot{x}$; 20 in./sec^2 per div.

t; 1 sec per div.

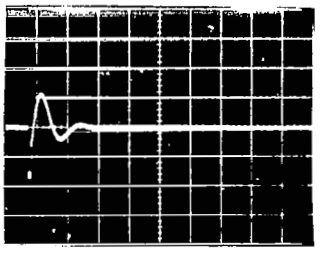

10,000 lb

12,000 lb

Figure 52: Response of nonlinear active isolation system with 10,000 lb. rigid payload to a 0.5 W force step applied at the payload for 0.37 Hz notch frequency. Relative displacement and velocity gains increased at $|\delta_1| = 4.0$ inches with displacement bias at $\delta_1 = 3.65$ inches.

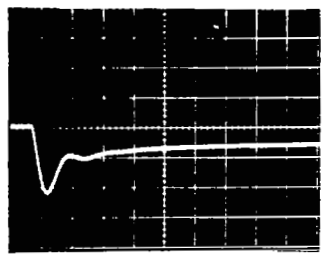

Payload relative displacement
δ_1; 1 in.per div.
t ; 1 sec per div.

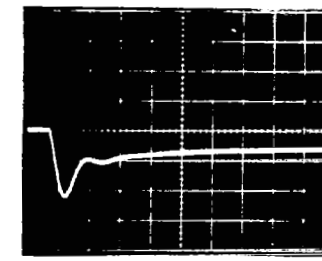

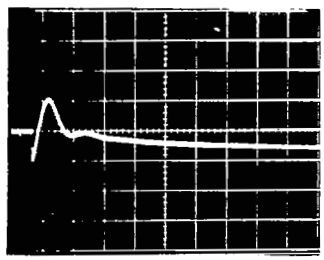

Actuator piston displacement
δ_2; 1 in.per div.
t ; 1 sec per div.

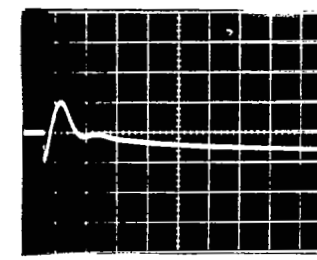

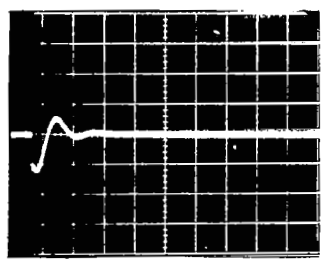

Actuator piston velocity
$\dot{\delta}_2$; 5 in./sec per div.
t ; 1 sec per div.

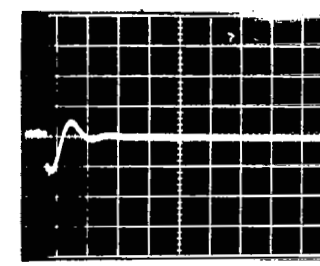

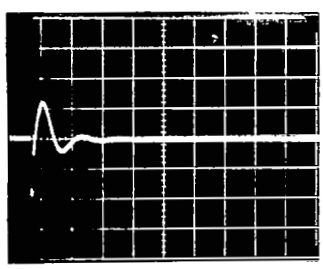

Payload Acceleration
$\ddot{x}$; 20 in./sec^2 per div.
t; 1 sec per div.

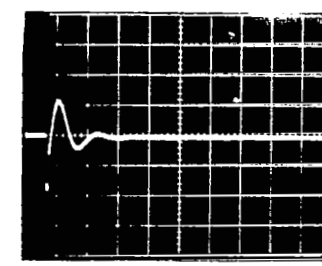

10,000 lb

12,000 lb

Figure 53: Response of nonlinear active isolation system with 10,000 lb. rigid payload to a 0.5 W force step applied at the payload for 8.8 Hz notch frequency. Relative displacement and velocity gains increased at $|\delta_1|$ = 4.0 inches with displacement bias at δ_1 = 2.15 inches.

TABLE XV

PEAK RIGID PAYLOAD RELATIVE DISPLACEMENT UNDER SIMULATED COMBINED VIBRATORY AND TRANSIENT EXCITATIONS FOR NONLINEAR ACTIVE SYSTEM

Payload Weight (lb.)	Notch Frequency (Hz)	Bias Displacement δ_c (in.)	Displacement From Bias Due to Transient $(\delta_1)_{max} - \delta_c$ (in.)	Total Peak Displacement $(\delta_1)_{max}$ (in.)
1,000	0.37	3.65	1.80	5.45
	2.93	3.65	1.95	5.60
	8.8	2.15	2.0	4.15
1,200	0.37	3.65	1.80	5.45
	2.93	3.65	1.80	5.45
	8.8	2.15	1.90	4.05
10,000	0.37	3.65	2.35	6.00
	2.93	3.65	2.35	6.00
	8.8	2.15	2.30	4.45
12,000	0.37	3.65	2.20	5.85
	2.93	3.65	2.25	5.85
	8.8	2.15	2.20	4.35

TABLE XVI

PEAK ACTUATOR PISTON DISPLACEMENT, PISTON VELOCITY, AND PAYLOAD ACCELERATION UNDER SIMULATED COMBINED VIBRATORY AND TRANSIENT EXCITATIONS FOR NONLINEAR ACTIVE SYSTEM

Payload Weight (lb)	Notch Frequency (Hz)	$(\delta_2)_{max}$ (in.)	$(\delta_2)_{max}$ (in./sec)	$\ddot{x}_{max}$	
				(in./sec^2)	(g)
1,000	0.37	1.09	5.5	20	0.052
	2.93	1.10	5.1	30	0.076
	8.8	1.13	6.4	36	0.093
1,200	0.37	0.95	4.9	28	0.074
	2.93	0.99	4.8	19	0.048
	8.8	1.08	5.1	29	0.074
10,000	0.37	1.15	6.4	36	0.093
	2.93	1.15	6.4	36	0.093
	8.8	1.05	6.4	38	0.098
12,000	0.37	1.00	5.3	34	0.088
	2.93	1.00	5.5	34	0.088
	8.8	1.10	5.7	34	0.088

Flexible Payload

The transfer functions for the system with flexible payload and nonlinear gains are identical to those for the linear system shown in Equations (25), (26) and (27) except that the displacement loop gain $G_d(s)$ is replaced by the nonlinear gain $G_d'(s)$ defined in Equation (28). The schematic and analog block diagrams of the nonlinear active system with flexible payload are shown in Figures 54 and 55, respectively.

The values of linear and nonlinear gains previously defined were used to evaluate the response of flexible payloads. The nonlinear gains are introduced in such a manner that the response to vibratory excitation is identical to that of systems employing linear gains. Therefore, only minor differences should exist between the response of the linear systems to transient or combined excitations, and that of systems with nonlinear gains.

In order to verify the effect of a flexible payload on the system response to the step force, values of transient variables are calculated for a 10,000 lb payload having resonant frequency of 5 Hz and 10 percent of critical damping, with a notch frequency of 2.93 Hz. Figure 56 shows a comparison between the time histories of the response variables with rigid and flexible payloads. The peak values at the variables are identical since they are primarily determined by the active portion of the system. The flexible payload exhibits lower displacement values of the second peak due to the additional damping introduced in the overall system. Therefore, it is concluded that the peak response of the 5 and 10 Hz resonant frequency flexible payloads is identical to that shown in previous paragraphs for the rigid payload.

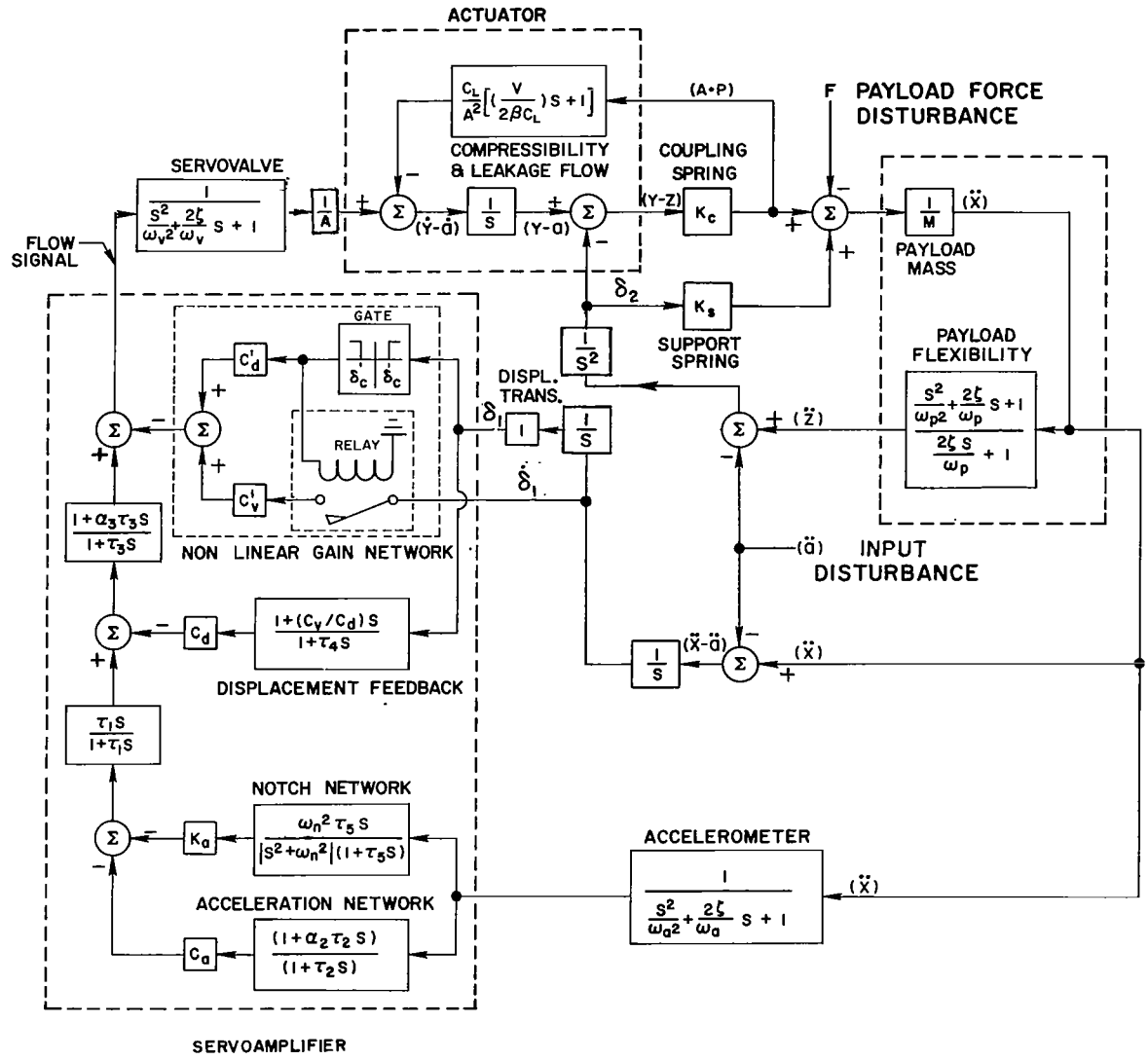

Figure 54: Schematic block diagram of nonlinear active system with flexible payload.

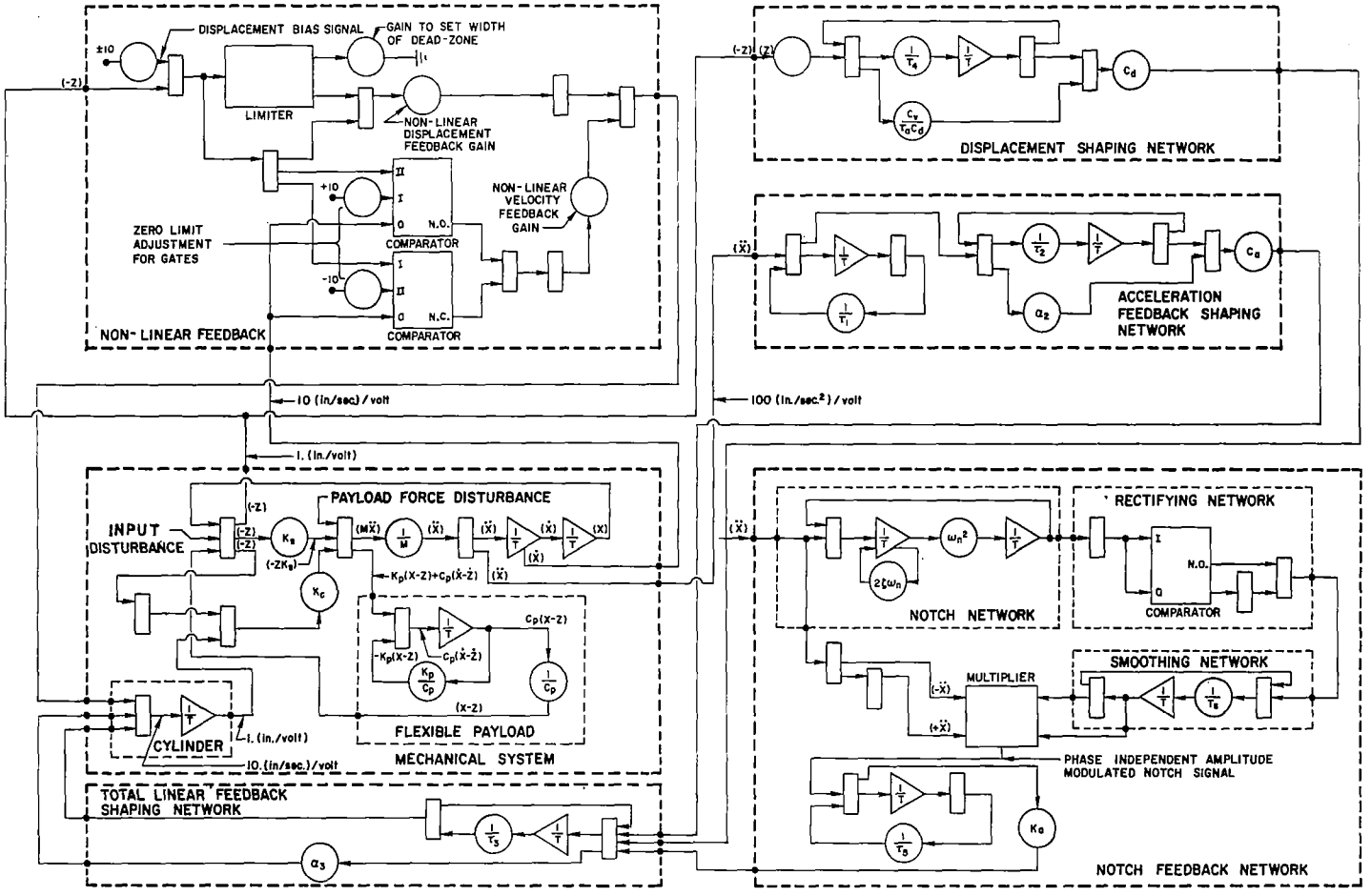

Figure 55: Analog block diagram of nonlinear system with flexible payload.

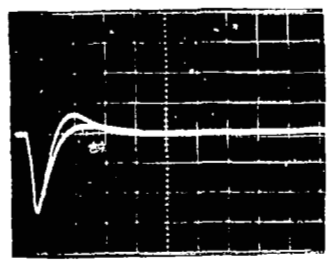

Payload relative displacement

δ_1; 2 in. per div.

t ; 2 sec per div.

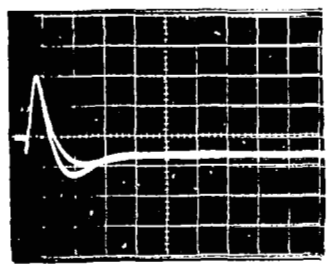

Actuator piston displacement

δ_1; 2 in. per div.

t ; 2 sec per div.

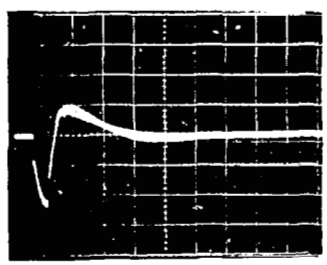

Actuator piston velocity

$\dot{\delta}_2$; 5 in./sec per div.

t ; 1 sec per div.

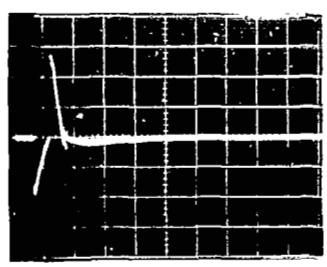

Payload Acceleration

$\ddot{x}$; 20 in./sec^2 per div.

t; 1 sec per div.

In all cases, the time histories with the highest absolute value at the second peak applies to the rigid payload.

Figure 56: Comparison between the response of rigid and flexible 10,000 lb. payloads to a 0.5 W force step applied at the payload for 2.93 Hz notch frequency. Relative displacement and velocity gains increased at $|\delta_1|$ = 4.0 inches.

SECTION 6: DISCUSSION OF RESULTS

Secondary suspension systems incorporating electrohydraulic isolation systems are designed to provide the degree of protection required for passenger comfort, and the displacement control necessary for vehicle stability, based on the postulated levels and frequency content of the vertical excitations reaching the payload of tracked air cushion vehicles. The active system consists of a fluidic static load support spring in parallel with an active isolator. The isolator as proposed contains: an actuator, flexible coupling, servovalve, servoaccelerometer, displacement transducer, and a servoamplifier. The servoamplifier includes: a narrow-band high-gain network (notch) for the isolation of the discrete vibration excitations emanating from the sag between guideway supports; a wide-band shaping network which, in combination with the flexible coupling, provides isolation of the wide-band excitations caused by guideway unevenness; and compensation networks to insure both system stability and displacement control.

The various components of the selected designs, with the exception of the absolute tracking notch network, have been used in previous applications. Experimental results have verified the feasibility of realizing a wide variety of analytically predicted performance characteristics. It is expected that, based on experience with basic tracking notch networks, electronic components of high reliability and low drift can be used to yield the absolute tracking notch circuit. A means must be incorporated, however, to insure that the notch frequency always equals the discrete frequency of sinusoidal excitation.

The frequency of the sinusoidal excitation is equal to the span length divided by the ground speed of the vehicle. Thus, since the span length can vary in a random fashion from span to span, it follows that the sinusoidal excitation frequency will also vary. The variation of the excitation frequency is almost a single function of the span length itself since the speed of the

vehicle will be nearly constant over the length of any given span. Therefore, the notch circuit must be capable of detecting very rapid changes in frequency as the vehicle traverses spans of varying lengths. One approach is to place code markers at the start of each span which identifies the span length ahead. The frequency of excitation for the forecoming span length is calculated by dividing the vehicle ground speed by the indicated span length detected from the code sensor. The frequency calculated is converted to a DC voltage proportional to the excitation frequency. This DC voltage is applied to the tracking notch network to set the notch frequency of the entire isolation system. In this manner the notch frequency can be changed almost instantaneously, giving the desired sinusoidal isolation for conditions of step changes in the excitation frequency.

The results presented in Sections 4 and 5 show that it is analytically feasible to provide the desired level of isolation and displacement control employing available hardware and experimentally proven techniques. Therefore, it is anticipated that such suspension systems will have application to a wide range of problem areas including TACV. In the following paragraphs the flow and power requirements for the selected designs are calculated. Comments regarding system reliability and weight estimates are presented in Section 7.

One final comment should be made which deals with the postulated levels of dynamic excitation. It is possible that the ± 3 inch level of vertical sinusoidal displacement excitation from the guideway is representative of a very "poor" guideway design. However, even if the postulated guideway unevenness is the most severe vibratory excitation, a wide-band isolation system having a 0.2 Hz resonant frequency would be required. Also, a vertical step force of 0.5W is probably too severe a design condition. Nevertheless, even lower values of transient forces at the payload would prevent use of a passive system since the desired degree of isolation could not be provided while

simultaneously limiting the displacement of a 0.2 Hz resonant frequency passive isolator under combined excitations to ± 6 inches.

Flow and Power Requirements. - The peak flow required to obtain the nonlinear gain system performance shown in Section 5 is equal to the sum of the flows required for: isolation of the discrete frequency sinusoidal excitation, Q_s; isolation of the sinusoidal broad-band excitation postulated by NASA LRC to be equivalent to the expected random excitations, $Q_{3\sigma}$; and the flow required to limit the deflections under transient force excitations to 6 inches, Q_F.

The peak flow required for isolation of the discrete frequency sinusoidal excitations Q_s is equal to the product of the peak excitation displacement and the flow value at the excitation frequency. Flow values are given in Appendix C. The peak flow required for isolation of the broad-band sinusoidal excitation $Q_{3\sigma}$ is given by

$$Q_{3\sigma} = 3\sqrt{\int_{\omega_1}^{\omega_2} Q^2(\omega)\, a^2(\omega)\, d\omega} \qquad (29)$$

where $Q(\omega)$ is the flow value as a function of frequency and $a(\omega)$ is the RMS displacement function specified as the broad-band displacement excitation. Table XVII shows the minimum and maximum peak flow requirements.

The flow output of the hydraulic servovalve depends upon the hydrostatic pressure drop across the servovalve. For conditions of steady-state vibration excitation, the pressure drop within the actuator times the actuator area is equal to the force which results from the deflection of the static load support springs; namely, ten percent of the payload weight divided by the net actuation area. Therefore, the pressure drop available across the servovalve for steady-state conditions is given by the difference between the supply pressure and the pressure drop

TABLE XVII

MINIMUM AND MAXIMUM PEAK FLOW REQUIREMENTS

Requirement	Nominal Payload (lb)	Q_s (in^3/sec)	$Q_{3\sigma}$ (in^3/sec)	Q_F (in^3/sec)	Required Peak Flow Q_T	
					(in^3/sec)	(gpm)
Minimum: (0.37 Hz notch; 50 mph)	1,000	4.80	1.1	6.05	11.95	3.08
	3,000	7.05	1.52	11.73	20.30	5.05
	10,000	21.90	4.72	35.2	61.82	15.90
Maximum: (8.8 Hz notch; 300 mph)	1,000	57.0	24.7	6.40	88.10	22.78
	3,000	89.5	38.8	12.93	141.23	36.4
	10,000	273.0	118.0	38.9	429.90	111.5

TABLE XVIII

MAXIMUM AVAILABLE STEADY-STATE SERVOVALVE FLOW

Payload (lb)	Supply Pressure (psi)	Pressure Drop Across Actuator (psid)	Available Pressure Drop Across Valve (psid)	Servovalve Type (Moog Inc.)	Available Peak Valve Flow (in^3/sec)
1,000	1892	149	1743	35	98
3,000	2833	306	2527	72	356
10,000	3000	335	2665	79	767

across the actuator. Table XVIII lists the peak actuator pressure drop under vibratory excitations, the resulting minimum servovalve pressure drop, and the maximum available flow output from each of the servovalves used. A comparison between the maximum required (Table XVII) and maximum available (Table XVIII) flows indicates that for the combined transient and vibratory excitations the servovalves selected in each case are capable of supplying the flow required to provide the desired vibration isolation characteristics and displacement control.

Finally, the required pump power can be calculated in terms of the time average flow since accumulators within the hydraulic power supply can integrate over the peak flow demands. The maximum required pump flow is given on Table XIX for the three payload weights. The required system power, equal to the product of average flow and system supply pressure, is also shown on Table XIX for each payload.

TABLE XIX

MAXIMUM REQUIRED PUMP FLOW AND POWER

Payload (lb)	Pump Flow (gpm)	Pump Power (HP)
1,000	13.4	15.0
3,000	18.1	30.0
10,000	54.3	94.5

SECTION 7: SYSTEM RELIABILITY, AND WEIGHT ESTIMATES

System Reliability

The system reliability is discussed in terms of reliability of individual components, and system failure and failsafe considerations. The comments are based on manufacturer's data and on Barry Controls' past experience with active isolation systems.

Component Reliability: The maintenance and reliability of the hydraulic portion of the isolation system are minimal and good, respectively. One of the most important precautions for obtaining an effective system is to start with and maintain a clean system. This requirement is paramount for obtaining required servovalve performance. Its performance depends on fine flapper valve orifices remaining open, sharp edges on control lands and ports remaining sharp, and tight sliding fits remaining free. Before assembling oil lines, fittings, and components, they must be thoroughly cleaned and flushed out to remove all traces of dirt and lint. Particular attention should be given to cylinder actuators, pumps, pressure and flow control valves, and reservoirs. Cleaned parts should be capped if they are to be stored for any length of time before being assembled. Oil to be used in the system should be purchased from companies that are capable of putting the oil through a high degree of filtration. In assembling the unit, all conections should be made tight so that no possible leakage can occur in a vibration environment.

The Moog model 35, 72 and 79 servovalves used in the selected systems are high precision instruments qualified for a variety of missile and aircraft applications. In many qualification programs these valves have met and even exceeded the environmental requirements of MIL-V27162, MIL-H-8775B, and MIL-E-5272C, and physical requirements of SAE ARP-490A, particularly in areas of vibration and shock. The servovalves will be maintenance free and give good reliable operation provided that all cleanliness

precautions are taken. The torque motor flapper of the servovalve's first stage is not affected by the input vibration and remains stable throughout the frequency range. The rated life expectancy should exceed 1000 hours continuous operation while providing tight servo control. Actually, servovalve operation could continue for a much longer time except for the wearing and rounding of the sharp-edged lands and ports due to erosion. This effect will cause a minor decrease in control action. However, vibration isolation would be maintained under these conditions.

The linear hydraulic piston actuator can be designed to provide long life operation limited only by effective sealing. the cylinder chamber is sealed along the piston rod by internal seals. The actuators should be guided in a manner that prevents radial loads or torques of the rod seals and bearings. The reliability and maintenance of the piston actuator will depend on the minimum leakage that can be tolerated over periods of time. The leakage levels considered here are very small and will not effect the piston's force capability.

The electrical analog system controller should be manufactured of high quality solid state operational amplifiers which can be designed to be relatively failure free over long periods of time, provided that routine maintenance checkout and adjustments are performed to detect and replace possible weakened components.

The proposed accelerometer transducer for sensing payload acceleration is a Kistler Model 305A type. This model utilizes a series of flexure arms to support and guide a symmetrical element along one well defined axis so as to insure true translational linear displacement. This design has been proven reliable in many missile telemetry system applications. The sealed case contains a solid state amplifier. The accelerometer should be handled with care and not dropped. Once assembled in its operation position it is a reliable, maintenance free unit.

The proposed relative displacement transducer for sensing displacement between the isolated body and input motion at the base of the isolator is a DCDT (direct current differential transformer). The transformer (Tresco, Inc.) has a built in 1000 Hz exciter carrier oscillator and phase sensitive demodulator. The input is 15 volts D.C. and the output is a voltage that is linearly dependent on relative displacement. The reliability is good and there should not be any maintenance required.

Failure and Failsafe Consideration: The loss of hydraulic pressure would gradually decrease and stop the operation of both the active isolation system and the static load support system. The passive flexible coupling would continue to provide vibration isolation at frequencies above 2 or 2.5 hz. If fluid loss occurs and the servovalve does not block the actuator ports, the payload will lower until the piston reaches the end of its stroke. Under such a condition it would be important to slow the vehicle to a speed wherein the passive isolation of the flexible coupling alone could provide the required degree of isolation for safe operation of the vehicle. Therefore, an automatic low pressure warning device should be incorporated within the system to warn the operator of a slight low pressure condition, and engage an automatic circuit as pressure loss occurs to slow the train to a safe speed. Failure of the electronics, although it can be minimized through proper design, would have effects similar to the loss of hydraulic pressure and should, therefore, be coupled to the automatic speed reduction device mentioned above.

Seal failure causing excessive leakage in the actuator or elsewhere would necessitate shutting down the system. Should the servovalve operation deteriorate due to clogging up of small passages, then the system would have to be shut down at a convenient time. The only precautions against this happening are, of course, the system filters and the initial precautions of starting with a clean system. Loss of the electrical control signal

to one or both of the valve torque motor coils will cause erratic operation or possible failure of the valve. Then the active isolation ceases.

The failure of the servoaccelerometer would result in the loss of the isolation characteristics. However, in the event of such a failure, the control system would remain stable and offer displacement control and high frequency passive isolation.

The loss of the displacement feedback signal would result in a system having acceleration feedback only. Such a system configuration leads to drifting of the actuator until the piston engages either the top or bottom cylinder block. The system would then chatter and bounce off the stroke limit position. Continued operation under these conditions could result in permanent damage to the actuator.

Failure of the electronics in the acceleration feedback loops can occur in two parallel modes. The first possibility is an operational amplifier failure which would apply a large DC voltage to the input of the following stage. This form of failure in either acceleration loop would saturate components common to both loops and block acceleration signals from performing their functions; thus such a failure would result in the loss of active isolation. The control system would be stable and exhibit displacement control only.

The second form of failure is that resulting in a gain change from the nominal settings. The complete loss of gain in either acceleration circuit would result in the same system changes as described for the failure of the accelerometers themselves. A failure resulting in a gain reduction within the servoaccelerometer feedback loop would result in a stable control system but a reduced bandwidth of the notch isolation. Failure resulting in a gain increase within this network will result in large notch bandwidth and larger resonant magnitudes. Extremely large (10 to 20 db) gain increases within the feedback loop

can result in an unstable condition of the control system. This results in large amplitude low frequency oscillations.

Failure resulting in a gain increase within this network would cause over correction of the feedback controls resulting in the loss of isolation or amplification of the high frequency excitations. Very large gain increases (10 to 20 db) could cause an unstable condition resulting in large frequency oscillations of the isolator as well as the loss or amplification of high frequency isolation characteristics.

Weight Estimates

The weight of the entire vibration isolation system cannot be determined since the mechanical configuration of the support system and air cushion structure for the TACV have not yet been determined. However, the weight of the principal components of the isolation system can be estimated based on the selected components, and the flow and hydraulic power requirements for each payload weight.

The weight of the electronic components would not vary with payload weight. The complete electronic control can be packaged in such a manner that the total weight does not exceed 50 lb.

The weight of the mechanical components is a function of the payload weight, and the flow and power requirements associated with each selected system. Estimates for each payload weight are given below and on the next page.

1,000 lb Payload Weight	Weight
Servovalve	3 lb
Actuator	20-40
Hydraulic Power Supply (Less motor and tubing)	75-150
Static Load Support Valve	1-3
Static Load Support System	20-30
	119-226

		Weight
3,000 lb Payload Weight		
Servovalve		8 lb
Actuator		30-50
Hydraulic Power Supply (Less motor and tubing)		200-250
Static Load Support Valve		1-3
Static Load Support System		30-40
	Total:	259-351 lb
10,000 lb Payload Weight		
Servovalve		20 lb
Actuator		90-150
Hydraulic Power Supply (Less motor and tubing)		400-600
Static Load Support Valve		1-3
Static Load Support System		120-150
	Total:	621-950 lb

The estimated combined total weight of the electronic and mechanical components are as follows:

1,000 lb Payload Weight:	119-226 lbs
3,000 lb Payload Weight:	309-401 lbs
10,000 lb Payload Weight:	671-1,000 lbs

It is anticipated that the TACV units will weigh more than 10,000 lbs. Whether the complete unit or separate compartments within the units are isolated would depend on strength consideration, flexibility of the unit, and location of passenger section within the unit. If the necessary weight associated with the mechanical interface between the isolation system itself, and the air cushions and payload are included, it is expected that the weight of the system for a 10,000 lb. payload would range from 1,000 to 1,500 lbs.

SECTION 8: CONCLUSIONS

Specific conclusions based on the results of the investigation are:

(1) Electrohydraulic isolators can be designed utilizing available components to provide isolation of high level vibratory excitations and limit the displacements due to transient loadings.

(2) In order to meet the postulated requirements for high speed ground transportation vehicles, isolation systems consisting of a static load support fluidic spring in parallel with a 0.2 Hz resonant frequency electrohydraulic isolator are selected. The isolator contains: an actuator, flexible coupling, servovalve, accelerometer, displacement transducer, and a servoamplifier. The servoamplifier includes a tracking narrow-band high gain network for the isolation of the discrete frequency vibratory excitations; a wide-band shaping network which, in combination with the flexible coupling, provides wide-band isolation; and compensation networks to insure both system stability and displacement control.

(3) In all cases, the vertical acceleration transmitted to isolated rigid and flexible payloads weighing 1,000, 3,000 and 10,000 pounds is maintained within levels compatible with human comfort (0.01g from 1.5 to 7.5 Hz). The maximum relative displacement under the combined vibratory excitations and step force at the payload is 6 inches.

(4) Isolation system flow requirements range from 13.4gpm for 1,000 pound payload, to 54.3gpm for 10,000 pound payload.

(5) For 3,000 psi supply pressure, the pump power requirements range from 15 HP for 1,000 pound payload, to 94.5 HP for 10,000 pound payload.

(6) Estimated system weights range from 119 pounds for 1,000 pound payload, to 1,000 pounds for 10,000 pound payload.

SECTION 9: RECOMMENDATIONS

The analysis presented in this report includes a representation of the dynamics of the various components. Therefore, the payload response to vibratory and transient excitations does take into consideration high frequency effects. However, the transfer functions selected for the components do not consider the higher order effects which are exhibited by actual hardware. Therefore, as is common practice in all active control systems, the values selected analytically prove the feasibility of the approach and serve as the starting point for final design. Final selection of gains and compensation networks must be made on the basis of laboratory testing.

In most applications the dynamic excitations occur in more than one direction. The isolation system selected on the basis of vertical excitations can be used for multidirectional inputs. However, from the point of view of system stability, it is important that active isolation systems of the type described in this report be evaluated based on multidirectional inputs.

Based on the results of this investigation and the comments made above it is recommended that:

(1) The results of the analysis be verified experimentally in the laboratory by the construction and testing of a single degree-of-freedom model.

(2) The same approach be taken to evaluate and test the application of similar active systems for the protection of rigid and flexible payloads subjected to severe multidirectional dynamic environments.

APPENDIX A

STATIC LOAD SUPPORT SYSTEM

The function of the static load support system is to remove all static weight from the hydraulic actuator, thereby allowing the use of a smaller actuating area and reducing the flow and power requirements of the control system.

Figure 57 indicates the schematic diagram of the static load support system. It consists of a single acting hydraulic cylinder connecting the payload to the TACV air cushion. The hydraulic actuator is connected to a large accumulator. The pressure within the accumulator P' is regulated by a small flow-control servovalve. The servovalve flow is, in turn, controlled by the differential pressure across the main hydraulic actuator of the active isolation system, P_d.

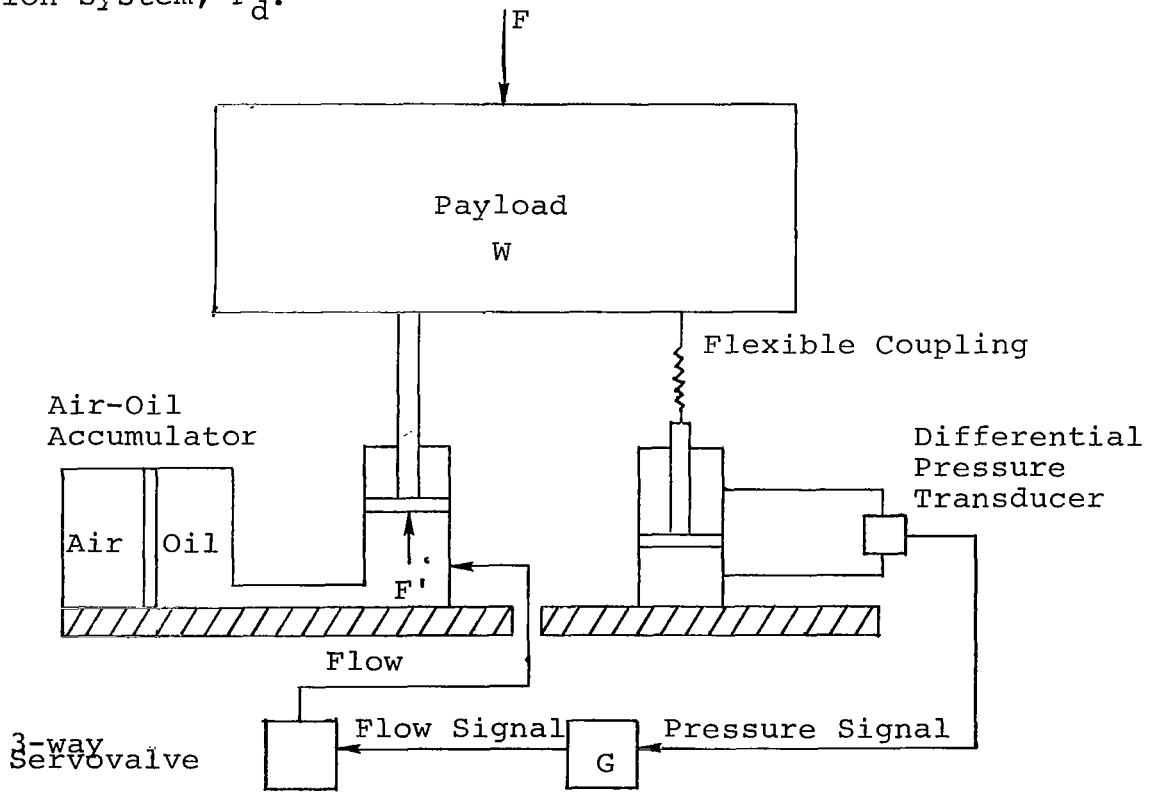

Figure 57: Schematic diagram of static load support system

The flow from the 3-way valve $Q'(s)$ in terms of the loop gain G and using Laplace notation, is given by

$$Q'(s) = G\, P_d(s) \tag{A-1}$$

The force summation at the main hydraulic actuator in terms of the main actuator area A, the payload applied force F, the payload weight W, and the force developed by the load support spring F', is given by

$$A\, P_d(s) = F(s) + W - F'(s) \tag{A-2}$$

The force summation at the load support spring in terms of the accumulator cross-sectioned area A', the accumulator preload pressure P_o, and the load support stiffness K is given by

$$F'(s) = P_o A' + \frac{Q'(s)}{A's} \tag{A-3}$$

For a large accumulator ($A_1 > A'$) the load support stiffness is a constant given by [Ref. 10]

$$K = \frac{2\, n\, P_i\, A_1^2}{V_o} \tag{A-4}$$

where

V_o = volume of air in accumulator
n = gas constant ≈ 1.2
P_i = accumulator nominal pressure
A_1 = cross-sectional area of the rod in load support system

The pressure drop in the main hydraulic actuator can be obtained by combining Equations (A-1) through (A-4) and is

given by

$$P_d(s) = \frac{\left[F(s) + W - P_o A'\right] s}{As + \frac{G}{A'} K} \qquad \text{(A-5)}$$

If the value of P_d is equal to zero for a steady force applied at the payload, the force at the actuator will also be zero. For a step load

$$F + W = \frac{\ell_o}{s} \qquad \text{(A-6)}$$

Substituting (A-6) in (A-5 results in

$$P_d(s) = \frac{\left(\frac{\ell_o}{s} - P_o A'\right) s}{As + \frac{G}{A'} K} \qquad \text{(A-7)}$$

Applying the final value theorem to evaluate the final value of the main actuator pressure drop [Ref. 11] results in

$$\lim_{t\to\infty} P_d(t) = \lim_{s\to o} s\, P_d(s)$$

$$= \lim_{s\to o} \left(\frac{\ell_o s - P_o A' s^2}{As - \frac{G}{A'} K} \right)$$

$$= 0 \qquad \text{(A-8)}$$

The loop gain G forces the load on the main actuator to reach zero as a static force is applied at the payload. Therefore, the static load is supported entirely by the load support system.

The time constant of the load support system is equal to AA'/GK. For long time constant (high loop gain), the flow required for minor differential pressure disturbances will be very small. To insure small flow requirements for vibratory disturbances a lag compensation can be added to the loop to filter out high frequency pressure changes.

APPENDIX B

DIGITAL COMPUTER PROGRAM

The solution of system steady-state equations as a function of frequencies for the open loop transfer function, absolute and relative transmissibility, flow, and stroke were programmed on a CDC 3600 time shared digital computer. The computer program is written in the Multicomp Fortran Language and is shown at the end of this appendix. A flow chart of the program is shown in Figure 58.

The program contains the system steady-state equations for the open and closed loop response of the electrohydraulic vibration isolation system with the flexible payload. A similar program was used for the calculation of the steady-state open and closed loop response of the electrohydraulic vibration isolation system with the rigid payload, with $K_p = \infty$ and $C_p = 0$.

The form of the system equations must show the numerator and denominator as a series of products and summations of complex polynomials by the expression

$$\frac{(R_{1,1}+ I_{1,1})\cdots(R_{1,10}+ I_{1,10})+\cdots(R_{10,1}+ I_{10,1})\cdots(R_{10,10}+ I_{10,10})}{(R_{11,1}+ I_{11,1})\cdots(R_{11,10}+ I_{11,10})+\cdots(R_{20,1}+ I_{20,1})\cdots(R_{20,10}+ I_{20,10})}$$

where R represents the real part of a complex polynomial, and I represents the imaginary part of a complex polynomial. Both the numerator and the denominator of each system formulation may contain up to ten sets of products of complex polynomials, and each product set may contain up to ten complex polynomials.

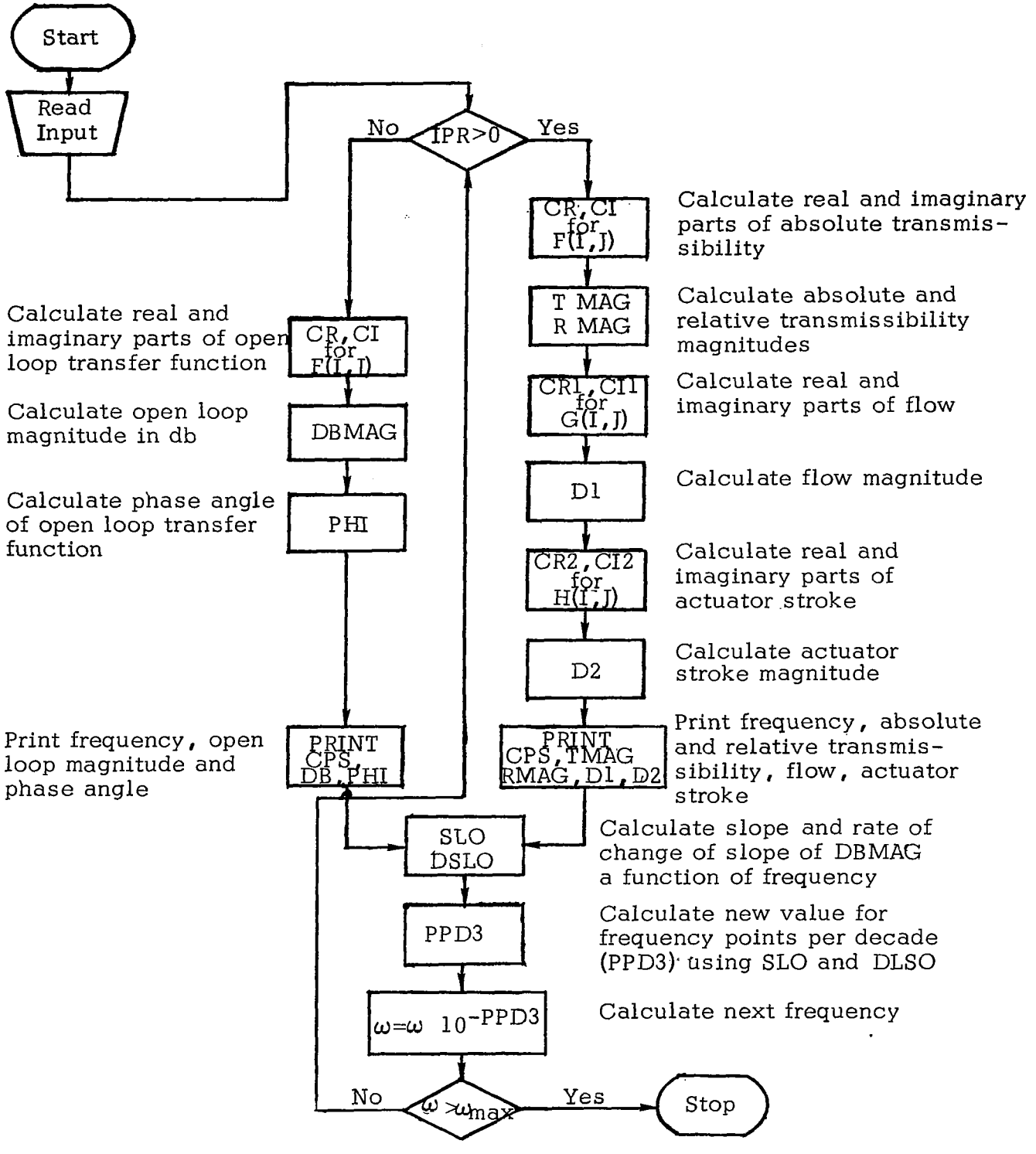

Figure 58 : Flow chart for digital computer program.

DIGITAL PROGRAM NOMENCLATURE

TERM	REPRESENTS
I	Identifies product chain set of each system equation.
J	Identifies complex polynomial of each product set defined by I. Odd J terms are real parts of complex polynomials and even J terms are imaginary parts of complex polynomials.
E(I,J)	Complex polynomials of open loop system transfer function.
NE(I)	Number of complex polynomials in I^{th} product chain set of open loop system transfer function.
F(I,J)	Complex polynomials of closed loop absolute transmissibility transfer function.
N(I)	Number of complex polynomials in I^{th} product chain set of absolute transmissibility transfer function.
G(I,S)	Complex polynomials of closed loop system flow transfer function.
NG(I)	Number of complex polynomials in I^{th} product chain set of system flow transfer function.
H(I,J)	Complex polynomials of closed loop system state transfer function.
NH(I)	Number of complex polynomials in I^{th} product chain set of system state transfer function.
A,L,LI	Run and casecount variables.
C(I)	Parameter coefficients of feedback system $C(1) = C_a/A$; $C(2) = K_a/A$; $C(3) = C_d/A$; $C(4) = C_v/A$; $C(5) = \tau_1$; $C(6) = \alpha_2$; $C(7) = \tau_2$; $C(8) = \alpha_3$; $C(9) = \tau_3$; $C(10) = \tau_4$; $C(11) = \tau_5$; $C(12) = F_n$; $C(13) = M$.
FB	Frequency at which solution starts (CPS).
WB	Frequency at which solution starts (RAD/SEC).
FE	Frequency at which solution ends (CPS).
WE	Frequency at which solution ends (RAD/SEC).

PPD4	Minimum number of frequency data points per decade.
lPR	Computer control parameter. For lPR = 0, only open loop transfer function is calculated. For lPR = 1, all closed loop transfer functions are calculated. For lPR = 2, only closed loop transmissibilities are calculated.
FN LOAD	Resonant frequency of undamped flexible payload, Hz.
2 LOAD	Fraction of critical damping of flexible payload.
CN	Isolation system constants. C1 = actuation area; C2 = K_c; C3 = K_s; C4 = K_p; C5 = C_p; C6 = β; C7 = V; C8 = C_L; C9 = ω_{sv}; C10 = ζ_{sv}.
WL1	Gain function for narrow-band feedback.
W	Frequency, RAD/SEC.
AWGAIN	Imaginary part of total wide-band gain.
ANGAIN	Real part of total narrow-band gain.
T1S	Imaginary part of wide-band lead network transfer function $(\frac{\tau_1 s}{1 + \tau_1 s})$.
A2T2S	Imaginary part of numerator of shaping lead-lag network $(\frac{1 + \alpha_3 \tau_2}{1 + \tau_2})$.
T2S	Imaginary part of denominator of shaping lead-lag network.
A3T3S	Imaginary part of numerator of compensation lag-lead network $(\frac{1 + \alpha_3 \tau_3 s}{1 + \tau_3 s})$.
T3S	Imaginary part of denominator of compensation lag-lead network.
T4S	Imaginary part of displacement feedback lag network $(\frac{1}{1 + \tau_4 s})$.
T5S	Imaginary part of narrow-band lead network $(\frac{\tau_5 s}{1 + \tau_5 s})$.
ANOTCH	Absolute value of denominator of narrow-band notch network.

SUREAL	Real part of denominator of servovalve transfer function.
SV1MAG	Imaginary part of denominator of servovalve transfer function.
AST1F	Represents $\frac{V}{2\beta A^2}$
ALEAK	Represents C_L/A^2
CR3	Real part of open loop transfer function.
CI3	Imaginary part of open loop transfer function.
DBMAG	Open loop magnitude in db.
CR,XREAL	Real part of absolute transmissibility.
CI,X1MAG	Imaginary part of absolute transmissibility.
TMAG	Absolute transmissibility.
RMAG	Relative transmissibility.
PHI	Phase angle of open loop transfer function.
SCO	Scope of transmissibility curve.

A listing of the computer program for the flexible payload is shown in the following pages.

```
LIST TACVF1
100↑       PROGRAM TACVF
110* FORM IS TEN CHAINS OF PRODUCTS OF TEN COMPLEX NUMBERS IN BOTH
120* NUMERATOR AND DENOMINATOR; THREE SUCH FUNCTIONS MAY BE CALCULATED
130* AT ONE TIME; IPR=0 GIVES MAG AND PHASE OF FIRST FUNCTION
140* IPR=1 GIVES MAG OF ALL THREE FUNCTIONS,F(I,J),G(I,J),H(I,J)
150* IPR>1. GIVES THE MAGNITUDES OF THE F(I,J) FUNCTION ONLY.
160* ODD J TERMS ARE REAL, EVEN J TERMS ARE IMAGINARY.
170        DIMENSION E(20,20),NE(20),F(20,20),N(20),G(20,20),NG(20)
171A H(20,20),NH(20),C(50)
175        DATA(NE=7,5,7,0,0,0,0,0,0,0,9,8,0,0,0,0,0,0,0,0)
180        DATA(N=9,7,0,0,0,0,0,0,0,0,0,9,9,7,5,7,0,0,0,0,0)
190        DATA(NG=8,6,8,7,0,0,0,0,0,0,0,8,0,0,0,0,0,0,0,0,0)
200        DATA(NH=3,3,2,0,0,0,0,0,0,0,1,0,0,0,0,0,0,0,0,0)
210        PI=3.14159265
220        A=1;L=1;L1=1
230↑    10 INPUT,C(6),C(7),C(8),C(9),C(12),FB,FE,PPD4,IPR
231        C(1)=0.5; C(2)=0.2; C(3)=0.576; C(4)=0.3
232        C(5)=8.63; C(10)=1.27; C(11)=1.
233        C(13)=2.5906
236        FNLOAD=10.
237        FNLOAD=2.*PI*FNLOAD
238        ZLOAD=0.
240        C1=0.673;C2=639.0; C3=14.3
241        C4=C(13)*FNLOAD**2; C5=ZLOAD*2.*C(13)*FNLOAD
242        C6=200000.; C7=7.*C1; C8=0.000266
243        C9=2.*PI*100.; C10=0.7
245        WB=2.*PI*FB;WE=2.*PI*FE;C(12)=2.*PI*C(12)
246        WL1=0.39788*(C(12)**2)
247        W=WB
250        PRINT 6,L1,L
255        A=A+0.5;L=A;WB=2.*PI*FB;WE=2.*PI*FE
260        IF(1-IPR) 203,204,205
270↑       204 PRINT 7;PRINT 3;PRINT 4;GO TO 14
280↑       203 PRINT 7;PRINT 3;PRINT 51;GO TO 14
290↑       205 PRINT 8;PRINT 3; PRINT 1
340↑    14 CONTINUE
345        IF(W-0.875*C(12)) 94,95,95
350↑    95 IF(1.125*C(12)-W) 94,96,96
355↑    96 PPD=0.7*PPD4; GO TO 97
360↑    94 PPD=PPD4
365↑    97 CONTINUE
370* - - - - PLACE ALL COMMON VARIABLES BELOW - - - -
375        AWGAIN=-C(1)*C(5)*(W**3);T5=C(11)/C(12)
376        ANGAIN=C(2)*C(5)*T5*WL1*C(12)*(W**4)
378        T1S=C(5)*W;T2S=C(7)*W;A2T2S=C(6)*C(7)*W
380        T3S=C(9)*W;A3T3S=C(8)*C(9)*W;T4S=C(10)*W
382        T5S=T5*W;ANOTCH=ABS((C(12)**2)-(W**2))
384        SVREAL=1-((W/C9)**2);SVIMAG=2.*C10*W/C9
386        ASTIF=C7/(2.*C6*(C1**2));ALEAK=C8/(C1**2)
```

```
      IF(1-IPR) 201,201,202
  202 CONTINUE
* - - - - PLACE E(I,J) EQUATIONS FOR OPEN LOOP BELOW - - - -
* ------------------------------------------------------------
      E(1,1)=0.;E(1,2)=AWGAIN;E(1,3)=C4;E(1,4)=C5*W
      E(1,5)=1.;E(1,6)=A2T2S;E(1,7)=1.;E(1,8)=A3T3S
      E(1,9)=1.;E(1,10)=T4S;E(1,11)=1.;E(1,12)=T5S
      E(1,13)=ANOTCH;E(1,14)=0.
* -------END OF E(1,J)-------
      E(2,1)=ANGAIN;E(2,2)=0.;E(2,3)=C4;E(2,4)=C5*W
      E(2,5)=1.;E(2,6)=T2S;E(2,7)=1.;E(2,8)=A3T3S
      E(2,9)=1.;E(2,10)=T4S
* --------END OF E(2,J) ---------
      E(3,1)=C(3);E(3,2)=C(4)*W;E(3,3)=C4-C(13)*(W**2);E(3,4)=C5*W
      E(3,5)=1.;E(3,6)=A3T3S;E(3,7)=1.;E(3,8)=T1S
      E(3,9)=1.;E(3,10)=T2S;E(3,11)=1.;E(3,12)=T5S
      E(3,13)=ANOTCH;E(3,14)=0.
* ---------END OF E(3,J) ----------
      E(11,1)=ALEAK;E(11,2)=W*(ASTIF+1/C2)
      E(11,3)=-C(13)*(C3+C4)*(W**2)+C3*C4
      E(11,4)=-C(13)*C5*(W**3)+C3*C5*W
      E(11,5)=1.;E(11,6)=T1S;E(11,7)=1.;E(11,8)=T2S
      E(11,9)=1.;E(11,10)=T3S;E(11,11)=1.;E(11,12)=T4S
      E(11,13)=1.;E(11,14)=T5S;E(11,15)=ANOTCH;E(11,16)=0.
      E(11,17)=SVREAL;E(11,18)=SVIMAG
* --------END OF E(11,J) ---------
      E(12,1)=-C5*(W**2);E(12,2)=-C(13)*(W**3)+C4*W
      E(12,3)=1.;E(12,4)=T1S;E(12,5)=1.;E(12,6)=T2S
      E(12,7)=1.;E(12,8)=T3S;E(12,9)=1.;E(12,10)=T4S
      E(12,11)=1.;E(12,12)=T5S;E(12,13)=ANOTCH;E(12,14)=0.
      E(12,15)=SVREAL;E(12,16)=SVIMAG
* --------END OF E(12,J) --------
* -----A,KC,KS,KP,CP,V,B,CL,WSV,ZSV, ARE FIXED ----
*     C1=A; C2=KC; C3=KS; C4=KP; C5=CP; C6=B
*     C7=V; C8=CL; C9=WSV; C10=ZSV; WL1=A*C(12)**2
* ------------------------------------------------
*     C(1)=CA/A; C(2)=KA/A; C(3)=CD/A; C(4)=CV/A
*     C(5)=T1; C(6)=A2; C(7)=T2; C(8)=A3; C(9)=T3
*     C(10)=T4; C(11)=T5*C(12)=WN; C(13)=M
* ------------------------------------------------------------
      CALL TRA(E,NE,CR3,CI3)
      TMAG=SQRT((CR3**2)+(CI3**2))
      DBMAG=20.*0.43429*ALOG(TMAG)
      CALL ARCTAN(CR3,CI3,ANGLE,ERROR)
      GO TO 207
  201 CONTINUE
* - - - - PLACE F(I,J) EQUATIONS FOR TRANSMISSIBILITY BELOW - - - -
* ------------------------------------------------------------
```

```
672         F(1,1)=ALEAK*C3;F(1,2)=(ASTIF*C3+1+(C3/C2))*W
674         F(1,3)=C4;F(1,4)=C5*W;F(1,5)=1.;F(1,6)=T1S
676         F(1,7)=1.;F(1,8)=T2S ;F(1,9)=1.;F(1,10)=T3S
678         F(1,11)=1.;F(1,12)=T4S;F(1,13)=1.;F(1,14)=T5S
680         F(1,15)=ANOTCH;F(1,16)=0.;F(1,17)=SVREAL;F(1,18)=SVIMAG
682* --------END OF F(1,J) --------
684         F(2,1)=C(3);F(2,2)=C(4)*W;F(2,3)=1.;F(2,4)=A3T3S
686         F(2,5)=C4;F(2,6)=C5*W;F(2,7)=1. ;F(2,8)=T1S
688         F(2,9)=1.;F(2,10)=T2S;F(2,11)=1.;F(2,12)=T5S
690         F(2,13)=ANOTCH;F(2,14)=0.
692* --------END OF F(2,J) --------
722         F(11,1)=0.;F(11,2)=W
724         F(11,3)=-(W**2)*(1.+(C4/C2)+(C3/C2))*C(13)+C4*(1.+C3/C2)
726         F(11,4)=-C(13)*(W**3)*C5/C2+W*C5*(1.+C3/C2)
728         F(11,5)=1.;F(11,6)=T1S;F(11,7)=1.;F(11,8)=T2S
730         F(11,9)=1.;F(11,10)=T3S;F(11,11)=1.;F(11,12)=T4S
732         F(11,13)=1.;F(11,14)=T5S;F(11,15)=ANOTCH;F(11,16)=0.
734         F(11,17)=SVREAL;F(11,18)=SVIMAG
736* --------END OF F(11,J) --------
738         F(12,1)=ALEAK;F(12,2)=W*ASTIF
740         F(12,3)=-(W**2)*C(13)*(C3+C4)+C3*C4
742         F(12,4)=-C(13)*(W**3)*C5+C5*W*C3
744         F(12,5)=1.;F(12,6)=T1S;F(12,7)=1.;F(12,8)=T2S
746         F(12,9)=1.;F(12,10)=T3S;F(12,11)=1.;F(12,12)=T4S
748         F(12,13)=1.;F(12,14)=T5S;F(12,15)=ANOTCH;F(12,16)=0.
750         F(12,17)=SVREAL;F(12,18)=SVIMAG
752* --------END OF F(12,J) --------
754         F(13,1)=0.;F(13,2)=AWGAIN;F(13,3)=1.;F(13,4)=A2T2S
756         F(13,5)=C4;F(13,6)=C5*W;F(13,7)=1.;F(13,8)=A3T3S
758         F(13,9)=1.;F(13,10)=T4S;F(13,11)=1.;F(13,12)=T5S
760         F(13,13)=ANOTCH;F(13,14)=0.
762* --------END OF F(13,J) --------
764         F(14,1)=ANGAIN;F(14,2)=0.;F(14,3)=C4;F(14,4)=C5*W
766         F(14,5)=1.;F(14,6)=T2S;F(14,7)=1.;F(14,8)=A3T3S
768         F(14,9)=1.;F(14,10)=T4S
770* --------END OF F(14,J) --------
772         F(15,1)=-C(13)*(W**2)+C4;F(15,2)=C5*W
774         F(15,3)=C(3);F(15,4)=C(4)*W
776         F(15,5)=1.;F(15,6)=A3T3S;F(15,7)=1.;F(15,8)=T1S
778         F(15,9)=1.;F(15,10)=T2S;F(15,11)=1.;F(15,12)=T5S
780         F(15,13)=ANOTCH;F(15,14)=0.
782* --------END OF F(15,J)----END OF D --------
970* ------------------------------------------------------------------
980         CALL TRA(F,N,CR,CI)
990         TMAG=SQRT((CR**2)+(CI**2))
1000         DR=CR-1.;DI=CI;XREAL=CR;XIMAG=CI
1010         TMAG=SQRT((CR**2)+(CI**2))
1020         RMAG=SQRT((DR**2)+(DI**2))
1030         IF(1-IPR) 207,206,208
```

```
1035↑  208 PRINT 9;STOP
1040↑  206 CONTINUE
1050* - - - - PLACE G(I,J) EQUATIONS FOR FLOW BELOW - - - -
1060* ------------------------------------------------------------
1062        G(1,1)=0.;G(1,2)=C1*C(1)*C(5)*(W**3)
1064        G(1,3)=C4;G(1,4)=C5*W;G(1,5)=XREAL;G(1,6)=XIMAG
1066        G(1,7)=1.;G(1,8)=A2T2S;G(1,9)=1.;G(1,10)=A3T3S
1068        G(1,11)=1.;G(1,12)=T4S;G(1,13)=1.;G(1,14)=T5S
1070        G(1,15)=ANOTCH;G(1,16)=0.
1075* --------END OF G(1,J) --------
1076        G(2,1)=-C1*ANGAIN; G(2,2)=0.
1078        G(2,3)=C4;G(2,4)=C5*W;G(2,5)=XREAL;G(2,6)=XIMAG
1080        G(2,7)=1.;G(2,8)=T2S;G(2,9)=1.;G(2,10)=A3T3S
1082        G(2,11)=1.;G(2,12)=T4S
1087* --------END OF G(2,J) --------
1088        G(3,1)=-C1*C(3); G(3,2)=-C1*C(4)*W
1089        G(3,3)=C4-C(13)*(W**2);G(3,4)=C5*W
1090        G(3,5)=XREAL;G(3,6)=XIMAG;G(3,7)=1.;G(3,8)=A3T3S
1092        G(3,9)=1.;G(3,10)=T1S;G(3,11)=1.;G(3,12)=T2S
1094        G(3,13)=1.;G(3,14)=T5S;G(3,15)=ANOTCH;G(3,16)=0.
1100* --------END OF G(3,J) --------
1102        G(4,1)=C(3)*C1;G(4,2)=C(4)*C1*W;G(4,3)=C4;G(4,4)=C5*W
1104        G(4,5)=1.;G(4,6)=A3T3S;G(4,7)=1.;G(4,8)=T1S
1106        G(4,9)=1.;G(4,10)=T2S;G(4,11)=1.;G(4,12)=T5S;G(4,13)=ANOTCH
1108        G(4,14)=0.
1112* --------END OF G(4,J) --------
1114        G(11,1)=C4;G(11,2)=C5*W;G(11,3)=1.;G(11,4)=T1S
1116        G(11,5)=1.;G(11,6)=T2S;G(11,7)=1.;G(11,8)=T3S
1118        G(11,9)=1.;G(11,10)=T4S;G(11,11)=1.;G(11,12)=T5S
1120        G(11,13)=ANOTCH;G(11,14)=0.;G(11,15)=SVREAL;G(11,16)=SVIMAG
1130* --------END OF G(11,J) AND ALL G(I,J) --------
1180* ------------------------------------------------------------
1190        CALL TRA(G,NG,CR1,CI1)
1200        FLOW=SQRT((CR1**2)+(CI1**2))
1210* - - - - PLACE H(I,J) EQUATIONS FOR STROKE BELOW - - - -
1220* ------------------------------------------------------------
1222        H(1,1)=-C(13)*(W**2)/C2;H(1,2)=0.
1224        H(1,3)=C4;H(1,4)=C5*W;H(1,5)=XREAL;H(1,6)=XIMAG
1230* --------END OF H(1,J) --------
1232        H(2,1)=1.+(C3/C2);H(2,2)=0.
1234        H(2,3)=C4-C(13)*(W**2);H(2,4)=C5*W
1236        H(2,5)=XREAL;H(2,6)=XIMAG
1244* --------END OF H(2,J) --------
1246        H(3,1)=-(1.+(C3/C2));H(3,2)=0.
1248        H(3,3)=C4;H(3,4)=C5*W
1255* --------END OF H(3,J) AND END OF N --------
1256        H(11,1)=C4;H(11,2)=C5*W
1260*   ------END OF H(I,J) ------------
```

```
1330* ------------------------------------------------------------
1340        CALL TRA(H,NH,CR2,CI2)
1350        STROKE=SQRT((CR2**2)+(CI2**2))
1360+   207 CONTINUE
1370        CPS=W/(2.*PI)
1380        IF(1-IPR) 209,211,212
1390+   212 PHI=180.*ANGLE/PI
1400        PRINT 2,CPS,PHI,DBMAG; GO TO 213
1410+   211 PRINT 5,CPS,TMAG,RMAG,FLOW,STROKE; GO TO 213
1420+   209 PRINT 53,CPS,TMAG,RMAG
1430+   213 CONTINUE
1440        DBMAG=10.*ALOG(TMAG)
1470        IF(WB-W) 24,23,23
1480+    23 TM1=DBMAG;TM2=DBMAG;TM3=DBMAG
1490        PPD1=PPD;PPD2=PPD;PPD3=PPD
1500        GO TO 25
1510+    24 TM1=TM2
1520        TM2=TM3
1530        TM3=DBMAG
1540        PPD1=PPD2
1550        PPD2=PPD3
1560+    25 DSLO=(TM3-TM2)*PPD2 - (TM2-TM1)*PPD1
1570        SLO=(TM3-TM2)*PPD2
1580        PPD3=PPD*ABS(DSLO)*.2+PPD*ABS(DSLO)*.02*SQRT(ABS(SLO))
1590        IF(PPD3-PPD) 27,27,26
1600+    26 IF(PPD-0.1*PPD3) 28,28,29
1610+    27 PPD3=PPD
1620        GO TO 29
1630+    28 PPD3=10.*PPD
1640+    29 IF((PPD2/PPD3)-1.20) 31,31,30
1650+    30 PPD3=0.707*PPD2
1660+    31 X=10.**(1./PPD3)
1670        W=X*W
1680        IF(W-WE) 14,14,32
1690+    32 PRINT 9; PRINT 3
1700        GO TO 10
1710+     1 FORMAT(  *     CPS      PHASE        DB-MAG*)
1720+     2 FORMAT(F10.4,3X,F7.2,3X,F7.2)
1730+     3 FORMAT(//1H0)
1740+     4 FORMAT(/*      CPS        ABS MAG       REL MAG*
1750A*        FLOW          STROKE*/)
1760+     5 FORMAT(F10.4,3X,F11.5,3X,F11.5,3X,F11.5,3X,F11.5)
1770+     7 FORMAT(* CLOSED LOOP TRANSFER FUNCTION*/)
1780+   6 FORMAT(*NASA TACV 1000-1,RUN *,I2,* CASE *,I2,/* SINGLE*
1790A* NOTCH FOR SINUSOIDAL EXCITATION, WIDEBAND FOR RANDOM EXCITATION*
1800A* LEAD, LEAD-LAG, LAG-LEAD ON CA; LEAD, LAG-LEAD ON KA;*/
1810A* LAG, LAG-LEAD ON CD AND CV, LEAD ON KA, FLEXIBLE 1000 POUND*
1820A* PAYLOAD */)
```

```
1830*      8 FORMAT(* OPEN LOOP TRANSFER FUNCTION*/)
1840* 9 FORMAT(/*-------------------------------------------------*/)
1850*    51 FORMAT( *     CPS          ABS MAG        REL MAG*)
1860*    53 FORMAT(F10.4,3X,F11.5,3X,F11.5)
1870        STOP
1880        END
1890        SUBROUTINE TRA(F,N,CR,CI)
1900* CALCULATES CR AND CI FOR F(I,J);G(I,J);H(I,J)
1910        DIMENSION F(20,20),N(20)
1920        DO 1 I=1,20
1930        IF(N(I)-1) 2,1,10
1940*     10 NT=(N(I)-1)*2-1
1950        DO 3 J=1,NT,2
1960        FIJ2=F(I,J+2)
1970        F(I,J+2)=F(I,J)*F(I,J+2)-F(I,J+1)*F(I,J+3)
1980*      3 F(I,J+3)=F(I,J)*F(I,J+3)+F(I,J+1)*FIJ2
1990        GO TO 1
2000*      2 F(I,1)=0.;F(I,2)=0.
2010        N(I)=1
2020*      1 CONTINUE
2030        BR=0.;BI=0.;TR=0.;TI=0.
2040        DO 4 I=1,10
2050        J=I+10
2060        TR=TR+F(I,2*N(I)-1)
2070        TI=TI+F(I,2*N(I))
2080        BR=BR+F(J,2*N(J)-1)
2090        BI=BI+F(J,2*N(J))
2100*      4 CONTINUE
2110        IF(ABS(TR)+ABS(TI)+ABS(BR)+ABS(BI)-1.E15) 6,6,5
2120*      5 TR=TR/1.E15;TI=TI/1.E15;BR=BR/1.E15;BI=BI/1.E15
2130*      6 CONTINUE
2140        DEN=BR**2+BI**2
2150        CR=(TR*BR+TI*BI)/DEN
2160        CI=(TI*BR-TR*BI)/DEN
2170*     11 RETURN
2180        END
2190        SUBROUTINE ARCTAN(X,Y,ANGLE,ERROR)
2200        ERROR=0.0
2210        PI=3.14159265
2220        IF(X) 10,30,20
2230*     10 ANGLE=ATAN(Y/X)+PI*SIGN(1.,Y)
2240*     18 RETURN
2250*     20 ANGLE=ATAN(Y/X)
2260*     19 RETURN
2270*     30 IF(Y) 40,100,50
2280*     40 ANGLE=-PI/2.0
2290*     21 RETURN
2300*     50 ANGLE=PI/2.0
2310*     22 RETURN
2320*    100 ERROR=1.0
2330*     99 RETURN
2340        END
2350 ENDPROG
```

APPENDIX C

FREQUENCY RESPONSE OF LINEAR ACTIVE FEEDBACK SYSTEM WITH FLEXIBLE PAYLOAD

Figures 59 through 70 show the closed loop, steady state response of flexible payloads supported on a linear feedback active isolator, in terms of absolute and relative transmissibilities, valve flow and stroke. The payload flexibility, notch frequency, and desired level of broad-band absolute transmissibility are shown in each case. Table XX shows the open loop phase and gain magnitude margins and the crossover frequencies at which they occur.

Payload Nominal Weight : 1,000 lb
% Critical Damping: 0.1
Natural Frequency : 5.0 Hz

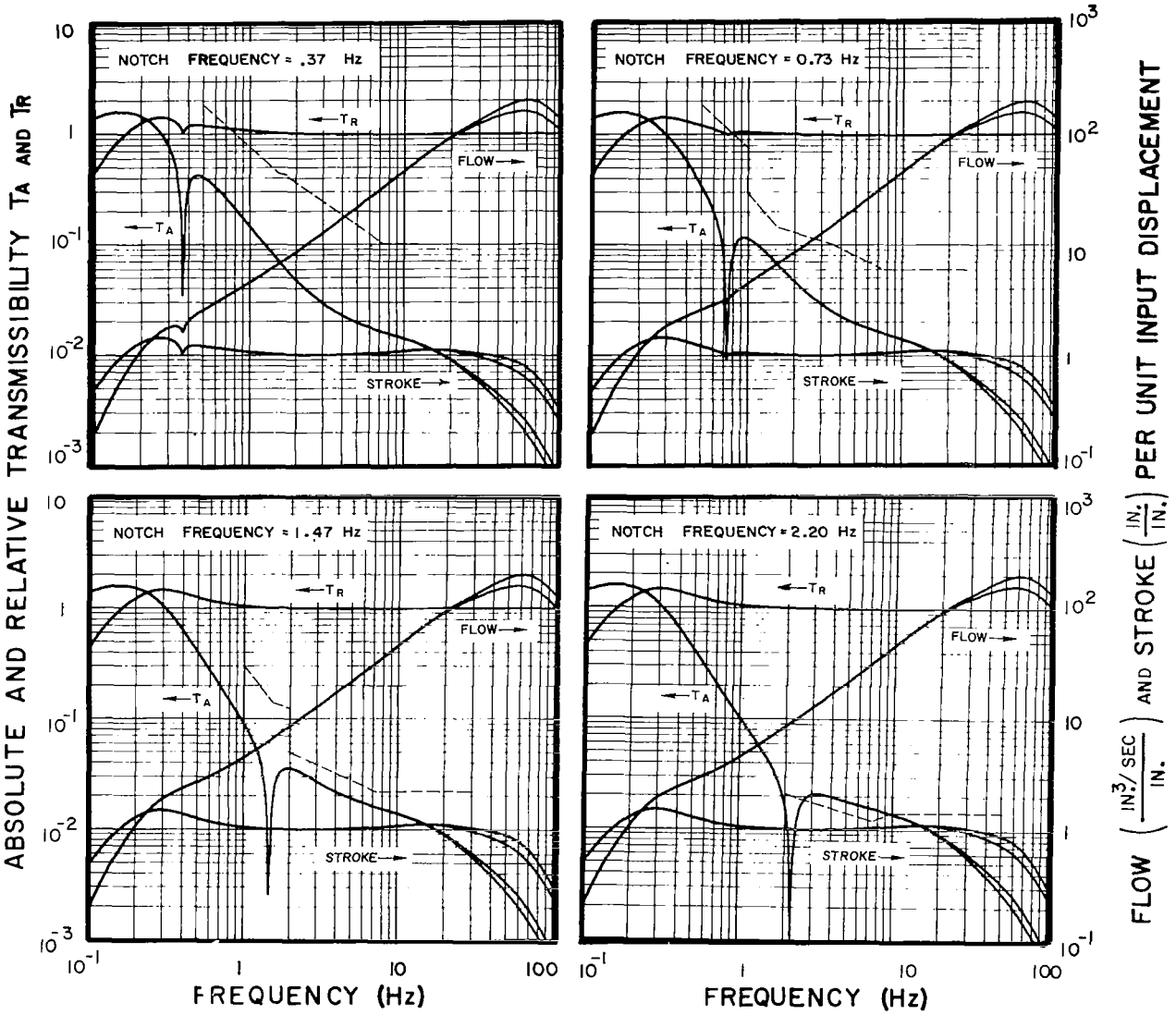

AT LOW FREQUENCIES, EACH CURVE APPLIES TO BOTH NOMINAL PAYLOAD AND A 20% INCREASE IN PAYLOAD. AT HIGH FREQUENCIES, THE UPPER CURVES APPLY TO THE NOMINAL WEIGHT AND THE LOWER CURVES TO THE INCREASED WEIGHT.

DASHED LINE REPRESENTS MAXIMUM ALLOWABLE ABSOLUTE TRANSMISSIBILITY FOR RANDOM INPUTS.

Figure 59: System absolute and relative transmissibility, valve flow, and actuator stroke for 1,000 lb flexible payload. Notch frequencies: 0.37, 0.73, 1.47 and 2.20 Hz.

Payload Nominal Weight : 1,000 lb
% Critical Damping: 0.1
Natural Frequency : 5.0

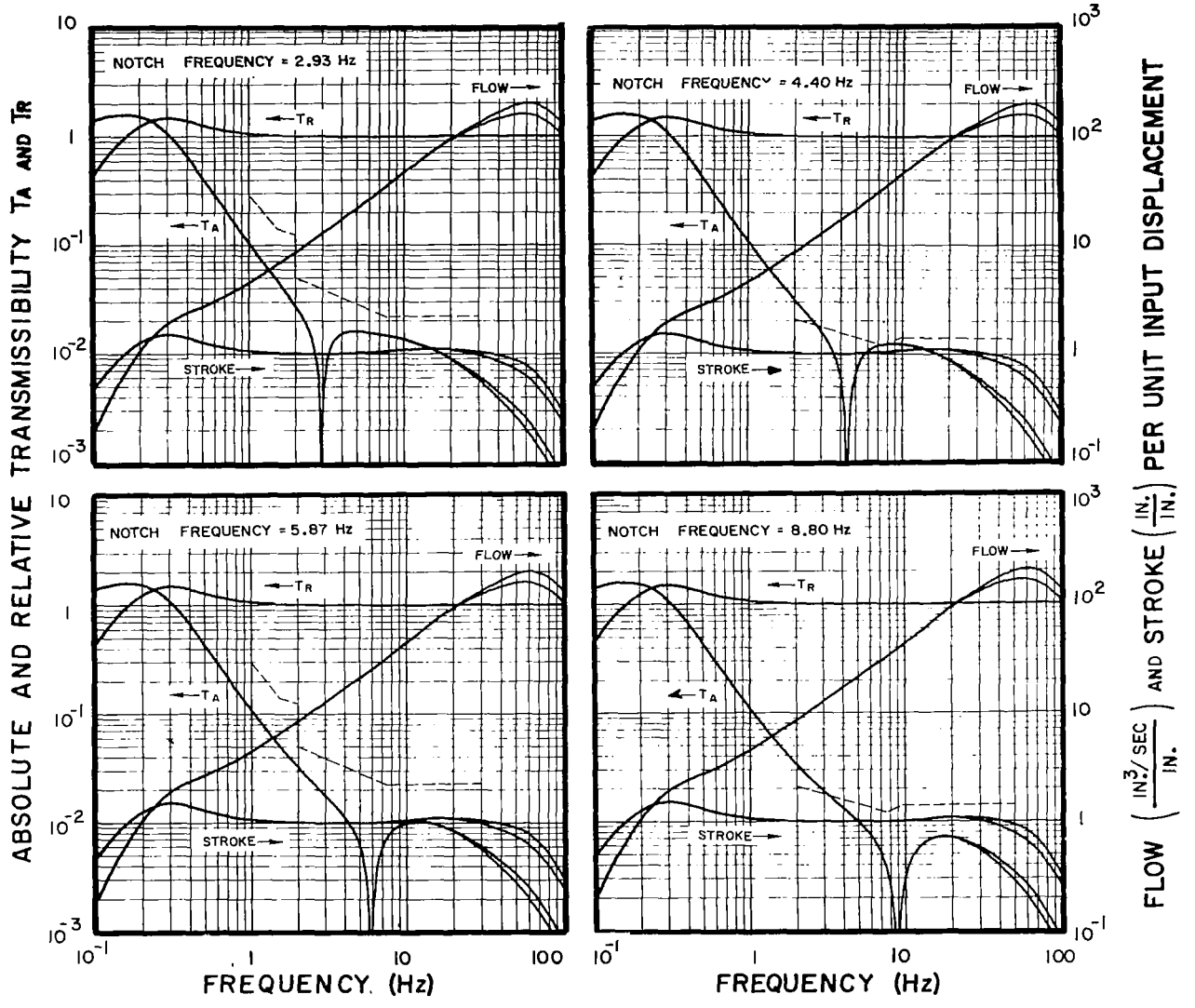

AT LOW FREQUENCIES, EACH CURVE APPLIES TO BOTH NOMINAL PAYLOAD AND A 20% INCREASE IN PAYLOAD. AT HIGH FREQUENCIES, THE UPPER CURVES APPLY TO THE NOMINAL WEIGHT AND THE LOWER CURVES TO THE INCREASED WEIGHT.

DASHED LINE REPRESENTS MAXIMUM ALLOWABLE ABSOLUTE TRANSMISSIBILITY FOR RANDOM INPUTS.

Figure 60: System absolute and relative transmissibility, valve flow, and actuator stroke for 1,000 lb flexible payload. Notch frequencies: 2.93, 4.40, 5.87 and 8.80 Hz.

Payload Nominal Weight : 1,000 lb
% Critical Damping: 0.1
Natural Frequency : 10.0 Hz.

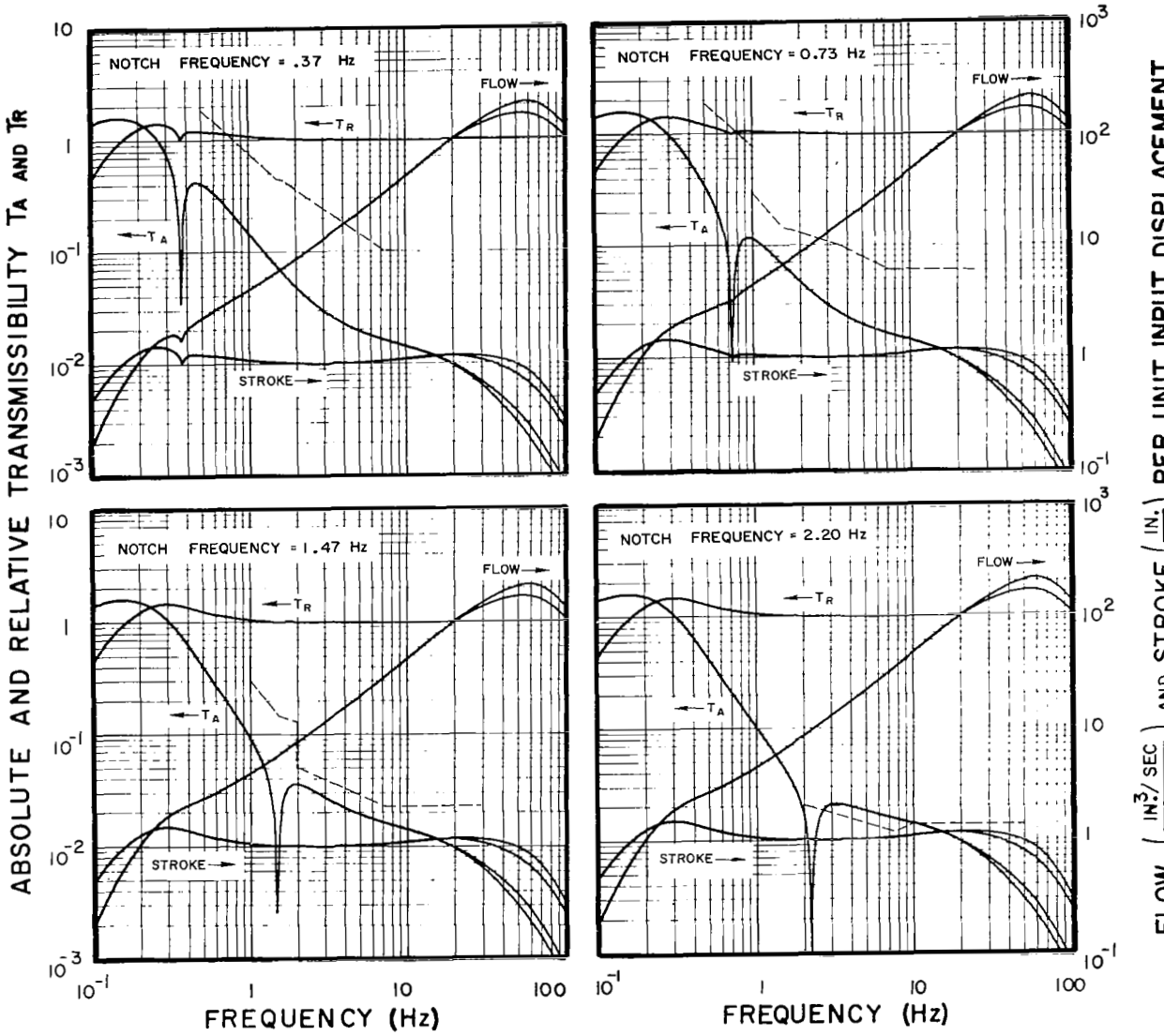

AT LOW FREQUENCIES, EACH CURVE APPLIES TO BOTH NOMINAL PAYLOAD AND A 20% INCREASE IN PAYLOAD. AT HIGH FREQUENCIES, THE UPPER CURVES APPLY TO THE NOMINAL WEIGHT AND THE LOWER CURVES TO THE INCREASED WEIGHT.

DASHED LINE REPRESENTS MAXIMUM ALLOWABLE ABSOLUTE TRANSMISSIBILITY FOR RANDOM INPUTS.

Figure 61: System absolute and relative transmissibility, valve flow, and actuator stroke for 1,000 lb flexible payload. Notch frequencies: 0.37, 0.73, 1.47 and 2.20 Hz.

Payload Nominal Weight : 1,000 lb
% Critical Damping: 0.1
Natural Frequency : 10.0 Hz

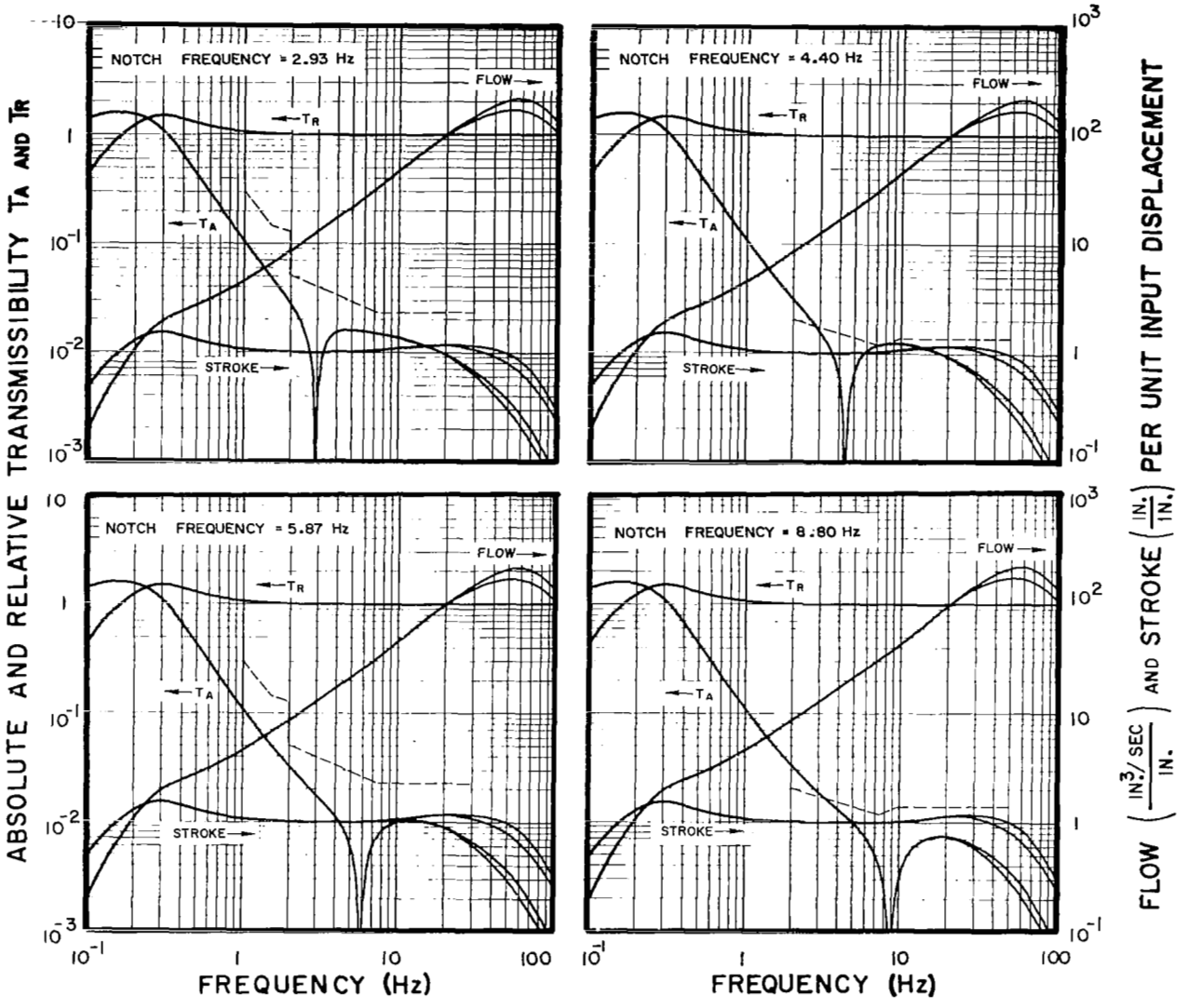

AT LOW FREQUENCIES, EACH CURVE APPLIES TO BOTH NOMINAL PAYLOAD AND A 20% INCREASE IN PAYLOAD. AT HIGH FREQUENCIES, THE UPPER CURVES APPLY TO THE NOMINAL WEIGHT AND THE LOWER CURVES TO THE INCREASED WEIGHT.

DASHED LINE REPRESENTS MAXIMUM ALLOWABLE ABSOLUTE TRANSMISSIBILITY FOR RANDOM INPUTS.

Figure 62: System absolute and relative transmissibility, valve flow, and actuator stroke for 1,000 lb flexible payload. Notch frequencies: 2.93, 4.40, 5.87 and 8.80 Hz.

Payload Nominal Weight : 3,000 lb
% Critical Damping: 0.1
Natural Frequency : 5.0 Hz

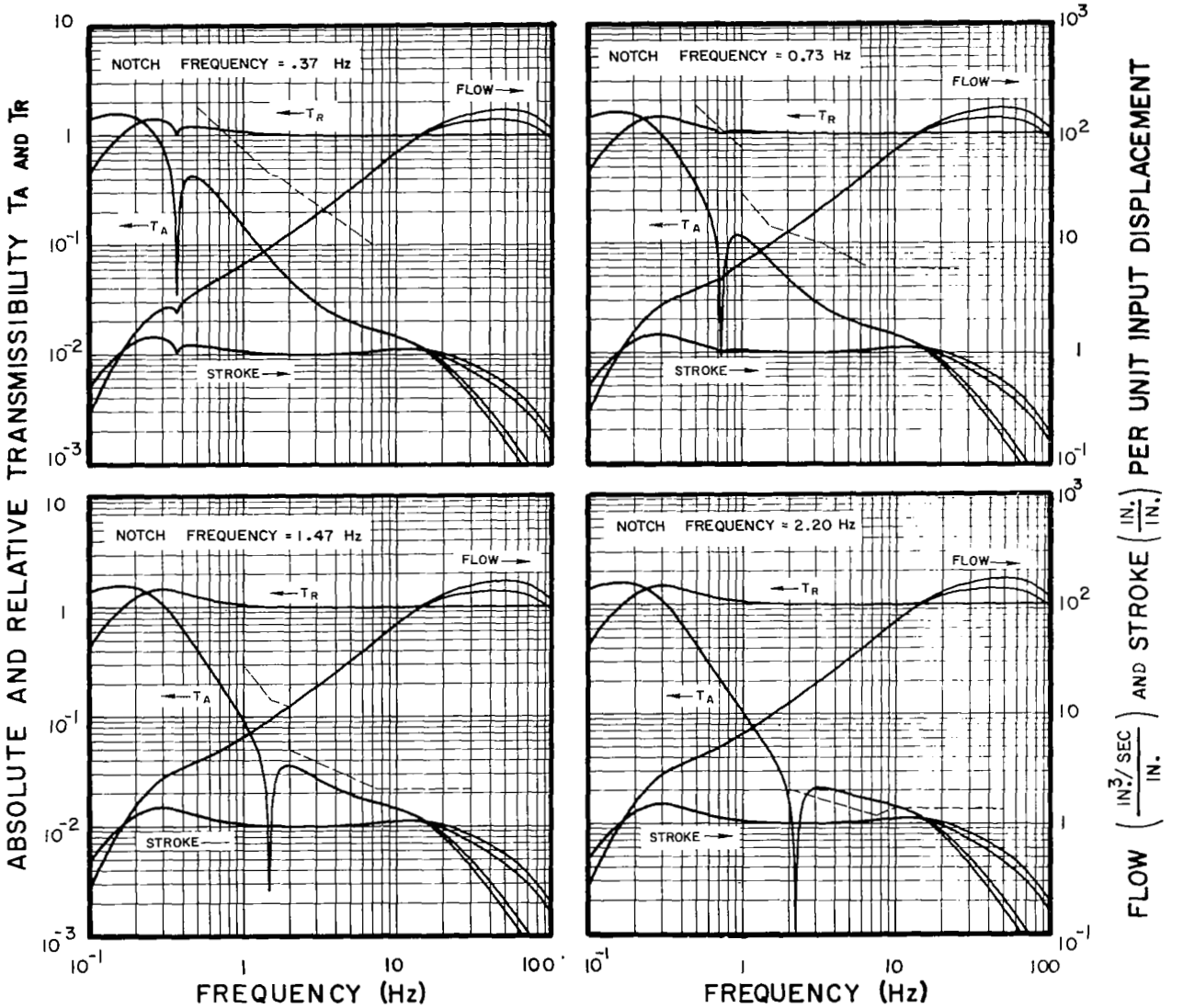

AT LOW FREQUENCIES, EACH CURVE APPLIES TO BOTH NOMINAL PAYLOAD AND A 20% INCREASE IN PAYLOAD. AT HIGH FREQUENCIES, THE UPPER CURVES APPLY TO THE NOMINAL WEIGHT AND THE LOWER CURVES TO THE INCREASED WEIGHT.

DASHED LINE REPRESENTS MAXIMUM ALLOWABLE ABSOLUTE TRANSMISSIBILITY FOR RANDOM INPUTS.

Figure 63: System absolute and relative transmissibility, valve flow, and actuator stroke for 3,000 lb flexible payload. Notch frequencies: 0.37, 0.73, 1.47 and 2.20 Hz.

Payload Nominal Weight : 3,000 lb
% Critical Damping: 0.1
Natural Frequency : 5.0 Hz

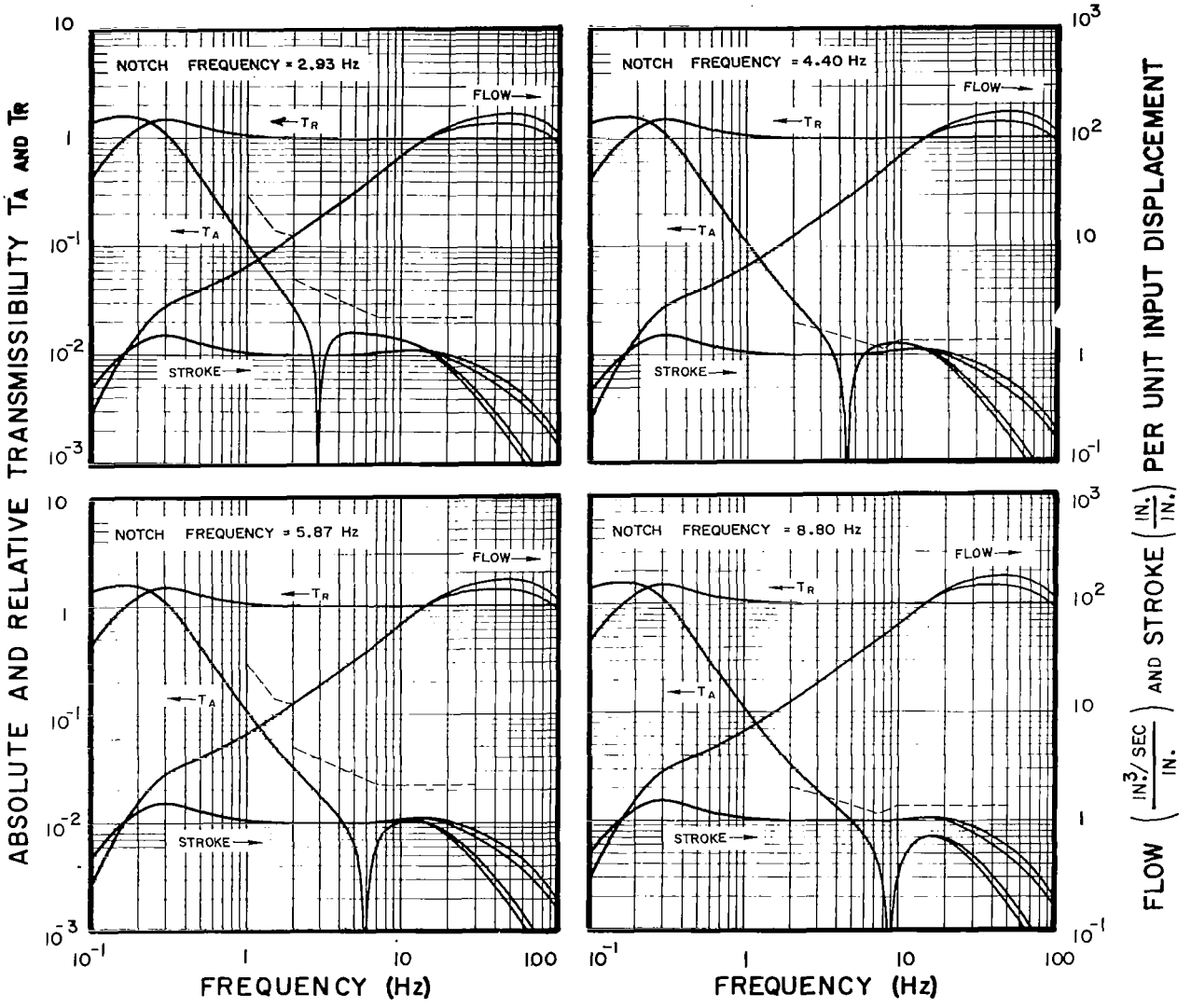

AT LOW FREQUENCIES, EACH CURVE APPLIES TO BOTH NOMINAL PAYLOAD AND A 20% INCREASE IN PAYLOAD. AT HIGH FREQUENCIES, THE UPPER CURVES APPLY TO THE NOMINAL WEIGHT AND THE LOWER CURVES TO THE INCREASED WEIGHT.

DASHED LINE REPRESENTS MAXIMUM ALLOWABLE ABSOLUTE TRANSMISSIBILITY FOR RANDOM INPUTS.

Figure 64: System absolute and relative transmissibility, valve flow, and actuator stroke for 3,000 lb flexible payload. Notch frequencies: 2.93, 4.40, 5.87 and 8.80 Hz.

Payload Nominal Weight : 3,000 lb
% Critical Damping: 0.1
Natural Frequency : 10.0 Hz

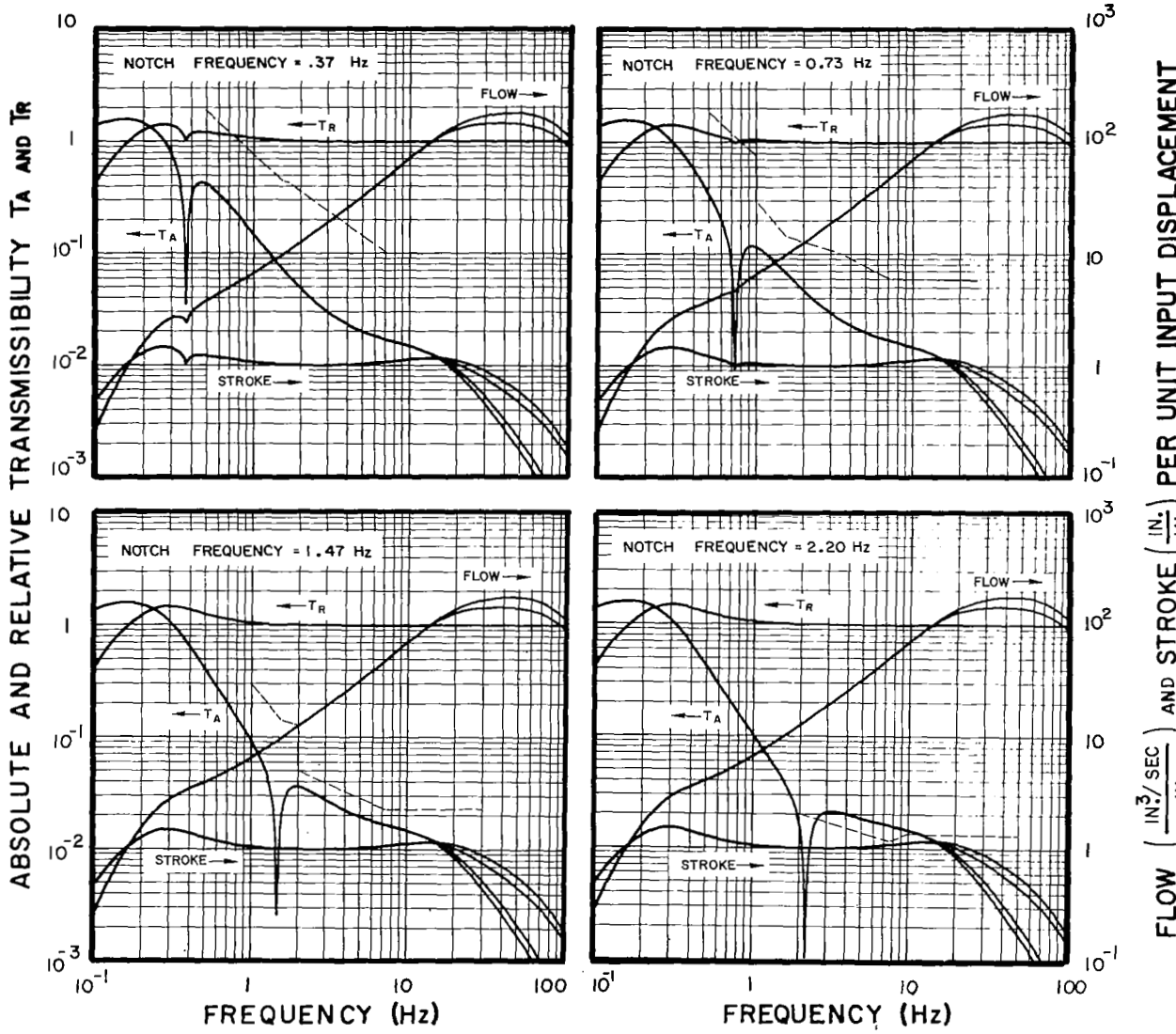

AT LOW FREQUENCIES, EACH CURVE APPLIES TO BOTH NOMINAL PAYLOAD AND A 20% INCREASE IN PAYLOAD. AT HIGH FREQUENCIES, THE UPPER CURVES APPLY TO THE NOMINAL WEIGHT AND THE LOWER CURVES TO THE INCREASED WEIGHT.

DASHED LINE REPRESENTS MAXIMUM ALLOWABLE ABSOLUTE TRANSMISSIBILITY FOR RANDOM INPUTS.

Figure 65: System absolute and relative transmissibility, valve flow, and actuator stroke for 3,000 lb flexible payload. Notch frequencies: 0.37, 0.73, 1.47 and 2.20 Hz.

Payload Nominal Weight : 3,000 lb
% Critical Damping: 0.1
Natural Frequency : 10.0 Hz

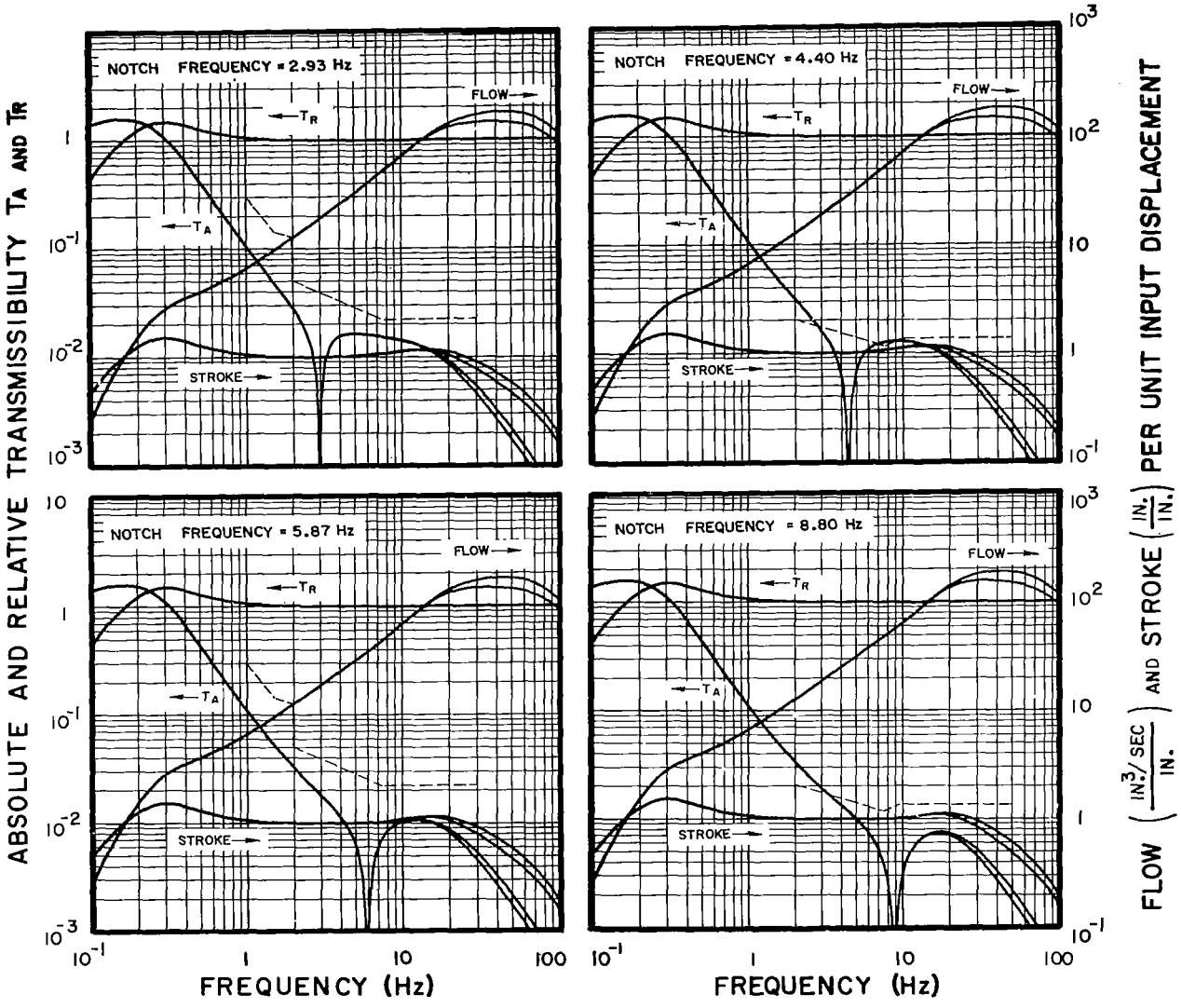

AT LOW FREQUENCIES, EACH CURVE APPLIES TO BOTH NOMINAL PAYLOAD AND A 20% INCREASE IN PAYLOAD. AT HIGH FREQUENCIES, THE UPPER CURVES APPLY TO THE NOMINAL WEIGHT AND THE LOWER CURVES TO THE INCREASED WEIGHT.

DASHED LINE REPRESENTS MAXIMUM ALLOWABLE ABSOLUTE TRANSMISSIBILITY FOR RANDOM INPUTS.

Figure 66: System absolute and relative transmissibility, valve flow, and actuator stroke for 3,000 lb flexible payload. Notch frequencies: 2.93, 4.40, 5.87 and 8.80 Hz.

Payload Nominal Weight : 10,000 lb
% Critical Damping: 0.1
Natural Frequency : 5.0 Hz

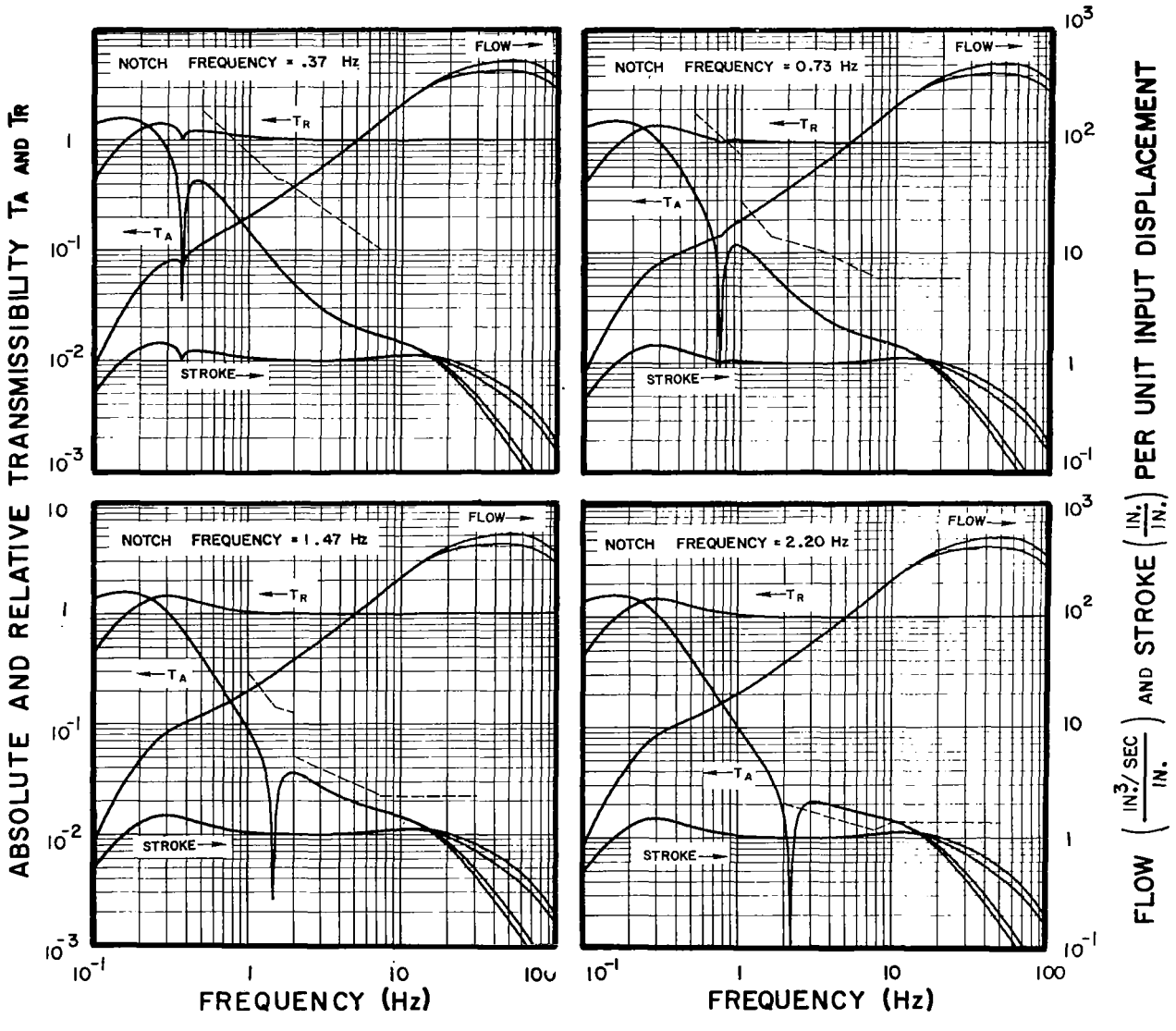

AT LOW FREQUENCIES, EACH CURVE APPLIES TO BOTH NOMINAL PAYLOAD AND A 20% INCREASE IN PAYLOAD. AT HIGH FREQUENCIES, THE UPPER CURVES APPLY TO THE NOMINAL WEIGHT AND THE LOWER CURVES TO THE INCREASED WEIGHT.

DASHED LINE REPRESENTS MAXIMUM ALLOWABLE ABSOLUTE TRANSMISSIBILITY FOR RANDOM INPUTS.

Figure 67: System absolute and relative transmissibility, valve flow, and actuator stroke for 10,000 lb flexible payload. Notch frequencies: 0.37, 0.73, 1.47, and 2.20 Hz.

Payload Nominal Weight : 10,000
% Critical Damping: 0.1
Natural Frequency : 5.0

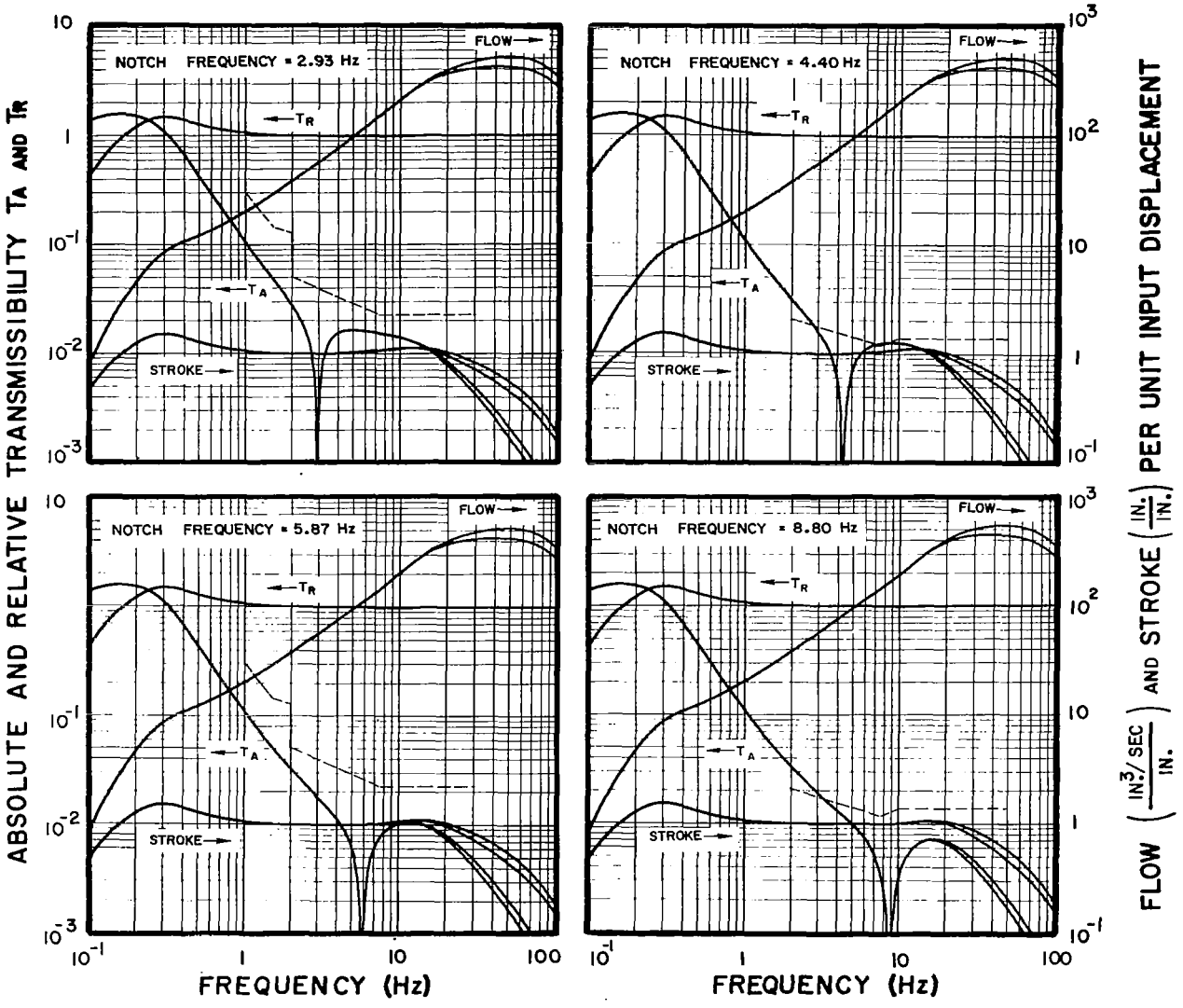

AT LOW FREQUENCIES, EACH CURVE APPLIES TO BOTH NOMINAL PAYLOAD AND A 20% INCREASE IN PAYLOAD. AT HIGH FREQUENCIES, THE UPPER CURVES APPLY TO THE NOMINAL WEIGHT AND THE LOWER CURVES TO THE INCREASED WEIGHT.

DASHED LINE REPRESENTS MAXIMUM ALLOWABLE ABSOLUTE TRANSMISSIBILITY FOR RANDOM INPUTS.

Figure 68: System absolute and relative transmissibility, valve flow, and actuator stroke for 10,000 lb flexible payload. Notch frequencies: 2.93, 4.40, 5.87 and 8.80 Hz.

Payload Nominal Weight : 10,000 lb
% Critical Damping: 0.1
Natural Frequency : 10.0

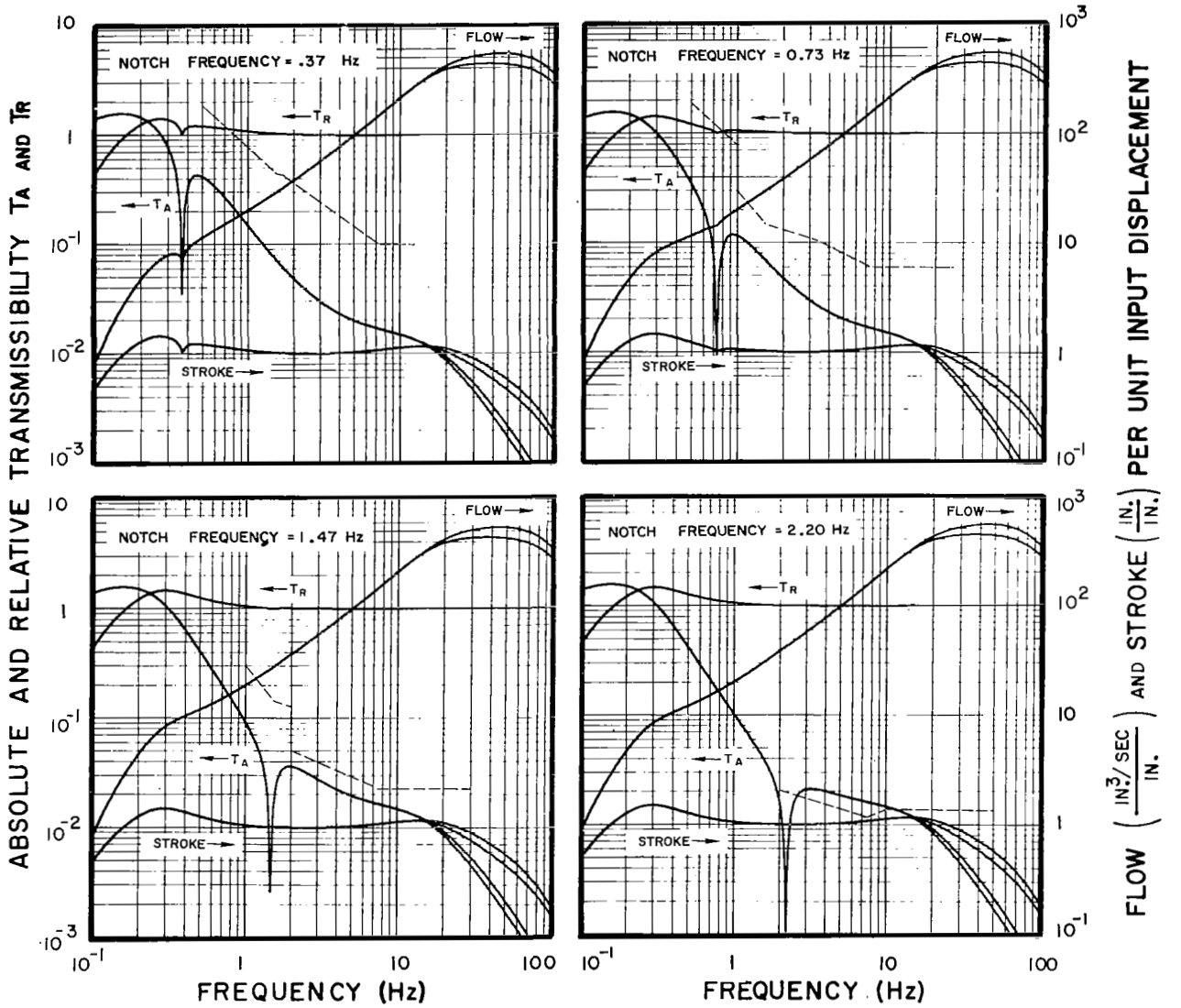

AT LOW FREQUENCIES, EACH CURVE APPLIES TO BOTH NOMINAL PAYLOAD AND A 20% INCREASE IN PAYLOAD. AT HIGH FREQUENCIES, THE UPPER CURVES APPLY TO THE NOMINAL WEIGHT AND THE LOWER CURVES TO THE INCREASED WEIGHT.

DASHED LINE REPRESENTS MAXIMUM ALLOWABLE ABSOLUTE TRANSMISSIBILITY FOR RANDOM INPUTS.

Figure 69: System absolute and relative transmissibility, valve flow, and actuator stroke for 10,000 lb flexible payload. Notch frequencies: 0.37, 0.73, 1.47 and 2.20 Hz.

Payload Nominal Weight : 10,000 lb
% Critical Damping: 0.1
Natural Frequency : 10.0 Hz

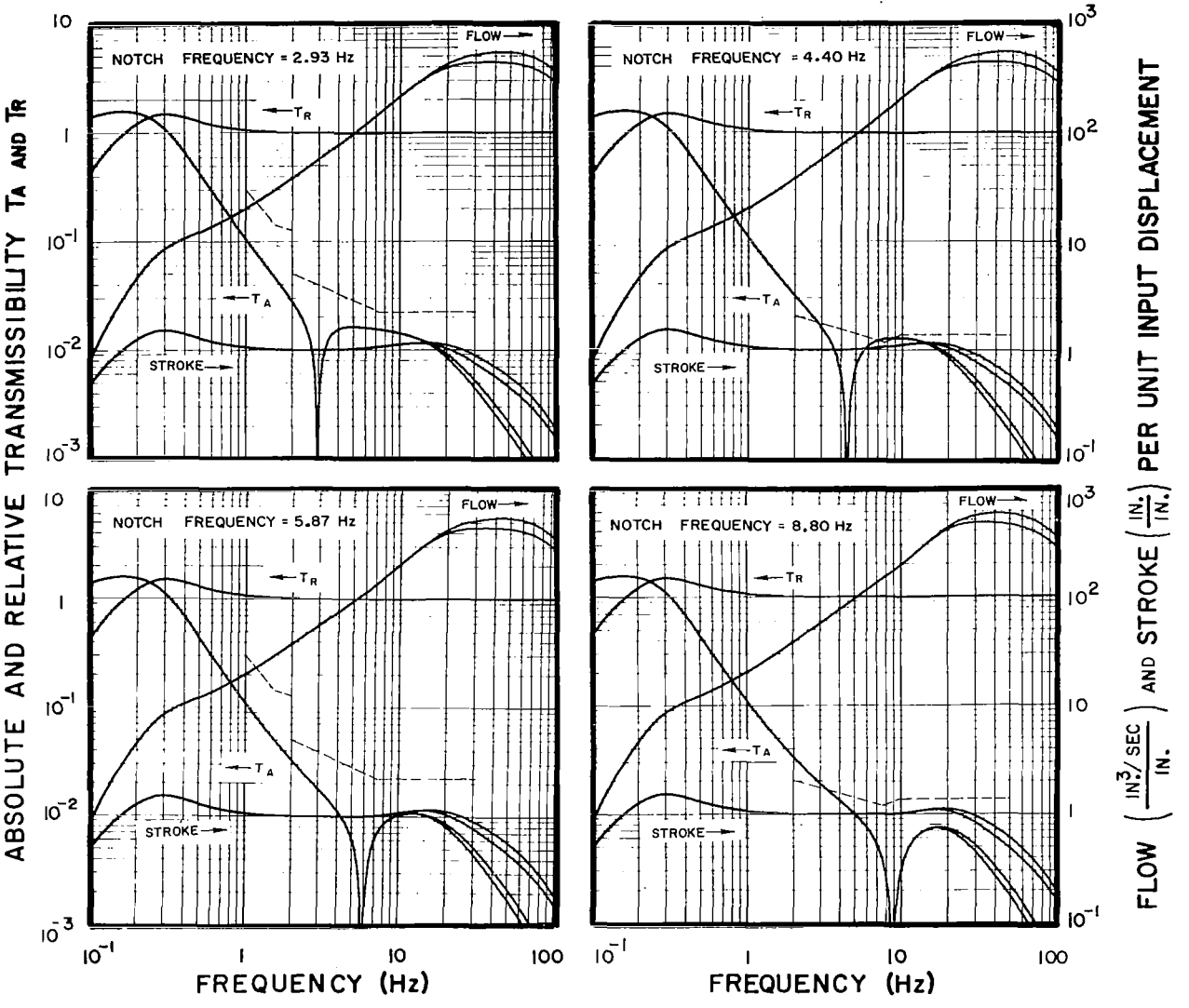

AT LOW FREQUENCIES, EACH CURVE APPLIES TO BOTH NOMINAL PAYLOAD AND A 20% INCREASE IN PAYLOAD. AT HIGH FREQUENCIES, THE UPPER CURVES APPLY TO THE NOMINAL WEIGHT AND THE LOWER CURVES TO THE INCREASED WEIGHT.

DASHED LINE REPRESENTS MAXIMUM ALLOWABLE ABSOLUTE TRANSMISSIBILITY FOR RANDOM INPUTS.

Figure 70: System absolute and relative transmissibility, valve flow, and actuator stroke for 10,000 lb flexible payload. Notch frequencies: 2.93, 4.40, 5.87 and 8.80 Hz.

TABLE XX

OPEN LOOP GAIN MAGNITUDE AND PHASE MARGINS

FOR FLEXIBLE PAYLOADS

Payload Weight (lb)	Payload Resonant Frequency (Hz)	Notch Frequency (Hz)	Phase		Gain	
			Crossover Frequency (Hz)	Margin (degrees)	Crossover Frequency (Hz)	Margin (db)
1,000	5	0.37	31.90	58.67	99.33	-12.53
		0.73	31.90	58.67	99.33	-12.53
		1.47	31.91	58.66	99.33	-12.53
		2.20	31.95	58.64	99.33	-12.53
		2.93	32.01	58.61	99.33	-12.52
		4.40	32.27	58.48	99.33	-12.52
		5.87	32.75	58.30	99.34	-12.50
		8.80	34.48	57.80	99.38	-12.45
1,200	5	0.37	27.28	60.25	98.65	-13.97
		0.73	27.28	60.25	98.65	-13.97
		1.47	27.29	60.24	98.65	-13.97
		2.20	27.33	60.23	98.65	-13.97
		2.93	27.40	60.20	98.65	-13.96
		4.40	27.67	60.11	98.65	-13.96
		5.87	28.19	60.02	98.65	-13.94
		8.80	30.07	59.91	98.69	-13.89
1,000	10	0.37	33.49	52.94	96.93	-12.08
		0.73	33.49	52.94	96.93	-12.08
		1.47	33.50	52.93	96.93	-12.08
		2.20	33.53	52.92	96.93	-12.08
		2.93	33.58	52.89	96.93	-12.07
		4.40	33.80	52.79	96.93	-12.07
		5.87	34.23	52.63	96.93	-12.05
		8.80	35.80	52.23	96.97	-12.00
1,200	10	0.37	28.65	55.34	96.63	-13.59
		0.73	28.66	55.34	96.63	-13.59
		1.47	28.67	55.33	96.63	-13.59
		2.20	28.70	55.31	96.63	-13.59
		2.93	28.76	55.28	96.63	-13.59
		4.40	29.02	55.20	96.63	-13.58
		5.87	29.49	55.11	96.64	-13.57
		8.80	31.22	55.02	96.68	-13.51

TABLE XX (Continued)

Payload Weight (lb)	Payload Resonant Frequency (Hz)	Notch Frequency (Hz)	Phase		Gain	
			Crossover Frequency (Hz)	Margin (degrees)	Crossover Frequency (Hz)	Margin (db)
3,000	5	0.37	21.85	61.36	97.87	-16.14
		0.73	21.85	61.36	97.87	-16.14
		1.47	21.86	61.35	97.87	-16.14
		2.20	21.90	61.34	97.87	-16.14
		2.93	21.98	61.32	97.87	-16.14
		4.40	22.32	61.31	97.87	-16.13
		5.87	22.93	61.40	97.88	-16.12
		8.80	24.99	62.08	97.92	-16.06
3,600	5	0.37	18.99	61.57	97.42	-17.63
		0.73	18.99	61.57	97.42	-17.63
		1.47	19.01	61.56	97.42	-17.63
		2.20	19.05	61.55	97.42	-17.63
		2.93	19.14	61.54	97.42	-17.63
		4.40	19.49	61.60	97.42	-17.63
		5.87	20.11	61.88	97.43	-17.61
		8.80	22.27	63.20	97.47	-17.55
3,000	10	0.37	22.93	57.57	96.29	-15.85
		0.73	22.93	57.57	96.29	-15.85
		1.47	22.95	57.56	96.29	-15.85
		2.20	22.98	57.55	96.29	-15.85
		2.93	23.06	57.53	96.29	-15.84
		4.40	23.36	57.50	96.29	-15.84
		5.87	23.89	57.58	96.29	-15.82
		8.80	25.82	58.15	96.33	-15.77
3,600	10	0.37	19.82	58.50	96.09	-17.39
		0.73	19.82	58.50	96.09	-17.39
		1.47	19.83	58.49	96.09	-17.39
		2.20	19.88	58.48	96.09	-17.38
		2.93	19.95	58.46	96.09	-17.38
		4.40	20.30	58.49	96.09	-17.37
		5.87	20.92	58.70	96.10	-17.36
		8.80	22.96	59.85	96.14	-17.30

REFERENCES

1. Ruzicka, J. E.: Active Vibration and Shock Isolation. Trans. SAE, vol. 77, Paper No. 680747, 1968, pp. 2872-2886.

2. Schubert, D. W.; and Ruzicka, J. E.: Theoretical and Experimental Investigation of Electrohydraulic Vibration Isolation Systems, ASME Paper No. 69-Vibr-40, May 1969.

3. Pepi, J. S.: Active Vibration Isolation of Aerial Cameras. Proceedings IES, April 1968, pp. 389-399.

4. Paul, Igor L.; and Bender, Erich K.: Active Vibration Isolation and Active Vehicle Suspension, MIT PB 173 648, November 1, 1966.

5. Calcaterra, P. C.; and Schubert, D.W.: Research on Active Vibration Isolation Techniques for Aircraft Pilot Protection, AMRL-TR-67-138, Oct. 1967.

6. Leatherwood, J. D.; and Dixon, G. V.: Active Vibration Isolation for Flexible Payloads, Proceedings IES, April 1968, pp. 407-413.

7. Calcaterra, P. C.; and Schubert, D. W.: Isolation of Helicopter Rotor-Induced Vibrations Using Active Elements, USAAVLABS-TR-68-9, June 1969.

8. Goldman, D. E.; and von Gierke, H. E.: Effects of Shock and Vibration on Man. Shock and Vibration Handbook (edited by C. M. Harris and C. E. Crede), vol. 3, chapter 44, McGraw-Hill Book Co., New York, 1961.

9. Harris, C. S.; and Shoenberger, R. W.: Human Performance During Vibration. AMRL-TR-65-204, Nov. 1965.

10. Cavanaugh, R. D.: Air Suspension and Servo-Controlled Isolation Systems, Shock Vibration Handbook (edited by C. M. Harris and C. E. Crede), vol. 3, chapter 33, McGraw-Hill Book Co., New York, 1961.

11. D'Azzo, J. J.; and Houpis, C. H.: Feedback Control System Analysis and Synthesis, McGraw-Hill Book Co., New York, 1966, p.91.